LEAKAGE CHARACTERISATION OF BULK WATER PIPELINES

Report

to the Water Research Commission

by

R Nsanzubuhoro, D Niebuhr and JE van Zyl

Department of Civil Engineering

University of Cape Town

WRC Report No. 2572/1/19

ISBN 978-0-6392-0062-0

July 2019

EXECUTIVE SUMMARY

INTRODUCTION

Leakage from bulk pipelines has received relatively little attention due to the difficulty of assessing the level of leakage from these pipes. However, recent developments in understanding the behaviour of leaks with changes in pressure have created opportunities for cost-effective, field-based leakage characterisation.

Field and laboratory studies have shown that leakage from water pipelines is substantially more sensitive to changes in pressure than conventionally believed. It has now been established that the major reason for this behaviour is that the areas of holes and cracks in pipes are not static, but that they change with variations in pressure.

A number of studies has shown that leak areas vary linearly with pressure under both elastic and visco-elastic material deformation conditions (Cassa et al., 2010; Cassa and Van Zyl, 2014; Greyvenstein and Van Zyl, 2007).

The aim of this project was to determine the characteristics and extent of water losses on bulk pipelines in the field. The study used pressure testing in combination with the latest models on the behaviour of leak areas with pressure to achieve this aim.

The project had the following objectives:

- A literature review of the latest research on the relationship between pressure, leakage rate and leakage area
- The design of equipment suitable for testing bulk pipelines
- Construction of the equipment and verification of its effectiveness in the laboratory
- Pilot testing of the equipment on a bulk pipeline
- Testing several bulk pipelines of different materials, diameters and ages to determine their leakage characteristics.

PIPE CONDITION ASSESSMENT EQUIPMENT

The pipe condition assessment equipment (PCAE) was based on the idea that if a pipe section is isolated from its users and the rest of the system, the only route for water to exit the pipe is through leaks that exist in the pipe. By connecting a water source and pump to the pipeline, it is possible to determine the leakage rate by measuring the inflow required to maintain a given pressure. Measuring the leakage rate at different pressures allows for the leakage flow rate, and subsequently the leakage area, to be estimated as a function of pressure.

This procedure can be used to identify existing leaks in a pipe and, if it has leakage, to estimate the leakage characteristics, which consist of the initial leak area and the head-area slope.

The following minimum design requirements were set for the PCAE:

- It must be suitable for testing both bulk and distribution system pipelines.
- It must consist of materials that can handle pressure up to 12 bar.
- It must be capable of accurately measuring and logging both flow rate and pressure.

- The water meter must be capable of measuring down to background flow rates (i.e. flow rates less than 250 ℓ per hour).
- The pressure transducer should allow for data logging at a frequency of 100 m/s.
- Excess air should be removed automatically.
- The full device must be mobile and robust enough to handle field environments.

Several components were incorporated into the PCAE to satisfy the aforementioned considerations. Figure 0.1 shows the PCAE, which contains a water tank on a trailer, valves, a magnetic flow meter, an inverter, a pump, unplasticised polyvinyl chloride (uPVC) pipes and a plastic reinforced hose adaptor.

Figure 0.1: The pipe condition assessment equipment

A procedure for the condition assessment of the pipelines in the field was developed and comprised the following steps:

- Flush the access point and initiate the PCAE.
- Establish the operational pressure of the test pipe.
- Set a minimum test pressure for the test pipe.
- Test whether the pipe is isolated after closing the isolation valves.
- Pump into the isolated pipe section to determine whether leaks exist and, if so, how the leakage rate responds to changes in pressure.
- End the test and put the pipe back into operation.

The data was then exported to a Microsoft (MS) Excel-compatible format. A spreadsheet was generated and the data was analysed.

FIELD TESTS AND RESULTS

The study could conduct 12 field tests, which is many more than originally planned. The tests allowed the equipment and methodology to be thoroughly tested, showing that it could provide a feasible, efficient and cost-effective method to evaluate bulk pipelines in the field.

A summary of the tests conducted is given in Table 0.1, which provides the leakage characteristics of the pipe, as well as the leakage rate at a pressure head of 50 m.

Table 0.1: Summary of the field tests conducted in this study

Test	A_0' (mm^2)	m' (mm^2/m)	Leakage at 50 m (ℓ/min)	Leakage at 50 m (m^3/a)	Comment
BS 8 pipeline Test 1	8.50	0.0032	16	8 600	Leaks confirmed in the field and repaired.
BS 8 pipeline Test 2	29.57	0.51	103	54 000	Test done several weeks after Test 1. Large new leak evident.
Wingfield Test 1-1	0	0	0	0	No leak on section between valves V2 and V3.
Wingfield Test 1-2	11.56	3.41	342	180 000	Leak found between valves V2 and V4.
Wingfield Test 2	-	-	-	-	Failure on hydrant – no test possible.
Wingfield Test 3	-	-	-	-	No test possible due to large leak occurring in the pipe while not in use.
University of Cape Town pipeline	-	-	3.4	1 800	Leak found, but too small for the meter to register it. Half of the meter starting flow assumed.
Simon Vermooten to Murrayfield Reservoir	-	-	-	-	No test possible due to isolation valve not sealing properly.
Lynnwood Road to Koedoesnek Reservoir	22.68	0.13	55	29 000	
Garsfontein to Parkmore High-level Reservoir	17.72	0.10	42	22 000	
Brickfields and Constantia Reservoir	-	-	-	-	No test possible due to isolation valve not sealing properly.
Fort Klapperkop Reservoir to Carina Street pipeline	137.66	3.09	549	288 000	
Average	**32.5**	**1.0**	**139**	**73 000**	

It was only possible to determine the leakage characteristics in eight (67%) of the 12 tests as shown in Figure 0.2. Two tests, both on the Wingfield pipeline, were not possible due to a very big leakage on the pipe. This line was not in active use, which may have contributed to its rapid deterioration. Two of the other tests could not be completed due to isolation valves not sealing properly, which is important additional information for the municipality to have. Should the pipe have to undergo repairs, non-sealing isolation valves may hamper the process and thus it is recommended that these valves are repaired.

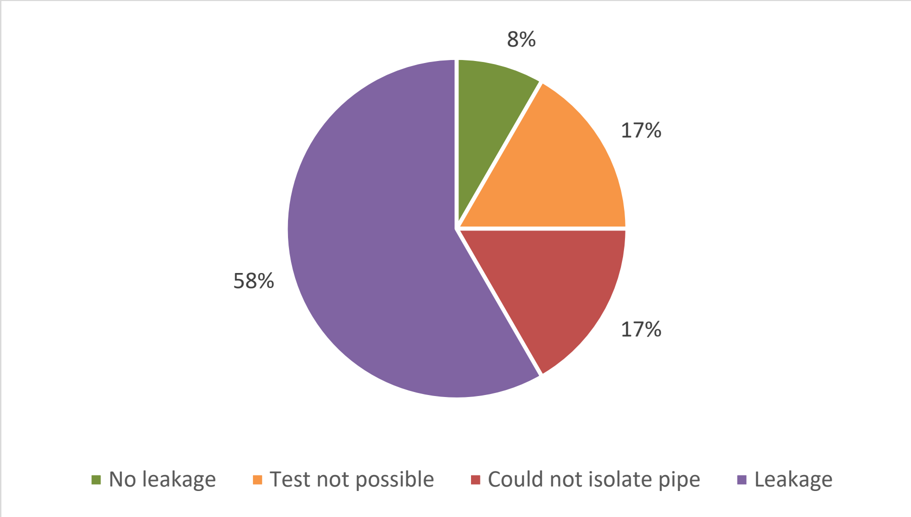

Figure 0.2: Summary of field test results

Of the eight successful pipe tests, only one pipe section (12.5%) was found to have no leakage. The other seven tests (87.5%) found leakage varying between 3.4 and 549 ℓ/min, or between 1 800 and 288 000 m^3 per area (see Figure 0.3). Assuming a production cost of R5/m^3, the leaks represent an annual loss of between R90 000 and R1 440 000.

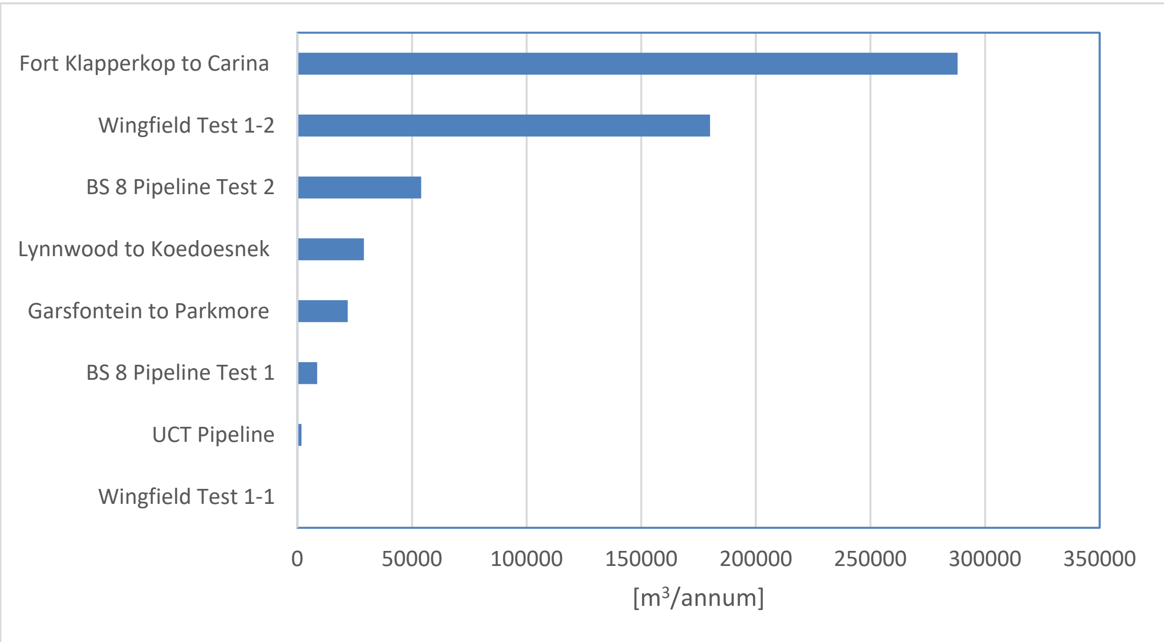

Figure 0.3: Annual leakage for the tested pipelines

CONCLUSION

The study showed that the PCAE provides an efficient, non-intrusive and cost-effective method to assess the condition of bulk pipelines. It seems that the vast majority of pipelines have some measure of leakage and that this leakage can have severe financial implications for water suppliers.

ACKNOWLEDGEMENTS

The project team wishes to thank the following people for their contributions to the project:

Reference Group	Affiliation
Dr N Kalebaila	Water Research Commission (Chair)
Ms Lelethu Bungu	Rand Water
Dr M Kumarasamy	University of KwaZulu-Natal
Mr S Moodlar	eThekwini Water and Sanitation
Mrs F Nel	Rand Water
Mr M Ncube	Development Bank of South Africa
Mr T Westman	City of Tshwane Metropolitan Municipality
Others	
Mr Pierre Maritz	City of Cape Town Metropolitan Municipality
Mr Alfred Wolfgang Moll	City of Cape Town Metropolitan Municipality
Ms Melissa De Sousa-Alves	City of Cape Town Metropolitan Municipality
Mr Motale E Selesho	Sol Plaatje Local Municipality
Mr Richard Sengani	Phokwane Local Municipality

TABLE OF CONTENTS

LIST OF FIGURES

LIST OF TABLES

ACRONYMS AND ABBREVIATIONS

BC	Brickfields to Constantia Reservoir
CCTV	Closed-circuit television
DMA	District metering area
DWS	Department of Water and Sanitation
EIF	Economic intervention frequency
EPA	Environmental Protection Authority
FAVAD	Fixed and variable area discharge
FC	Fort Klapperkop Reservoir to Carina Street
FEA	Finite element analysis
GP	Garsfontein to Parkmore High-level Reservoir
GPR	Ground-penetrating radar
HDPE	High-density polyethylene
ILI	Infrastructure Leakage Index
IWA	International Water Association
LK	Lynnwood Road to Koedoesnek Reservoir
MDPE	Medium-density polyethylene
MS	Microsoft
NPSH	Net positive suction head
NRW	Non-revenue water
OWB	Overberg Water Board
PCAE	Pipe condition assessment equipment
PCP	Pre-stressed concrete pipes

PE	Polyethylene
PVC	Polyvinyl chloride
RFEC	Remote field eddy current
RFET	Remote field eddy current technique
SVM	Simon Vermooten to Murrayfield Reservoir
TC	Transformer coupling
UCT	University of Cape Town
UN	United Nations
uPVC	Unplasticised polyvinyl chloride

CHAPTER 1: INTRODUCTION

1.1 INTRODUCTION

A great deal of work has been done over the past two decades on managing water losses in distribution systems. The Water Loss Task Force of the International Water Association (IWA) played a leading role in this effort, with its standard water balance now widely used as a basis in municipal water loss programmes.

One of the areas that has received relatively little attention is leakage on bulk pipeline systems. Bulk pipelines connect water treatment plants to bulk reservoirs, and distribute water from reservoirs to different towns or water supply zones. Bulk pipes may be operated using pumps or gravity, and generally do not supply consumers directly.

Bulk pipelines transport large quantities of water, often at high pressures. Thus, it is critical that bulk pipelines are well maintained, and that leaks are detected and repaired when they occur. Unfortunately, leaks seldom appear on the ground surface, and individual leaks are difficult to detect.

It is also difficult to determine the water losses in a bulk pipeline: the high flow rates make it impractical or prohibitively expensive to measure flow rates at both ends of bulk pipelines. Cheaper solutions, such as clamp-on ultrasonic flow meters or reservoir drop tests, are prone to problems and do not have the required accuracy.

Due to the lack of measured values, water loss on bulk pipes is often assumed to be 2% or 3%. However, these losses may be much greater in practice, and due to the large flows of water transported by bulk pipelines, even small fractions of losses represent large volumes of water.

Field and laboratory studies have shown that leakage from water distribution systems is substantially more sensitive to changes in pressure than conventionally believed. It has now been established that the major reason for this behaviour is that the areas of holes and cracks in pipes are not static, but that they change with variations in pressure.

A number of studies has shown, through experimental and finite element modelling studies, that leak areas vary linearly with pressure under both elastic and visco-elastic material deformation conditions (Cassa et al., 2010; Cassa and Van Zyl, 2014; Greyvenstein and Van Zyl, 2007; Ssozi et al., 2015). While non-linear variations may occur when plastic deformation or fracture occurs in the pipe material, these phenomena only occur when the load on a pipe is increased (i.e. pressure is increased), and not when the pressure is lowered as is the case for pressure management.

A distribution system or pipeline will generally have many leaks of different types and sizes that make up the total leakage. However, if the area of each individual leak varies linearly with pressure, it follows that the total leakage area of the system or pipeline will also vary linearly with pressure. The hydraulic behaviour of orifices (and thus leaks) is well understood, and thus the total leakage area at any pressure can be estimated from the standard orifice equation (the discharge coefficient can either be assumed or incorporated in the area calculation to obtain the effective area).

If the total leak area of the system is estimated at different pressures, the leakage area can be plotted against pressure, and a linear function fitted to the data points. The intercept of this line with the area axis gives the initial leak area, and the slope of this line the head-area slope.

The head-area slope has been studied for different leak types (Cassa and Van Zyl, 2013; Cassa and Van Zyl, 2014). Its value is reasonably well understood as a function of the pipe material (elasticity modulus, Poisson's ratio), pipe section (diameter, wall thickness) and leak parameters (shape, dimensions). Thus, it can be used to identify the characteristics of the dominant leaks in the system.

Finally, a dimensionless leakage number can be calculated for the leak, representing the ratio between the leakage from the expanding to the original parts of the leak area (Cassa and Van Zyl, 2014). A simple formula has been proposed to convert between the leakage number and the more commonly used N1 leakage exponent, and thus the leakage characteristics can be expressed in terms familiar to leakage practitioners.

1.2 AIM AND OBJECTIVES

The aim of this project was to determine the characteristics and extent of water losses on bulk pipelines. The proposed method uses pressure testing in combination with the latest models on the behaviour of leak areas with pressure to achieve this aim.

This was achieved through the following objectives:

- Conduct a literature review of the latest research on the relationship between pressure, leakage rate and leakage area.
- Design equipment suitable for testing bulk pipelines.
- Construct the equipment and verify its effectiveness in the laboratory.
- Pilot test the equipment on a bulk pipeline.
- Test several bulk pipelines of different materials, diameters and ages to determine their leakage characteristics.
- Develop guidelines for the condition assessment of pipelines using the methodology developed in this study.

CHAPTER 2: LITERATURE REVIEW

2.1 INTRODUCTION

The demand for water, an already strained resource in many countries and areas, is increasing, while cities are continuing to expand and populations are continuing to grow. Urbanisation, population growth, migration and industrialisation are all contributing to this ever-increasing need (United Nations, 2015; World Bank, 2016). According to a United Nations (UN) assessment, two-thirds of the world's population will have insufficient water supply by the year 2020 (Rogers, 2014). Furthermore, by 2025, it is estimated that 1.8 billion people will be living in countries or regions with absolute water scarcity, with two-thirds of the population living under water-stressed conditions (United Nations, 2012).

In many countries, water scarcity is further increased by climate change. Climate change has different effects on different regions of the world, leading to either increases or decreases in temperatures and precipitation, as well as to the occurrence of more extreme weather events, such as prolonged droughts and extreme flooding (United Nations, 2012). Generally, however, climate change tends to cause decreased precipitation in countries that already experience low precipitation (De Wit and Stankiewicz, 2006), thereby significantly contributing to the worrying trends of water scarcity.

With all the current and anticipated water scarcity in the world, it would be expected that the value of water is recognised and that water is treated as one of the world's most precious and valuable resources. This is, however, not the case, and a lot of water is lost and wasted. In the year 2006, for instance, the total cost of non-revenue water (NRW) worldwide was already estimated at $14 billion per year, with the contribution of developing countries amounting to one-third of this amount (Kingdom et al., 2006). Such huge loss of water, in a world that is entirely dependent on this limited resource, is clearly unacceptable, and all interventions to counter this loss deserve to be investigated.

2.2 WATER MANAGEMENT

2.2.1 Introduction

As water infrastructure ages, it deteriorates structurally and hydraulically. This leads to significant impacts on the water quality, the water lost, system reliability and efficiency. Water infrastructure must therefore be effectively and continuously managed to limit the impacts and to ensure renewal of the system when it is most cost effective to do so.

Unfortunately, in many systems, a large volume of water is lost without any intervention taking place. Gonzalez-Gomez et al. (2011) (in Van den Berg, 2015) conclude, in their study of high NRW in developing countries, that the main reason for the high NRW is a lack of incentives, not enough funds allocated to reduce water losses, and a lack of knowledge about NRW. This is supported by Frauendorfer and Liemberger (2010), who state that utility owners must be made aware that they are "sitting on a gold mine" and that their staff must be incentivised by informing them of the consequences and effects of NRW.

For effective water management, a strategy must be developed and put in place. Farley (2003) presented the following central questions that must be answered when developing a strategy:

1. How much water is being lost?
2. Where is it being lost?
3. Why is it being lost?
4. What strategies can be introduced to reduce losses?
5. How can the strategy be maintained?

The first steps to developing a suitable strategy therefore require a detailed assessment of the water entering and exiting the system. As stated by Lambert and Hirner (2000), the most important part of determining how much water is being lost in a system is to accurately quantify the volume of water that is entering the system. This view is supported by Rogers (2014), who states that an immediate and precise way of quantifying leakage is needed that is not subject to measurement errors. In distribution networks, Rogers suggests that the minimum night flow approach was developed for this precise reason.

For municipal systems, the results of such an assessment can be summarised in the form of a water balance. A water balance presents the different components of NRW and provides guidance on how much water is lost through real losses, such as leaks, and how much through apparent losses. It clearly indicates how the water entering the system is allocated. Based on a study of leakage management technologies in the UK, the Environmental Protection Authority (EPA) (2007) suggests that before any pipe testing strategy is developed, the approximate water balance must first be determined with available equipment, such as flow meters.

System Input Volume M^3/year	Authorised Consumption M^3/year	Billed Authorised Consumption M^3/year	Billed Metered Consumption (including water exported)	Revenue Water M^3/year
			Billed Unmetered * Consumption	
		Unbilled Authorised Consumption M^3/year	Unbilled Metered Consumption	Non-Revenue Water** M^3/year
			Unbilled Unmetered Consumption	
	Water Losses M^3/year	Apparent Losses M^3/year	Unauthorised Consumption	
			Metering Inaccuracies	
		Real Losses M^3/year	Leakage on Transmission and/or Distribution Mains	
			Leakage and Overflows at Utility's Storage Tanks	
			Leakage on Service Connections up to point of Customer metering	

Figure 2.1: The International Water Association's water balance (Lambert and Hirner, 2000)

For the water management strategy to be most effective, it is important that the most critical pipelines, which leak the most, are identified and rehabilitated in priority sequence (Bennis et al., 2011). It therefore follows that, with the state of the leakage of all the pipe systems known, an engineering evaluation must be conducted to identify and prioritise pipes and pipe sections in need of repair or replacement (Prinsloo et al., 2011).

For such an evaluation, not only the amount of leakage, but a proper understanding of the physical condition of the pipe asset must exist. The type of deterioration mechanisms present, the existing and potential failure modes, as well as the expected frequencies of the failures are valuable data on which the risk of the asset can be determined (Liu et al., 2012).

Decisions, such as whether to undertake leakage reduction work and up to what level of leakage is acceptable, are ultimately economically motivated. The cost of treating and pumping water that never reaches the customer is an economic loss. An economic investment that increases exponentially as the allowable leakage is lowered is needed to recover it. An optimum balance therefore exists between savings and investment, which is specific to each network (Rogers, 2014).

It is therefore advisable that the economic level of leakage for every pipe system is known before a decision is made on the leakage strategy for that pipe system (Farley, 2003; EPA, 2007). The economic level of leakage is the level of leakage below which the cost of identifying and repairing the leaks will be higher than the value of the water lost. The total elimination of all leaks will never be economically or physically feasible, and thus the economic level of leakage can be used as a guideline to determine whether a leakage reduction strategy is justifiable (Fantozzi and Lambert, cited in Bennis et al., 2011).

Once the water leakage strategies for reducing pipeline losses have been implemented successfully, the last question from Farley (2003) still remains: How can the strategy be maintained?

One way of maintaining a functioning system is by implementing monitoring programmes that track the deterioration of the system (Prinsloo et al., 2011). With such a strategy, continuous monitoring or regular testing of the infrastructure must be carried out. The advantage of this strategy is that intervention is only carried out on pipe systems that are in need of attention, while the disadvantage is the cost of continuous condition monitoring.

Another method calls for planned intervention at suitable intervals. The economic intervention frequency (EIF) (Lambert and Lalonde, 2005, cited in Laven and Lambert, 2012]) is the frequency at which the cost of intervention equals the value of the water lost through leaks since the previous intervention. Determining the EIF for all pipe systems would be the ideal first step in determining the ideal intervals between interventions. A suitable frequency can also be determined by statistically modelling historic failure rates or by modelling and forecasting deterioration based on measured deterioration (Liu et al., 2012). For both these methods, however, accurate and detailed historic data obtained from pipe inspections is required.

With water leakage strategies in place for the pipe systems, funds, tools and available technologies can be proactively allocated to where they are most needed (Prinsloo et al., 2011).

It should be clear that all the above steps to developing and implementing a sound water strategy strongly depend on information available on the condition of the pipe system. This information should form the basis of such a strategy (Prinsloo et al., 2011). Therefore, in cases where the condition of the pipe infrastructure is not known, an effective water management strategy depends on an efficient, and preferably low-cost, pipe condition monitoring technique.

2.2.2 Municipal water losses in South Africa

South Africa is a water-scarce country, with its current water supply already stretched to its limits in order to meet the growing demand. It is therefore of great importance that the water of this country is managed efficiently and that water losses are kept to a minimum.

In South Africa, the focus in the recent past was mainly on developing new water infrastructure to satisfy the growing demand. Little attention was given to the existing water infrastructure, which is now rapidly ageing past its original design life. In 2011, the weighted average age of South Africa's water infrastructure was approximated to be 39 years (Prinsloo et al., 2011) – a concerning fact, considering that the design life of water infrastructure is generally 40 years. Reliability, as well as water leakage, is therefore not expected to improve without serious intervention. Van Vuuren (2014) quotes Muller stating that 30% of the bulk water supply systems monitored by South Africa's Department of Water and Sanitation (DWS) already require water resource security interventions.

In a study by McKenzie and co-workers (McKenzie et al., 2012), data of the municipal water supply of 132 of the possible 237 municipalities throughout South Africa was gathered through surveys and analysed.

The NRW was estimated to be 36.8%, of which 25.4% constitutes losses through physical leakage. The apparent losses, however, vary considerably between the municipalities, with losses estimated at 80% in some municipalities and only 5% in others.

The NRW of 36.8% is similar to the world average of 36.6%, which is high compared to developed countries, but low compared to developing countries. Similarly, the average Infrastructure Leakage Index (ILI) value is estimated at 6.8%, which is on par with the world average. McKenzie et al. (2012) state that even though South Africa's water losses are on par with world norms, considering that this is a water-scarce country, South Africa has a significant scope for savings through reducing water losses.

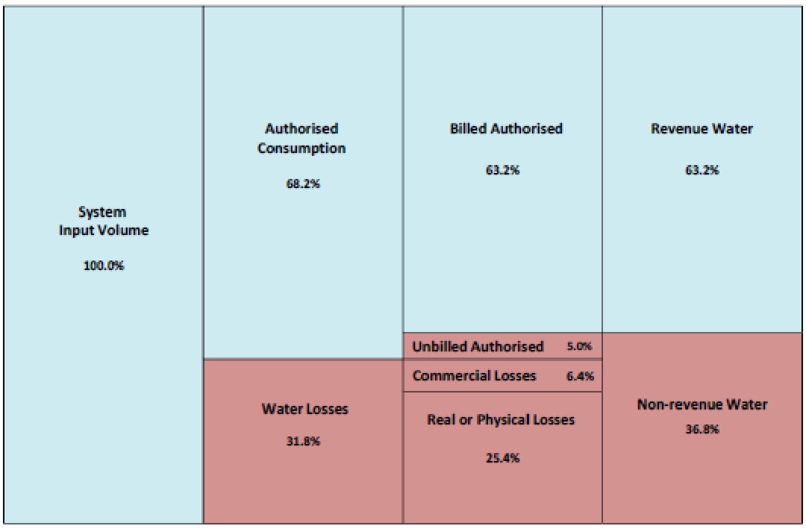

Figure 2.2: South Africa's national water balance in 2009/10 (McKenzie et al., 2012)

Another concern highlighted by McKenzie et al. (2012) is that a significant number of municipalities (45%) could not report on the volumes entering and leaving their networks, indicating that no water demand management was taking place at these municipalities. Reasons were found to be, among others, a lack of resources and metering, ignorance and apathy. Appropriate planning is therefore impossible. More recently, figures from DWS (Van Vuuren, 2014) reveal that only 52% of municipalities participated in a later study, indicating a further drop in participation.

A recent development, "No Drop" certification, was designed to combat the problem of poorly managed municipalities. This certification programme will be implemented to assess, verify and validate the efficiencies of municipalities (Herbst and Raletjena, 2015). An assessment of every water supply system will be made on a yearly basis and a score will be given to each municipality. This programme aims to acknowledge good practice, but also to direct necessary regulatory and support interventions to remedy non-compliance. The underlying aim is to encourage continuous improvement in water-use efficiency and water management. Therefore, one of the key objectives of this programme is to encourage condition monitoring and to identify water losses.

From the above, it should be clear that South Africa has the potential to drastically improve its water efficiency through improved water management and increased investment in water infrastructure. According to DWS studies (McKenzie et al., 2012), a realistic target of 25% NRW is achievable over a period of 10 years (starting from 2012) if approximately R2 billion is invested annually. Another source puts the required investment at 2% of the value of South Africa's current water infrastructure (Van Vuuren, 2014). With water becoming increasingly scarce and valuable, this seems to be a justifiable expense.

2.2.3 Leakage in bulk pipelines

Bulk pipelines have long been challenging components to be effectively addressed in water network audits and the modelling of real losses. This is due to the lack of reliable methods for assessing this component of real water loss (Laven and Lambert, 2012).

Leak detection has historically relied on acoustic methods that send signals of the sound emitted by the water escaping from the pipeline. These acoustic methods have been used to detect and locate leaks. They rely on the sound travelling through the ground to the surface directly above the leak, or travelling along the pipeline to appurtenances to which sensors can be attached.

Bulk pipelines, however, present challenges to both these two approaches. They tend to be buried deeper, and in less accessible locations when compared to distribution lines, often making it impractical to detect the sound rising to the surface.

They also tend to have few appurtenances, and generally do not transmit broad bands of sound for long distances as many distribution pipes do. This renders conventional historic approaches to leak detection on bulk pipelines ineffective.

In order for acoustic leak detection methods to work in transmission mains, Laven and Lambert (2012) suggest that two fundamental approaches are taken into account: detecting the sound of leaks at greater distances in pipelines (transmission main correlators) or finding a way to bring the acoustic sensor to the sound (inline methods).

2.2.4 Factors affecting pipe leaks

Through an acoustic analysis of over 3 000 km of international transmission lines from 25 countries (Laven, 2012; Laven and Lambert, 2012), it was revealed that between 22 and 166 unreported bursts per 100 km exist, with an average of 92 per 100 km.

The effect of the pipe material, geographic location, diameter and age was investigated, with age showing the strongest and most consistent correlation to the unreported burst rate, in the form of a linear relationship. This strong correlation hints to the possibility that leaks are forming and accumulating continuously at approximately 1.6 bursts per 100 km per year.

By adapting the available international data on unreported leaks in distribution mains in accordance to the equation for unavoidable annual real losses and the bursts and background estimate methodology, it was shown that, at realistic pressure heads, burst frequencies on well-maintained transmission lines can be expected at one burst per 100 km per year, confirming the rate obtained from data analysis. This leads to Laven (2012) concluding that the majority of transmission line bursts, if not reported immediately, will never be reported and will continue to exist throughout the lifetime of the pipe. This finding again highlights the importance of an active leakage control strategy.

The following tables, adapted from Laven and Lambert (2012), provide an interesting perspective on how the number of unreported bursts vary by region, by pipe material and by pipe diameter.

Table 2.1: Burst frequency for different geographic regions (Laven and Lambert, 2012)

Region	Distance (km)	Leaks	Leaks per 100 km
Worldwide	3 221	2 966	92
North America	711	496	70
Latin America	186	40	22
Europe	1 583	2 023	128
Africa	383	244	64
Asia and South Pacific	298	150	50
Middle East	60	13	22

It is clear from the table above that Europe has the highest leak concentration. This is partially due to the age of the pipes and partially due to the old pipes in Europe that consist largely of cast iron. This is seen in Table 2.2 to be a significant contributor to burst frequency.

Table 2.2: Burst frequency for different pipe materials (Laven and Lambert, 2012)

Material	Distance (km)	Leaks	Leaks per 100 km
Cast iron	1 127	1 871	166
Ductile iron	199	142	71
Steel	296	87	29
Concrete	961	417	43

Welded steel pipes are seen in Table 2.2 to contribute the least to burst frequency.

The pipe diameter had an interesting effect, with burst frequency increasing with decreasing pipe diameter, except for pipes below 600 mm, for which the burst frequency was observed to be lower. The small sample size of pipes with pipe diameters smaller than 600 mm may, however, have contributed to this observation.

Table 2.3: Burst frequency for different pipe diameters (Laven and Lambert, 2012)

Diameter (mm)	Distance (km)	Leaks	Leaks per 100 km
<600	47	31	66
600-900	302	267	88
1 050-1 500	399	141	35
>1 500	368	52	14

In a study of water distribution networks in England, Skipworth et al. (1999) (cited in Van den Berg, 2015) show that other technical and environmental factors, not mentioned above, can also influence pipe leakage. These conditions include climate, soil conditions, traffic loading and the density of the connections.

Whereas the above factors are based on the number of observed leaks, the main factor affecting the leakage rate through these leaks is pressure. There is a clear relation between leakage and pressure, which many utilities ignore.

Lambert (2000) and Thornton and Lambert (2005) highlight the importance of pressure management when developing an effective leakage strategy to reduce leakage rate and the rate of occurrence of new leaks. This importance is validated in a case study by Charalambous (2005) on 15 district metering areas (DMAs), in which he observed a reduction of approximately 38% in background and locatable losses, as well as a reduction of 40% to 45% in reported leaks due to a pressure reduction of 32%. Pressure management therefore plays a major role in leakage reduction.

2.3 LEAKAGE AND WATER LOSS ON PIPELINES

2.3.1 Leak hydraulics

The bulk pipeline condition assessment tool will make use of fundamental scientific principles to characterise water losses in bulk pipeline systems. The hydraulics of orifices is well understood and a great deal of research has been conducted on different orifices. A leak in a pipe can be considered as an orifice, for which the leakage flow rate (Q) can be described as a function of the orifice area (A) and pressure head (h) by the orifice equation given as:

$$\mathrm{Q} = \mathrm{C_d A}\sqrt{2\mathrm{gh}} \qquad \textit{Equation 2.1}$$

where C_d is the discharge coefficient that accounts for the energy losses and jet contraction; and g is the gravitational acceleration (Cassa and Van Zyl, 2014).

While the orifice flow equation predicts leakage to be proportional to the square root of pressure, field tests have shown that this equation does not provide a satisfactory model for the behaviour of system leakage with pressure. Practitioners have since adopted a more general equation in the form:

$$\mathrm{Q} = \mathrm{Ch}^{\mathrm{N1}} \qquad \textit{Equation 2.2}$$

where C is the leakage coefficient; h is the pressure head and N1 is the leakage exponent.

Field tests have found a large range of the reported leakage exponent (Wu, 2011), varying from 0.36 to 2.95, the vast majority of leakage exponents being between 0.5 and 1.5.

May (1994) then introduced the fixed and variable area discharge (FAVAD) concept that assumes that some leaks are rigid, while others expand with increasing pressure. May (1994) suggested that leaks in flexible materials have leakage exponents of 1.5. Combining this with the orifice equation (shown as Equation 2.1), he proposed a new leakage equation in the form:

$$\mathrm{Q} = \mathrm{k_1 h^{0.5}} + \mathrm{k_2 h^{1.5}} \qquad \textit{Equation 2.3}$$

The FAVAD concept introduced by May (1994) was later confirmed by Cassa et al. (2010) using finite element analysis. The study concluded that the leak area (whether circular, a longitudinal crack or a circumferential crack) is a linear function of pressure, regardless of the pipe material, as long as the pipe material behaves elastically. Therefore, all leak areas vary linearly with pressure. The pressure response of a leak can be characterised by an initial area (under zero pressure conditions), A_0, and the head-area slope (gradient of the linear line), *m*. The expression for the leak area as a function of the pressure head is given by:

$$\mathrm{A} = \mathrm{A_0} + \mathrm{mh} \qquad \textit{Equation 2.4}$$

Substituting Equation 2.4 into Equation 2.1 results in the modified orifice equation (MOE) in the form:

$$Q = C_d\sqrt{2g}(A_0h^{0.5} + mh^{1.5}) \qquad \textit{Equation 2.5}$$

While this modified FAVAD equation is similar to Equation 2.3 proposed by May (1994), it is interpreted differently: instead of interpreting leaks as either fixed or variable, all leaks in a system can be considered to have variable areas. In other words, all leaks will increase in area when the pressure is increased. The terms “modified orifice” and “FAVAD” are used interchangeably in this report.

For leaks with small head-area slopes, the first term of Equation 2.5 is likely to be dominant, resulting in an effective leakage exponent of 0.5. Conversely, for flexible leaks with high head-area slopes, the second term of the equation will be dominant, resulting in a leakage exponent of 1.5.

The modified FAVAD equation presents the theory on which the bulk pipeline condition assessment equipment is based. The pressure response of the leak is estimated at different pressures. The leakage area can then be plotted against the pressure and a linear function can be fitted to the data points. The intercept of this line with the area axis gives the initial leak area, and its slope lines the head-area slope.

Cassa et al. (2010) tested three leaks 60 mm long in a 110 mm Class 6 uPVC pipe. The cracks were oriented in the longitudinal, circumferential and spiral directions, and were analysed using finite element modelling. The leak areas were determined at different pressures and plotted against the pressure head as shown in Figure 2.3.

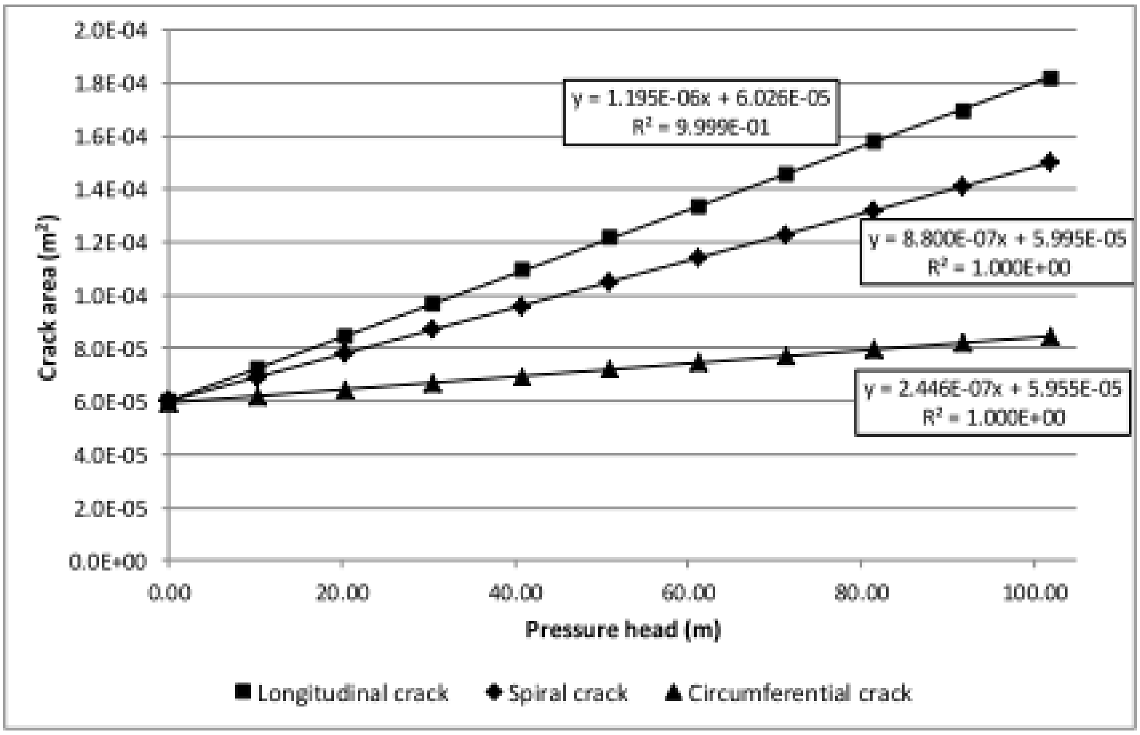

Figure 2.3: The areas of cracks 60 mm long in a Class 6 uPVC pipe as a function

As indicated by Figure 2.3, the intercept of the line with the area axis shows the initial area, A_0, and the slope of the line gives the head-area slope. Longitudinal cracks have the highest head-area slopes, followed by the spiral crack and then the circumferential cracks.

2.3.2 The FAVAD equation

The FAVAD equation defines the leakage through the initial area plus the leakage through the additional area created by the expansion of the leak area under pressure. These two components are clearly represented in the FAVAD equation, with the first term being identical to the orifice equation, and the second term accounting for the variation in flow under pressure according to the head-area slope.

2.3.2.1 FAVAD equation for individual leaks

The factors that influence the variables of the FAVAD equation are similar to those for the N1 exponents. The influences of some of these factors are, however, more accurately modelled with the FAVAD equation. In this paragraph, the results of a number of studies that have been conducted to characterise the relationship between leakage area and pressure with the FAVAD equation are discussed, with a focus on the factors that can be modelled more accurately with the FAVAD equation.

For pipe materials with linear-elastic properties, Cassa and Van Zyl (2010), Cassa and Van Zyl (2011) and Ssozi et al. (2015) make use of finite element modelling to show that the areas of all types of leak openings increase linearly with pressure. Under elastic conditions, therefore, the pressure response of any leak can be fully characterised by the initial area and the head-area slope. This finding is supported in experimental studies conducted by Malde (2015).

De Miranda et al. (2014) derived a physically based analytical formula to accurately predict leakage in linear-elastic pipes with longitudinal cracks. This formula takes pipe material and pipe geometry properties into account. The author considers the longitudinal strip in the cracked pipe as a classical beam with elastic restraints and derives the following formula for the head-area slope of the FAVAD equation:

$$m = \frac{12\rho g L R^4 \pi (1-v^2)}{Es^3\left(\left(\frac{s_0}{s}\right)^2 \left(\frac{A_1 L}{R}\right)^{-A_2} + 1\right)}$$

The above equation was validated by De Miranda et al. (2014) through comparison with published experimental results of leakage exponents for various materials. Good correlations with the predictions of Cassa and Van Zyl (2013) (cited in De Miranda et al., 2014), as well as various experimental results, were achieved for polyvinyl chloride (PVC), steel and cast iron pipes.

In an investigation by Cassa and Van Zyl (2014), an equation for the head-area slopes of a longitudinal crack is proposed:

$$m_{long} = \frac{2.93157 \cdot d^{0.3379} \cdot L_c^{4.80} \cdot 10^{0.5997(\log L_c)^2} \cdot \rho \cdot g}{E \cdot t^{1.746}}$$

The crack width was observed to have a negligible effect on the head-area slope, while its effect on the initial leak area was major. Cassa and Van Zyl (2014) provided ranges of possible head-area slopes for PVC, asbestos cement and cast iron pipes.

2.3.2.2 FAVAD equation for pipe systems

In a study on the feasibility of the FAVAD equation for pipe systems, Schwaller et al. (2015) found that the initial leakage area and head-area slope of a system with many leaks can be estimated using the FAVAD equation with the leakage rate and average zone pressure-head before and after pressure reduction.

These initial leakage areas, as well as the head-area slopes, were found to provide good estimates of the sums of the individual leakage areas and head-area slopes of all the leaks in the system.

Schwaller and Van Zyl (2014) also investigated the application of the FAVAD equation for characterising pressure management areas through a statistical approach. A spreadsheet model was developed with a number of random distributions of leak quantities, areas, discharge coefficients and head-area slopes typically found in real distribution systems. Simulations were then carried out with this data to reproduce conditions of typical distribution systems with two pressures, as experienced during night tests performed in practice. Leakage exponents were then determined using these random scenarios. Repeatability analysis was applied to this data for distributions with 100, 1 000 and 10 000 leaks.

In order to perform realistic statistical analyses, Schwaller and Van Zyl (2014) estimated fitting distributions and ranges for the various leak parameters. The discharge coefficient, C_d, and the initial leak area, A_0, were modelled using normal distributions. The head-area slope, m, was modelled as a power function of the leak area as proposed by Cassa and Van Zyl (2011) (cited in Schwaller and Van Zyl, 2014) and the pressure head, h, was modelled with a uniform distribution. The distribution system was assumed to exist on a constant elevation.

The resulting N1 leakage exponents were then estimated, as displayed in Table 2.4:

Table 2.4: Leakage exponents for 100 random networks with 100, 1 000 and 10 000 leaks respectively (Schwaller and Van Zyl, 2014)

Number of system leaks	Mean N1	Range of N1
100 leaks	0,66	0,46 to 1,67
1000 leaks	0,92	0,46 to 1,59
10 000 leaks	1,08	0,81 to 1,26

As seen above, the N1 values largely ranged between 0.5 and 1.5, as expected from field studies. This investigation, therefore, shows that the combined effect of individual elastically deforming leaks, characterised by the FAVAD equation, can produce a range of leakage exponents that is typical to the range observed in field studies.

In another study, Schwaller et al. (2015) conducted a sensitivity analysis on 300 artificial network models with randomly distributed leaks. The following graphs resulted and indicate that the initial leakage area, A_0, is approximately equal to the sum of all the individual initial leakage areas, and that the head-area slope. m, is approximately equal to the sum of all the individual head-area slopes.

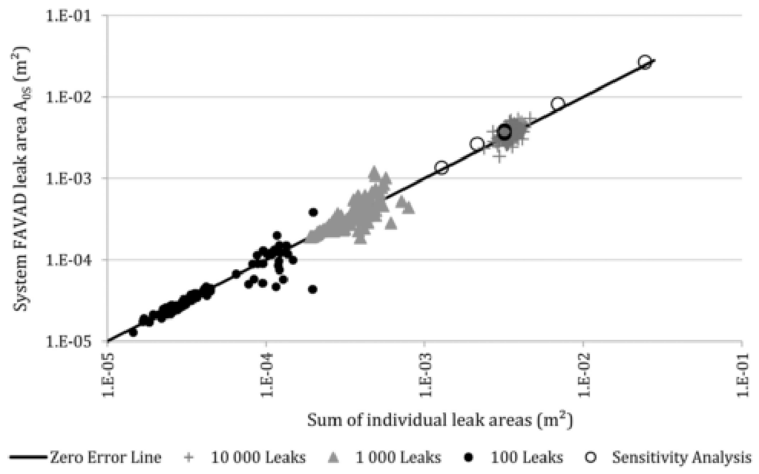

Figure 2.4: Initial leakage area of the system in comparison to the sum of individual leakage areas (Schwaller et al., 2015)

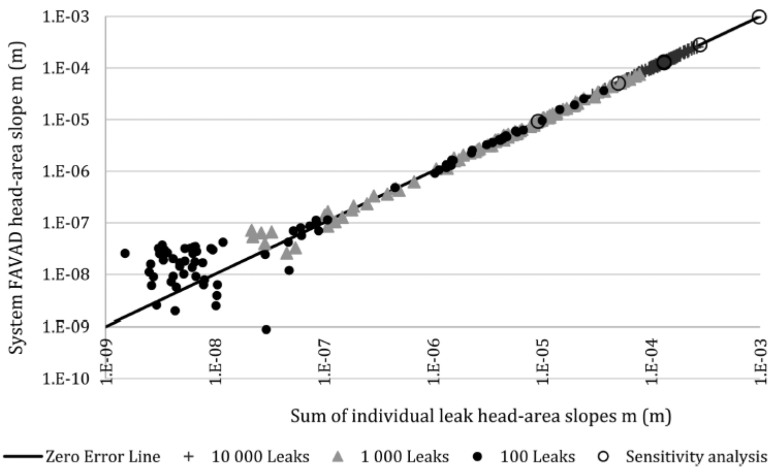

Figure 2.5: System head-area slope in comparison to the sum of the individual head-area slopes (Schwaller et al., 2015)

Schwaller et al. (2015), therefore, showed that the FAVAD equation can be used to characterise the leakage of a system, and that the system head-area slope can provide insights on the type of leaks in the system. Errors were observed, but they remained small in comparison to the range that the parameters can adopt.

Schwaller et al. (2015) concluded that the application of the FAVAD equation to systems is feasible, because leak areas change linearly with pressure. The initial area of the system and the system's head-area slope are meaningful properties, independent of pressure, characterising the state of the system. Estimates of the total initial leakage area, as well as the sum of all head-area slopes, can therefore be obtained by applying the FAVAD equation together with pressure reduction.

One concern was observed, namely the high errors that result when varying elevations are taken into consideration. By performing a sensitivity analysis, Schwaller et al. (2015) showed that the FAVAD parameters are sensitive to the slope of the system and that the equation works most accurately on horizontal systems. The errors, however, remain small, even on significant slopes, and the relation still provides a good estimate of the state of the system.

Deyi et al. (2014) also performed field studies on pressure management zones and attempted to characterise the leakage with the FAVAD and N1 equation. An unrealistically large range of N1 values between 0.18 and 3.33 was obtained. They concluded that all N1 values higher than 1.5 signified a system leakage area smaller than zero, which is not physically possible. Reasons for this anomaly are suggested to be measurement errors, an underestimated role played by plastic deformation, or the leaking of valves on the system boundary. This study therefore highlights the complexity and high error potential of implementing this method to large pressure management zones.

It can be concluded that the FAVAD equation is good for characterising individual elastically deforming leaks, but it is also suited for investigating systems with multiple leaks. For systems with multiple leaks, however, the applicability of the FAVAD equation to accurately characterise these systems must be investigated further.

2.3.3 The N1 equation

2.3.3.1 Equation description

The N1 power equation has the form:

$$Q = Ch_{AZP}^{N1} \qquad \textit{Equation 2.6}$$

By measuring the average pressure zone head and by estimating the leakage of a system before and after pressure management, the leakage coefficient and the N1 leakage exponent can be estimated (Schwaller et al., 2015).

The N1 exponent can be calculated by dividing the N1 equation before pressure management by the N1 equation after pressure management, resulting in the elimination of the unknown leakage coefficient, C.

$$\frac{Q_1}{Q_2} = \left(\frac{h_{AZP1}}{h_{AZP2}}\right)^{N1} \qquad \textit{Equation 2.7}$$

With the N1 exponent known, the discharge coefficient, C, can easily be calculated.

2.3.3.2 Factors affecting the N1 exponent

From a fluid mechanics point of view, and based on the laws of fluid mechanics, the N1 equation cannot be fully defined, unless the leak is a perfect orifice and the exponent remains at 0.5. Through experimental methods and field tests, however, fairly accurate leakage characterisations have been obtained by fitting observed flow-pressure curves with curves obtained from the N1 equation with varying N1 exponent values.

The N1 exponent values are found to vary considerably in practice, with ranges between 0.36 and 2.79 obtained in field studies on leaks of water distribution systems in various countries. The variations in these N1 values affect the leakage considerably. As discussed by Walski et al. (2009), by halving the pressure, the leakage is reduced by 29% for an exponent value of 0.5; 65% for an exponent value of 1.5; and 82% for an exponent value of 2.5, proving the high dependence of leakage on pressure.

In an experimental investigation by Greyvenstein and Van Zyl (2007), for instance, N1 values of between 0.4 and 2.3 were observed for individual leaks. In most studies, however, the vast majority of N1 values fall between 0.5 and 1.5 (Ogura, 1979; Farley and Throw, 2003, cited in Greyvenstein and Van Zyl, 2007). The most common leakage exponent can be assumed to be 1 (Lambert, 2000; Ogura, 1979).

Various investigations have been conducted to explain this phenomenon (Clayton and Van Zyl, 2007; May, 1994; Schwaller and Van Zyl 2014, cited in Schwaller et al. (2015), and the following conclusion was made: An N1 equation, with an N1 value of 0.5, is based on fluid mechanics principles that assume the following:

- The leakage area stays constant at all pressures.
- The flow is fully turbulent (Van Zyl, 2014).
- The surrounding soil has no effect.

These conditions are not encountered in real leaks, and therefore the assumptions are not valid for these conditions. By adjusting the N1 exponent value, however, the equation can be adjusted to fit the behaviour of real leaks, resulting in a range of N1 exponent values.

Walski et al. (2009) summarised the N1 values obtained from various field and experimental studies. The following table originates from the study of Walski et al. (2009), but has been extended considerably to include the results of even more studies:

Table 2.5: Summary of N1 values reported in literature (adapted from Walski et al., 2009)

Author	N1 values	Conditions
Ogura (1979)(in Schwaller and Van Zyl, 2014)*	1.39-1.72	Slits
Hiki (1981)	0.5	Drilled holes
May (1994) (in Walski et al., 2009)*	0.5 1.5 2.5	Fixed area Size = f (pressure) Longitudinal
Lambert (2001) Lambert (1997) (in Schwaller et al., 2015)*	0.52-2.79 0.5 1.5 0.36-2.79	Literature UK metal pipes UK plastic pipes Literature
Farley and Throw (2003)(in Cassa and Van Zyl, 2014)*	0.70-1.68 0.63-2.12 0.52-2.79	UK (1977) Japan (1979) Brazil (1999)
Thornton and Lambert (2005)	0.5-1.6 0.5 0.5-1.0 >1.0 0.5- 2.0 0.8-1.0	Function of ILI, based on literature Circular holes, Re >4 000 Small circular leaks in general Corrosion clusters Longitudinal cracks: Length to width ratio = low Length to width ratio = high (for PVC pipes) Asbestos cement pipes
Walski et al. (2006)	0.66-0.76	Drilled holes
Walski et al. (2009)	0.47-0.74** Mean = 0.58 Median = 0.54	Slits and holes of various lengths and sizes for a number of pipe diameters in the PVC pipe
Greyvenstein and Van Zyl (2007)	0.52 1.38-1.85 0.79-1.04 0.41-0.53 0.67-2.3	Round hole Longitudinal PVC pipe Longitudinal asbestos cement pipe Circumferential Corrosion steel
Noack and Ullanicki (2007) in (Walski et al., 2009)*	0.5-1.2	f (soil permeability)

Author	N1 values	Conditions
Ashcroft and Taylor (in [56])*	1.39-1.72 1.23-1.97 1.52	10 mm slit in plastic pipe 20 mm slit in plastic pipe Average under varying pressure
Deyi et al. (2014) in (Lambert, 2000)	0.18-3.33	Mainly plastic distribution systems in South Africa.
Charalambous (2005)	0.64-2.83 Average = 1.47	Field study on 15 DMAs in Cyprus for mixed asbestos cement, PVC and medium-density polyethylene (MDPE) pipes
*These works are not referenced in this study, and can be found in the references indicated. **These are exponent values resulting from a slightly adapted N1 equation that eliminates the effect of system demand changes.*		

A number of factors were found to significantly affect leakage rate and the N1 exponent, as seen in Table 2.5. Four factors, as suggested by Clayton and Van Zyl (2007), and a fifth factor later added by Schwaller and Van Zyl (2014), are discussed in more detail below:

2.3.3.3 Soil hydraulics

The nature and size of the orifice was found through numerous studies to have a much greater effect on the leakage rate, compared to the effect of the porous media flow through the soil (Walski et al., 2009; Walski et al., 2006). It is therefore often deemed unlikely that soil plays a significant role in variation in leakage exponents (Van Zyl, 2014). This is mainly due to the soil being able to drain more water than exits the pipe through the leak.

As early as in 1981, however, Hiki (1981) investigated the influence of the medium surrounding the leak on the leakage exponent. Exponents were measured for leaks discharging into air, water and sand, but no direct influence could be detected.

Soil, however, plays a role in controlling the leak in cases where the orifice is large and the soil permeability low. For large leaks in certain soil conditions, the water will create its own path upwards to the surface, essentially creating a water column that creates a static head immediately outside the leak. When permeability is low, even small leaks can build such an additional friction head outside the leak, resulting in situations where the soil head loss can exceed the orifice head loss (Walski et al., 2006).

Walski et al. (2006) describe an orifice or soil number that indicates whether the leak is more soil dependant or more orifice dependant. Through a number of field tests, they also found that, for most real-world situations, leaks are dominated by orifice dependence, rather than by soil dependence.

Clayton and Van Zyl (2007) discuss a number of factors that highlight the complexity of the role played by the soil surrounding a leak, with its effect depending on the leak size and soil type. They conclude that flow rates in the soil-leak interface will unlikely be a linear function of the pressure.

2.3.3.4 Pipe material behaviour

The pipe material behaviour is considered to contribute significantly to the variation. By comparing PVC pipes to steel pipes, Bennis et al. (2011) found that the leakage was greatest in flexible pipes under high pressure. Cassa et al. (2010) support this phenomenon and further show, through a finite element analysis (FEA), that the effect of the crack type and crack size on the N1 value also varies, depending on the material type.

Thornton and Lambert (2005) proposed the following N1 values in relation to the ILI for various pipe material flexibilities. The upper curve displays this relationship for fully flexible pipes, while the lowest curve represents fully rigid pipes.

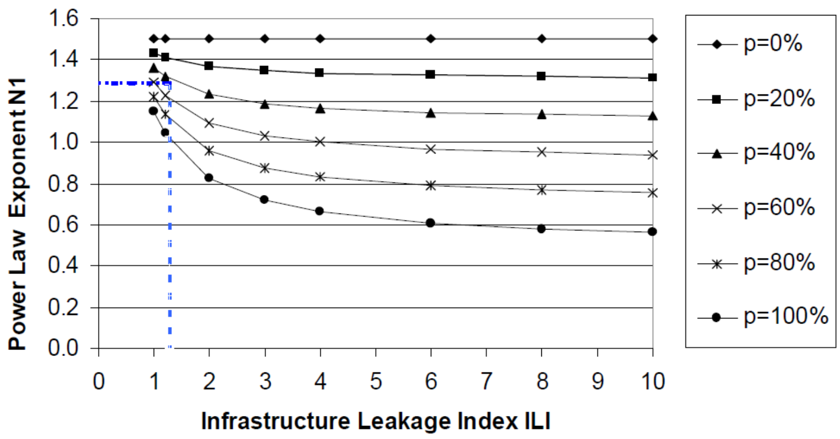

Figure 2.6: The N1 exponent relation to the ILI number for various pipe materials with varying rigidity (Thornton and Lambert, 2005)

These relations were used to predict a number of exponents obtained from test data and proved to be quite accurate.

In another FEA study by Ssozi et al. (2015), the visco-elastic behaviour of pipe materials is investigated. The study found that visco-elastic behaviour, which strongly depends on material type, will lead to higher N1 exponent values if it occurs.

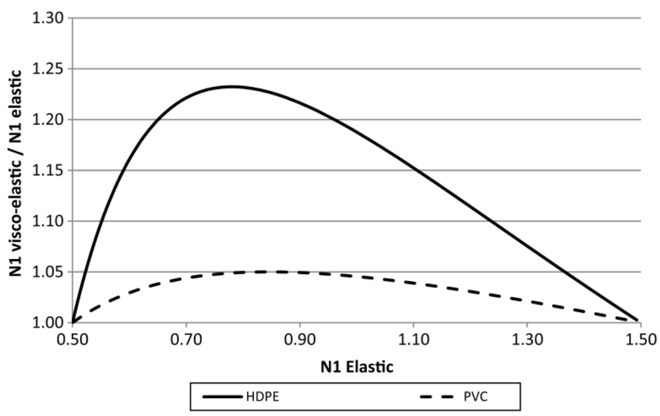

Figure 2.7: The effect of visco-elastic behaviour on the N1 exponent (Ssozi et al., 2015)

Clayton and Van Zyl (2007) also discuss the fact that pipes of different materials fail in certain characteristic ways. Asbestos cement pipes commonly fail through having longitudinal cracks, while leaks in steel and cast-iron pipes commonly result from corrosion holes. Circumferential cracks are also more common in cast iron pipes with a small diameter due to bending. Knowledge of the most common leak types depending on the pipe material can be valuable to predict and model the pressure response of pipe systems.

2.3.3.5 Leak hydraulics

According to Hiki (1981), leakage through round holes can be characterised by a leakage exponent of 0.5. This finding is supported by Greyvenstein and Van Zyl (2007), who, through laboratory tests, showed that the leakage exponent for round holes remains close to 0.5, irrespective of the hole diameter or pipe material. Bennis et al. (2011), however, showed that, for steel and PVC pipes, the exponent N1 decreases slightly as the hole diameter increases.

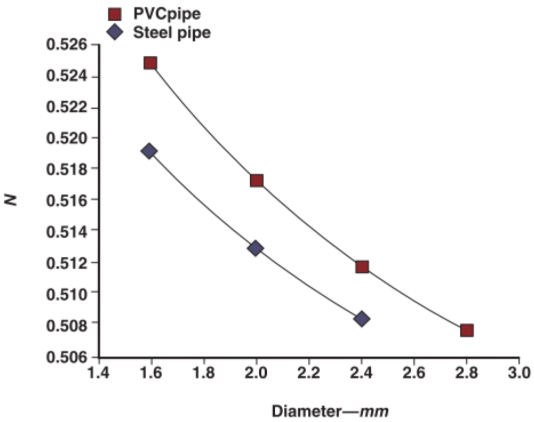

Figure 2.8: Variation of the N1 exponent with a leak diameter for round leaks (Bennis et al., 2011)

Cassa et al. (2010), however, show, through an FEA study, that an increase in the hole diameter causes an increase in the N1 exponent, with this effect emphasised as the elasticity of the material increases. This strengthens results obtained by Hiki (1981), who also observed a slight increase in leakage exponent values with increasing hole diameter.

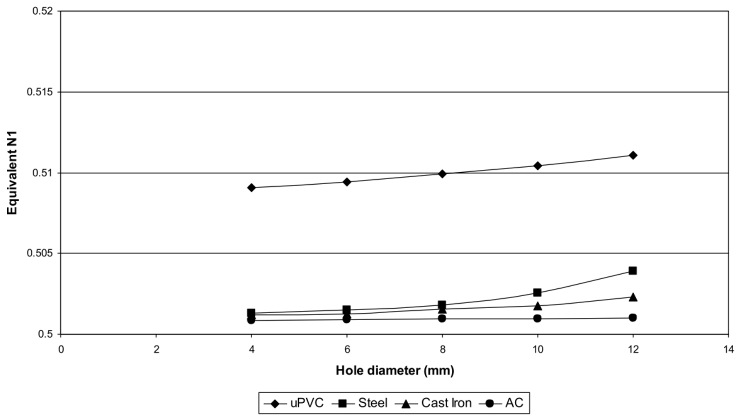

Figure 2.9: Variation of N1 with increasing hole diameter for various pipe materials (Cassa et al., 2010)

Corrosion holes in steel pipes, in contrast, were found to exhibit considerably higher exponent values of between 0.67 and 2.3 (Greyvenstein and Van Zyl, 2007). The high exponents were observed in pipes with significant corrosion damage to the pipe wall and surrounding material. It is suggested that the weakened support around the hole contributes to higher stresses and strains around the hole, in turn leading to higher exponent values. This is supported by Cassa et al. (2010), who showed, with an FEA study, that pipe stresses are significantly affected by the leak opening and that the material yield strength is easily exceeded in the vicinity of the opening.

Cassa et al. (2010) also show that an increase in the length of a longitudinal or centrifugal crack has an exponential effect on the N1 value; again, with this effect emphasised by the elasticity of the pipe material.

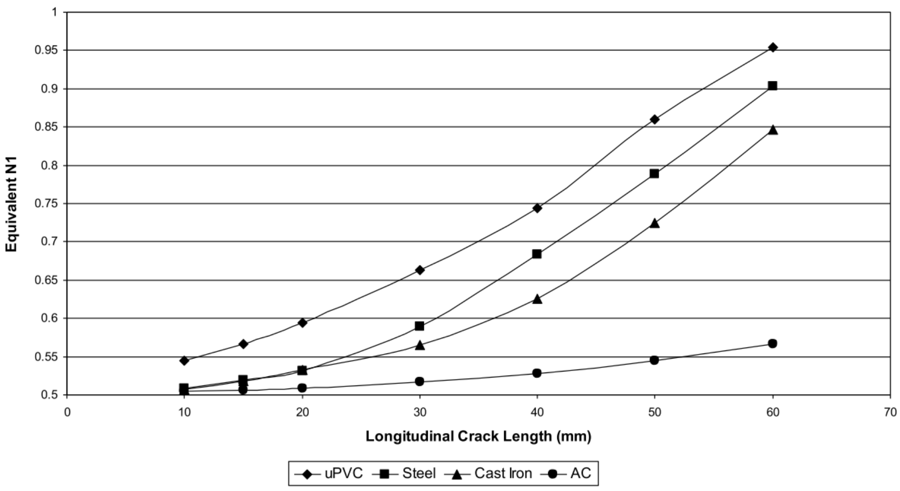

Figure 2.10: Variation of N1 with increasing length of the longitudinal crack for various pipe materials (Cassa et al., 2010)

Longitudinal cracks can show considerably higher exponent values of between 0.79 and 1.85 (Greyvenstein and Van Zyl, 2007; Avila, 2003, cited in Cassa and Van Zyl, 2014), while circumferential cracks exhibit lower values between 0.41 and 0.52. Again, the FEA study of Cassa et al. (2010) supports this phenomenon by predicting that longitudinal cracks will show the most expansion with pressure, followed by circumferential cracks and then round holes.

Narrow cracks also have higher leakage exponents than wider cracks of equal length. The high exponent values in longitudinal cracks are attributed to the fact that circumferential stresses are higher than longitudinal stresses in pipes, resulting in the widening of longitudinal cracks as pressure increases (Greyvenstein and Van Zyl, 2007). Clayton and Van Zyl (2007) also discuss the effect of the larger wetted perimeter of cracks in comparison to round holes, resulting in a higher possibility of laminar or transitional flow rates, which in turn result in higher N1 exponent values. If the crack closes up completely under zero pressure conditions, the leakage exponents will be 1.5 (Cassa and Van Zyl, 2014).

Cassa and Van Zyl (2014) showed that different N1 values can be obtained for the same leak when the pressures are varied. In this study, it is shown that N1 values tend to 0.5 as the system pressure tends to zero, and tends to 1.5 as pressure tends to infinity.

Through experiments on steel and PVC pipes, Bennis et al. (2011) showed that the range over which the pressure is applied also plays a role. A higher initial pressure resulted in a higher value for N1, meaning that, for a given pressure reduction, the reduction of flow rate will be greater for higher initial pressures.

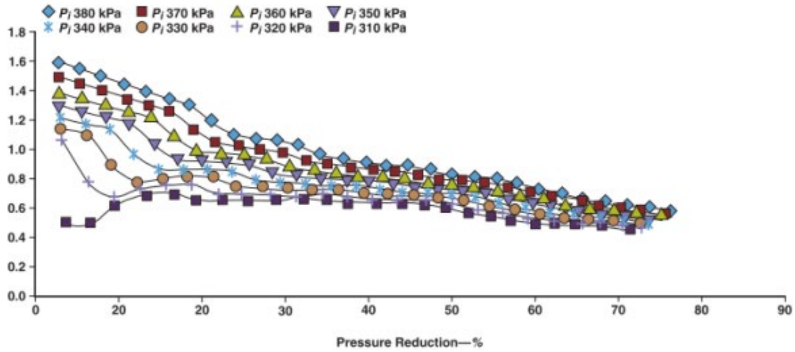

Figure 2.11: Variation of N1 in response to pressure reduction rates for various initial pressures on steel pipes (Bennis et al., 2011)

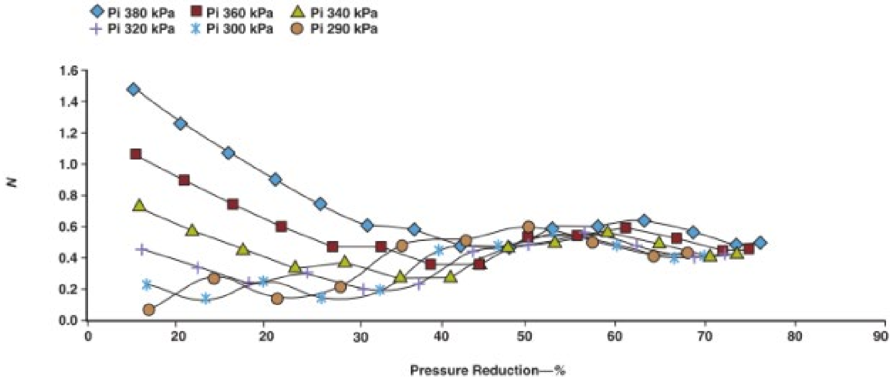

Figure 2.12: Variation of N1 in response to pressure reduction rates for various initial pressures on flexible PVC pipes (Bennis et al., 2011)

Cassa and Van Zyl (2014) also show that the leakage exponent for a given leak is higher at higher pressures. Ultimately, through an FEA study, Cassa et al. (2010) show that the effect of pressure on the leak opening increases exponentially with increasing hole diameter or crack length. The N1 exponents were therefore predicted to increase moderately with increasing hole diameter, and extensively with increasing crack length.

2.3.3.6 Leak flow type

The type of flow depends on a number of the abovementioned factors, and can vary from turbulent flow to laminar flow. Fully turbulent flow is a requirement for the theoretical leakage exponent of 0.5 for an orifice. Laminar flow can explain leakage exponents of 1, as flow rate and pressure become linearly related during laminar flow (Van Zyl, 2014). Thornton and Lambert (2005) quote experimental results from John May that clearly show that N1 values increase to above 0.5 as the Reynolds number is decreased to below 4 000, representing transitional or laminar flow.

Through a simple example, however, Van Zyl (2014) shows that laminar flow will be extremely unlikely. Clayton and Van Zyl (2007) also show that, for flow in leaks to be laminar, the leak must be less than 3 ℓ per day for a leak with an aspect ratio of 10 000. Transitional flow is more likely, but is still unlikely to contribute significantly to a leakage exponent larger than 0.5 (Van Zyl, 2014).

2.3.3.7 Disadvantages of the N1 equation

Schwaller and Van Zyl (2014) referred to a number of disadvantages of the N1 equation:

- The N1 equation is empirical and not founded on fundamental fluid mechanics theory. The overall form of the equation is based on orifice theory, but the constants can only be determined experimentally.
- The values of the constants ($C$and $N1$) are not fixed, but vary with pressure.
- The units of C include the variable N1, which complicates the equation and makes it difficult to interpret and distinguish between the factors affecting the N1 exponent and the constant C.

In addition to the above factors, the C constants and N1 exponents do not provide a lot of information on the characteristics of a leak. Ferrante (2011) and Ferrante et al. (2011) also demonstrated, by experimenting with leaks in thick steel pipes, thin steel pipes and polyethylene (PE) pipes, that leaks cannot be accurately characterised by this equation, as the variation of the leak area with head is not accurately represented. Even though the N1 exponent provides an indication of how sensitive the leak is in respect to pressure variation, it fails to accurately model a direct relationship between pressure and the leakage area.

2.3.4 Relation between FAVAD and the N1 equation: the leakage number

Cassa and Van Zyl (2014) conducted a study to compare the performance of the FAVAD and N1 parameters with each other. A leak 60 mm long in a PVC pipe was tested and the leak area measured at different pressures and compared to finite element results. It was concluded that the N1 exponent does not provide a good characterisation of the leak in comparison to the FAVAD equation. The leakage number was therefore derived and defined by Cassa and Van Zyl (2014) as a more consistent way to characterise pressure leakage response.

The N1 and FAVAD equations were equated, and after manipulation, the following expression was found.

$$N1 = \frac{\ln(N_L+1)-\ln C}{\ln h} + \frac{1}{2}$$ *Equation 2.8*

with the leakage number defined as:

$$L_{NS} = N_L = \frac{mh}{A_0}$$ *Equation 2.9*

with the leakage number defined as the ratio between the flow through the expanded leak and the initial area of the leak.

Thus, with the above relation, the leakage exponent can be easily determined for any leak if the head-area slope and initial area are known.

A plot was generated of the leakage exponent versus the leakage number. This showed that the relationship remains the same, irrespective of the values of A_0, m and h (Cassa and Van Zyl, 2014).

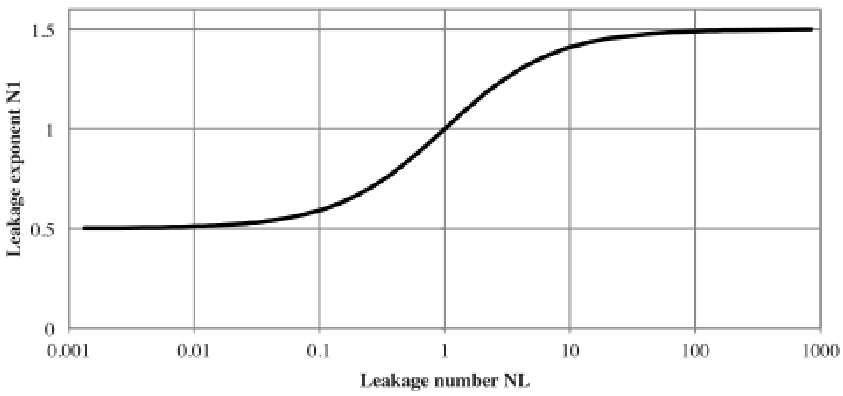

Figure 2.13: Leakage number N_L corresponding to leakage exponent N1 (Cassa and Van Zyl, 2014)

The formula that describes this relationship was manipulated to the following form:

$$N_L = \frac{N1-0.5}{1.5-N1} \;\; or \;\; N1 = \frac{1.5N_L+0.5}{N_L+1} \qquad \textit{Equation 2.10}$$

The leakage number will equal 1 if the leakage amount through the expanded portion of the leak equals the leakage through the initial leakage area. A leakage number smaller than 1 indicates that the leakage through the initial area contributes more than the leakage through the expanded area (Schwaller et al., 2015).

In a field study by Deyi et al. (2014), the N1 exponents, as well as the FAVAD variables, were obtained for existing distribution systems. Even though the resulting N1 values reflected an unrealistic range of between 0.18 and 3.33, an interesting observation was made when plotting the N1 exponents with the leakage number. As can be seen in Figure 2.14, the N1 exponents higher than 1.5 are plotted on a seemingly different line, compared to the N1 values below 1.5, which followed the expected relationship:

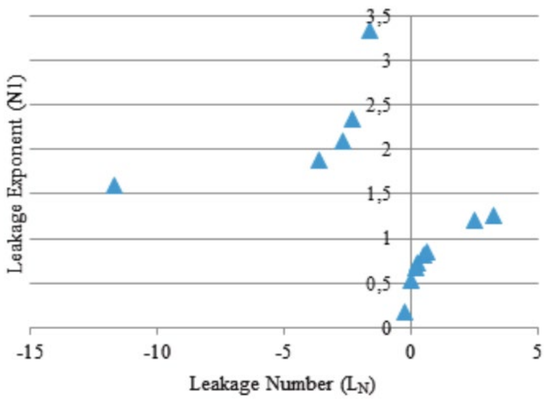

Figure 2.14: Relationship between N1 and the leakage number (Deyi et al., 2014)

Schwaller et al. (2015) also investigated the application of the leakage number to systems, using the system leakage area and the system head-area slope. This study concluded with the recommendation that the leakage number can and should be used for future field applications as errors, which are introduced when assumptions on the leak discharge coefficients are made, are eliminated with this approach.

2.4 BULK PIPE MATERIALS

This section will look at the range of pipe materials that are commercially available and are used on bulk water duties. Liu (2003) rightfully claims that an engineer cannot make a wise selection of the best pipe that is required for a given project without some understanding of the characteristics of the various types of pipes that are available commercially.

Site location is not the only factor considered when selecting a pipeline. According to the Council for Scientific and Industrial Research (CSIR) (2005) the following factors must also be considered when selecting suitable pipe materials for a particular project:

- The life cycle cost (initial capital cost plus maintenance costs)
- The chemical composition of the water to be transmitted
- The corrosive nature of the soil and ground water, and the possible existence of stray electric currents
- The structural strength of the pipes and the components

For the material discussion, two broad classifications of pipeline material will be used; metallic and non-metallic.

2.4.1 Ductile iron

Ductile iron pipes are made of iron containing approximately 3.5% carbon in spheroidal or nodular form and a magnesium alloy (Liu, 2003). It is a material that is ductile and does not rupture easily, and is a natural successor of cast iron material.

According to Rajani and Kleiner (2003), when ductile iron pipes were introduced in North America in the late 1950s, producers and users focused primarily on their mechanical properties, which were superior to those of cast iron. These pipes were initially laid and used with minimal or no corrosion protection. Within a few years, it became apparent that unprotected ductile pipes placed in aggressive soils tend to corrode at a rate slower than that observed in cast iron pipes. However, because the wall thickness of the ductile iron was smaller than that of cast iron pipe, holes such those shown in Figure 2.15 appeared soon after installation.

Figure 2.15*: External corrosion of ductile iron pipes*

Currently, many methods and techniques have been developed or adopted to protect ductile iron pipes from corrosion. These methods typically include PE encasement, stray current control and cathodic protection (Kroon et al., 2011). Rajani and Kleiner (2003) further explain that these protection methods perform well under some circumstances and poorly under others. It is often difficult to tell whether a reported success or failure can be attributed to the quality of implementing a method or whether it is inherent in the method’s ability to perform under a given set of conditions.

Figure 2.16(a) shows an example of how some ductile iron pipes are protected. In Figure 2.16, an internal centrifugal applied cement mortar is lined inside the ductile iron pipe, Outside the pipe is a zinc coating that forms a stable protective layer of insoluble zinc salts. Finally, a second layer of bituminous coating further enhances the corrosion resistance of the pipe. Figure 2.16(b) shows the finished protected ductile iron product.

(a) *(b)*

Figure 2.16: Ductile iron pipes used for drinking water: (a) showing the various components (TPLI Metal Casting Industries, 2010); and (b) showing some commercially available ductile iron pipes (Henan Wein Industry Co. Ltd, 2012)

With regard to ductile iron pipe fittings, there are fittings available to form a complete ductile iron system. However, due to the unique angles of most site bends, prefabricated steel bends (specials) are sometimes used with mechanical couplings. In many instances, it is possible to find a short branch line being 25% steel and 75% ductile iron (Burstall, 1997).

With regard to pipe joints, standard ductile iron pipes are provided with spigot and socket ends. There are also special joint types that provide full axial restraint, thus avoiding the need for anchor blocks on bends, etc. When it comes to rubber ring joints, repairing one that has leaked may involve cutting out a section and splicing in a new section (e.g. steel) with two mechanical joints. This can be a relatively expensive procedure. It is possible to weld it successfully. However, according to Burstall (1997), ductile iron welders are hard to find.

The ductile iron pipe is now used extensively in water supply and waste water systems (Liu, 2003).

2.4.2 Cast iron

Ordinary cast iron pipe is made of iron containing 3% to 4% of carbon in the form of graphite flakes. The pipe is cast either by using a stationary mould (horizontal or vertical) or a centrifugal mould (Liu, 2003). The mould is usually either a metal mould cooled by water, or a sand-lined mould. The centrifugal mould often produces better results when compared to the stationary mould.

Cast iron pipes generally exhibit good corrosion resistance and a long life. Rust tubercles, shown in Figure 2.17, form on the inside. This requires periodic scraping to be done to remove them.

Figure 2.17: Cast iron rust tubercles (http://dofbill.com/category/lead-poisoning/)

An economic solution to extend the asset life of a cast iron pipe is to deploy *in-situ* cement mortar lining or other methods of lining. These lining solutions improve the flow and water quality for approximately a third to a quarter of the cost of a new main. The chemical cleaning of unlined pipes is an alternative to relining (Burstall, 1997).

Knowing the extent of the internal and external corrosion of the pipe is important before any relining is undertaken. This is because a "good" wall thickness must be determined to know if the metal left is sufficient for relining. If the good metal left is found to be insufficient, sections of the pipeline will have to be replaced. A stress analysis is usually conducted along the pipe. For operational reasons, a full survey of a main may not be possible. In this case, sample sections of the main can be removed for further investigation.

The main disadvantage of the cast iron pipe is that it is not ductile. It is a brittle material and can fail catastrophically under excessive loads or impact. According to Burstall (1997), if the leakage history of a cast iron pipe shows frequent breaks, it is worth considering replacing the whole line. Another operational problem encountered with cast iron pipes is leakage at lead-packed joints.

Cast iron pipes cannot be welded. This is because of their microstructure and mechanical properties. Because of coarse graphite flakes, they are inherently brittle and cannot withstand the stresses set up by a cooling weld.

Failures of cast iron pipes can often be attributed to rapid pressure variations, e.g. surges. Control valves that open or close too quickly and malfunctioning air valves are also culprits. Manually operated line valves should not cause problems if they are operated under the proper waterworks procedure.

Circumferential cracks in cast iron flanges cannot be repaired. For such cases, Burstall (1997) recommends a replacement steel fabrication. For longitudinal cracks that run between the spigot and the socket joints, both joints will have to be cut out and a length of pipe spliced in using two mechanical couplings.

2.4.3 Steel

Steel that is used in water pipelines is inherently strong, yet ductile, and does not fracture easily. It is usually easily worked and welded. The main problem with steel pipes is corrosion, which causes pinhole leaks and may result in loss of wall thickness within the pipe (Burstall, 1997). Cathodic protection that prevents external corrosion should be an integral part of steel water pipeline design.

Ordinary steel pipes are made of carbon steel. They are either seamless or seamed (welded). The seamed pipelines are made of steel sheets or plates that are rolled or press-formed into circular shapes, with the edge (seam) of each pipe closed by welding.

Steel has a brittle or ductile transition zone at low temperatures. This means that, at this temperature, its ability to absorb energy is low and its ability to blunt cracks and prevent them from expanding is significantly reduced. Older steel pipelines that are found in very cold climates can potentially fail catastrophically at the welds under normal operating conditions (Phillips, 1972).

Large splits in steel pipes can be repaired if the curved plates are welded over the affected area, or a repair clamp can be fitted. Burstall (1997) suggests that old methods of rubber wedged against the leak under a girth clamp should not be used for permanent repairs as, inevitably, a leak will eventually appear.

2.4.4 Plastic materials

Plastic pipes are well accepted for distributing water. Several different plastic materials are used. All types of plastic that are used are corrosion resistant, ductile and relatively impervious (Burstall, 1997). Generally, the strength of plastic materials is less than the strength of steel and ductile iron materials. This limits the plastic pipe sizes that are available for high operating pressures.

The plastic pipes that are most often used when it comes to underground utility construction are PE and polyvinyl chloride (PVC). Both materials are light in weight, corrosion resistant, and are resistant to chemical and bacteriological buildup. Besides the fact that PE pipes are more flexible than PVC, the other main difference between the two plastic pipes is the way the length of pipes are joined together and how they are joined to other pipe materials.

Plastic pipes have limitations when it comes to cases where they are above ground. The span between supports is usually made shorter than steel, resulting in extra supports and increased costs. Plastic pipes may also not be the best choice for replacement pipe crossings that are rugged in difficult places to access.

Other uses of plastic pipes are in raw water lines in catchment areas. They are also suitable for scour valve (drain valve) tail pipes. Plastic pipes are particularly favourable when it comes to chemical lines at treatment plants. for example conveying chemical solutions into bulk mains for disinfection purposes.

When constructing a plastic pipeline, more care is often required because it can easily be damaged. Careless backfilling, for example, can lead to damage of the plastic pipeline. Plastic bulk pipelines usually have smaller diameters; thus longer pipe lengths with fewer joints can be achieved. In addition, plastic pipes are easily inserted inside older, larger cast iron mains, instead of replacing older mains.

When it comes to plastic pipe joints, a number of systems are available. Unplasticised PVC materials are usually welded with a solvent, allowing the solvent to glue the fitting and form an integral system. Polyethylene plastic pipes, on the other hand, are fusion-welded, using heat to join and integrate the pipe systems. Rubber rings are also sometimes used in uPVC. Plastic pipes jointed with rubber rings are comparable in certain respects to ductile iron systems jointed with rings.

Two fusion methods are commonly used for high-density polyethylene (HDPE): butt welding and electrofusion couplings (Burstall, 1997). The butt-welding process is similar to metal welding. The electrofusion method uses built-in electric heating elements that are used to weld the joint together. An electrical current that is timed heats the coupling and pipe to give controlled temperature and consistent weld.

2.4.5 Asbestos cement

Asbestos cement is made of asbestos fibres mixed into concrete. The pipe ends are usually plain, and fit sockets with rubber ring seals. When it comes to bends and fittings, asbestos cement pipelines use cast iron or ductile iron. Asbestos cement is a brittle material and can fail catastrophically. Sometimes, when an asbestos cement pipe bursts, an excavator is not required for the repairs because the burst can scour its own hole, enabling access to the burst pipe (Burstall, 1997).

2.4.6 Concrete

Concrete pipes can be divided into low-pressure and high-pressure pipes. Low-pressure pipes are normally made of plain concrete. These are used in applications that do not operate under high or even moderate internal pressure, for example sewers or culverts. Plain concrete pipes can easily withstand high external pressure that is imposed on it by the earth and traffic above it, because it has a high compressive strength. Furthermore, concrete pipes can be made to withstand moderate to high internal pressure by placing reinforcement in the concrete – either by using pre-stressed concrete or by using ordinary reinforced concrete.

2.5 LEAK DETECTION AND CONDITION MONITORING

2.5.1 Introduction

Two different types of general leakage control strategies exist: passive control and active control (Farley, 2003). Passive control is a strategy in which the operation team attends to leaks that are reported to them or that they come across. Only leaks with a significant effect on the functioning of the system and visible leaks are attended to with this strategy. Active leakage control involves the deployment of staff to investigate systems and detect leaks that have not been reported. This approach includes regular surveys and the monitoring of leakage and pipe condition.

The following factors must be considered before the most suitable leakage control strategy for a network is chosen:

- *Financial constraints on equipment and labour:* Due to the high cost associated with the equipment and labour required for active leakage control, this strategy appears to be expensive. In many cases, funds available for such strategies are constrained, as the monetary benefits are not realised. Passive strategies, however, result in failures being identified at much later stages, after which the consequences of the failures, as well as the increased effort required to rectify the failures, require considerably more funding than would have been required if an active strategy was implemented.

- *Risk and consequences of failure:* The consequences of unexpected downtime due to pipe failure also affect the leakage control strategy. If, for instance, the pipe system supplies critical consumers that are solely dependent on the supply, the consequences may be detrimental and expensive. Active control would be an absolute necessity in such cases.

- *Pipe accessibility and geological conditions:* Active control can be difficult and expensive to implement in some cases because access to the pipe may be restricted. This can be due to the pipe passing through rough terrain or through restricted areas. Passive control, in turn, may be ineffective in rural areas where pipe bursts can remain unnoticed for long periods. Geological conditions, such as the soil type and moisture content, also play a role in determining the most suitable strategy. In pipe environments where bursts do not show on the ground surface, passive control methods may be ineffective, while the applicability and effectiveness of certain active control methods are also influenced by ground conditions.

- *Scarcity and value of water:* Passive control strategies can be justified in water-abundant environments and in cases where little energy has been transferred to the water. In water-scarce countries, however, a high level of activity and investment in leakage monitoring is justifiable.

Unfortunately, in most developing countries, passive leakage control is the most common strategy (Farley, 2003), even though active strategies would be more suitable in many cases. Reasons for this include funding constraints, poor management and a lack of knowledge of active assessment technologies.

With passive leakage control strategies, the need for rehabilitation or the replacement of pipes is decided on criteria such as the number of recent failures, age, material and risk. Significant costs and savings can, however, be made with active approaches, because they allow the water utility to maintain their pipelines and identify only specific sections in need of replacement, instead of replacing the entire pipeline (Prinsloo et al., 2011).

In this section, active leakage control and condition assessment methods that are commercially available will be discussed.

For active leakage control methods, a number of distress indicators exist for water pipes that, if detected, can give the operator a good indication of the condition and risk of failure of the pipe system. The distress indicators that are most commonly detected include pipe leakage, corrosion, pipe wall defects and lining defects.

Methods used for the active condition monitoring of pipes are generally of one of two types. Direct condition assessments involve the direct assessment and identification of the pipe condition and defects, as well as the interpretation of signals emitted from these defects. Indirect condition assessments involve the analytical interpretation of data obtained from conditions induced onto the pipe systems.

2.5.2 Leak noise correlators

2.5.2.1 Description

With this method, leakage noise is measured at two pipe contact points and is then transmitted to a device that determines the position of the leak by measuring the time shift of the maximum correlation between the two signals. The noise can be measured by either hydrophones (underwater microphones) or low-frequency vibration sensors (Gao et al., 2005), or a combination of both (Liu et al., 2012). With the propagation velocity of the sound in water known, as well as the distance between the two sensors, the location of the leak can be detected.

This system can be effectively implemented on water transfer and distribution systems, because water-filled pipes can transmit acoustic leak signals over long distances without the shape of the leak signal changing significantly, and at almost constant propagation velocities (Hunaidi et al., 2004). Multiple leaks can also be detected between the two sensors, as each leak will have its unique signal peak. This peak varies considerably on metal pipes, while the peaks on plastic pipes vary much less and are therefore harder to distinguish (Hunaidi et al., 2004).

2.5.2.2 Limitations

A difficulty that arises when implementing acoustic leak detection to large diameter pipelines, such as bulk transmission lines, is that the intensity of the sound waves weakens at faster rates as the diameters of the pipes increase (Laven and Lambert, 2012; Hao et al., 2012).

Larger pipes also result in lower pipe rigidity and consequently lower predominant frequencies that are more susceptible to low-frequency interference (Hunaidi et al., 2004). This leads to the requirement of more access points at closer proximity to each other, posing a problem to bulk transmission lines, where access points are much fewer than in distribution networks. Applying acoustic leak detection with the above methods is therefore ineffective (Laven and Lambert, 2012).

The performance of this type of acoustic leak detection, and acoustic leak detection in general, can be greatly compromised by high environmental acoustic noise that can hide sounds emitted from leaks, especially for low water pressure pipes (Cataldo et al., 2015; Hunaidi et al., 2004).

A further drawback of this method is that its effectiveness depends on a number of factors that influence the amount of noise created by leaks. Higher pressure pipe leaks, for instance, generate more noise than low pressure leaks (Hunaidi et al., 2004). Small pinhole leaks and leaks created by corrosion pits emit clear noise signals, while large splits, leaking valves and leaking joints emit lower noise levels that are not easily detected by acoustic methods (Hunaidi et al., 2004; Rogers, 2014). If the pipe is below the water table, the acoustic signals are muffled (Hunaidi et al., 2004).

Pipe material has a significant effect, with a large amount of signal attenuation experienced in plastic pipes, while signals travel furthest in metal pipes. Rigid pipe materials also lead to higher predominant frequencies that are less susceptible to low-frequency interference (Hunaidi et al., 2004). It is therefore clear that this method is not equally effective for all types of pipe systems. Large, low pressure pipe bursts in plastic pipes, for instance, are harder to detect than small, high pressure pinhole leaks in steel pipes (Rogers, 2014).

Finally, for this method to be effective, a blanket survey approach of the whole pipe system is required to quantify the possible leakage. The method further requires a highly skilled and experienced operator that can identify and distinguish between leakage signals and acoustic noise (Hunaidi et al., 2004). Therefore, for large and complex networks, this can be an inefficient and time-consuming process.

2.5.3 Ultrasonic guided waves

2.5.3.1 Description

A sleeve fitted with a transducer and a ring of dry-coupled piezo-electric elements, which act as both emitters and receivers, is positioned around the outer circumference of the conductive pipe. Waves at frequencies below 100 kHz are emitted and the reflections of the waves are recorded and analysed (Leinov et al., 2015). Signals are reflected from both the front and back ends of defects, allowing the size of the defect to be estimated from the time lag between the two signals. The depth of the defects can be roughly estimated from the amplitude of the reflected signal, as it has been found that the depth is roughly proportional to the amplitude of this signal (Tse and Wang, 2009). This system can perform its function while the pipe is in full operation. Numerous defects can be identified with this technique by separating the reflected signals. This method is ideal for identifying corrosion in steel pipes (Hao et al., 2012).

2.5.3.2 Limitations

This method is strongly compromised by the limited distance of pipe that can be analysed from the fixed probe position. This technique is most effective for pipes above the surface, where it is effective over a range of 30 m (Liu et al., 2012). In buried pipes, however, this range is less, as more energy is lost to the surrounding medium. The bedding material and pipe coatings significantly affect the attenuation of the signals, and coatings with strong isolating properties can greatly reduce signal attenuation even further (Leinov et al., 2015).

Another drawback is that this method can only be applied to continuously conductive pipes, such as welded steel pipes. The method can also not indicate whether the defect is on the inside or outside of the pipe.

2.5.4 Ultrasonic inline inspection

2.5.4.1 Description

One way of implementing acoustic leak detection to bulk distribution pipes is by bringing the acoustic sensor closer to the source of the sound (Laven and Lambert, 2012). This can be achieved by implementing devices that travel inside the pipeline during operation.

The ultrasonic inline inspection method is used to detect either cracks or metal thinning through emitting and receiving very high-frequency waves from equipment installed on a carrying device that is pulled through the pipe. The waves are transmitted vertically through the pipe wall and reflections from the pipe features, such as from the inner and outer wall of the pipe, are recorded and analysed according to the time-of-flight principle. With this analysis, a high-resolution data image of the pipe's wall thickness can be obtained. Similarly, the signals can be emitted from slanted probes, causing the signals to propagate through the pipe at angles. These signals then reflect from vertical cracks in the pipeline, which are difficult to detect with vertical reflections.

2.5.4.2 Limitations

The length of time required for this labour-intensive pipe inspection and the high resulting cost of implementing this technique are the main drawbacks (Liu et al., 2012).

Similar to other acoustic methods, the leak detection efficiency is strongly dependent on the amount of noise emitted from the leak. The pipe material, pipe pressure, leak size and leak type therefore have similar influences on the probability of leak detection as leak-noise correlators.

2.5.5 SmartBall

2.5.5.1 Description

This method utilises an untethered and free-swimming ball, fitted with acoustic monitoring equipment. The acoustic listening equipment is fitted inside an aluminium sphere that is located in the centre of a foam ball. The device is launched through any flanged pipe opening 100 mm in diameter isolated by a valve. It propels itself through the entire length of the pipe.

Since it was commercially introduced in 2006, this method has rapidly gained popularity. In the short period starting in the middle of 2009 and ending in the beginning of 2012, it has already been used to survey more than 1 500 km of pipe (Liu et al., 2012).

One major advantage of this system is that it is small and untethered, allowing it to pass through valves and other obstacles encountered in large and generally unpiggable pipelines, bringing it within close range to all potential leaks. The round shape of the device ensures that the shape generates minimal noise as it travels in the pipe, largely eliminating external interference (Oliviera et al., 2011), and allowing for the detection of leaks smaller than 0.4 ℓ per minute, depending on the pipe material and leak type (Prinsloo et al., 2011).

This method also allows for the pipe to be surveyed in minimal time, while remaining in full operation.

2.5.5.2 Limitations

The main disadvantage of this technique is that the leak's magnitude and severity cannot be determined qualitatively. The severity of the leak can only be roughly estimated by the noise emitted from it (Liu et al., 2012). The noise is, however, dependent on a number of factors. Similar to the limitations discussed for leak noise correlators, the leak noise is influenced by pipe material, pipe pressure, leak size and leak type.

2.5.6 Closed-circuit television (CCTV) inspection

2.5.6.1 Description

This is a direct, inline condition assessment technique that utilises a camera, fitted on a carrier device, to capture and transmit video and images to a ground station as it travels through a pipeline (Liu and Kleiner, 2013). The carrying device, which is usually self-propelled, is inserted into the pipeline after it has been taken out of operation and drained completely.

2.5.6.2 Limitations

Major disadvantages of this system are the slow pace at which a pipe is analysed and the fact that the pipe must be emptied and must remain out of operation for the duration of the investigation. The device is commonly limited to a speed 15 cm/s (Liu and Kleiner, 2013) to allow for quality recordings, and stops frequently to assess suspected locations in the pipeline, resulting in extensive downtime. Although a lot of research and development has taken place to allow for automatic crack detection, interpretation of the footage is mostly performed manually by an experienced operator, which makes this method expensive and time consuming (Costello et al., 2007).

Newer side-scanning evaluation technology is, however, now available, which generates 360˚ images of the pipe surface (Liu and Kleiner, 2013), considerably reducing the time required for scanning the pipeline.

Unfortunately, this method can only be used to assess the interior of the pipeline, and gives little indication of the depth and seriousness of detected cracks (Hao et al., 2012). Further, limitations exist on the sizes and types of leaks that can be detected through visual inspection. This method is highly dependent on the skills of the operator.

2.5.7 Laser scan

2.5.7.1 Description

This is a direct, inline inspection method and involves a device that projects a ring of laser light onto the inner surface of the emptied pipe. A camera captures the images of the projected ring. The profile of the pipe is reconstructed digitally from images captured by the laser ring. The advantage of this method is that the reconstructed profile can be unfolded and manipulated to allow for effective review and analysis to detect and pinpoint potential pipe corrosion.

2.5.7.2 Limitations

Although this method is superior to normal CCTV inspection in terms of its capabilities for detecting potential leak sites, it is still limited by its long surveying time, as well as the fact that the pipeline must be taken out of operation and emptied for the duration of the assessment.

2.5.8 Ground-penetrating radar

2.5.8.1 Description

Ground-penetrating radar (GPR) is a direct assessment technique that surveys the ground in the general vicinity of the pipe by sending high-frequency electromagnetic pulses from a device that is guided over the pipe on the ground surface. Waveforms obtained from the pulse reflections from materials that have sufficiently differing electrical characteristics are then plotted and analysed (Lai et al., 2016).

This method can be used for the leak detection of all pipe material types, as it indicates leaks by detecting certain changes in the di-electric characteristics of the soil surrounding a leak, irrespective of the pipe material (Hunaidi and Giamou, 1998). Underground voids that are created by the leaking water, for instance, slow down the radar wave and give an appearance of deeper energy (Stampolidis et al., 2003).

2.5.8.2 Limitations

A number of studies confirm that GPR is highly sensitive to changes in moisture and is limited in highly conductive soil types, such as clay and silty soils (Hunaidi and Giamou, 1998; Stampolidis et al., 2003). The GPR is also susceptible to any conductive objects in the vicinity of the pipe (Cataldo et al., 2014), with noise dominating the waveform plots at depths deeper than 3 m. Even to successfully survey at depths of between 2 m and 3 m, the conditions must be very favourable. Furthermore, for successful leakage detection, highly skilled staff is required to accurately interpret the waveform plots, which is also a time-consuming and expensive process (Hao et al., 2012).

2.5.9 Time domain reflectometry

2.5.9.1 Description

With time domain reflectometry, an electromagnetic signal is generated, which then propagates along a sensing element close to the pipe. The signal is partially reflected as it encounters varying degrees of electric impedance (Cataldo et al., 2014). By analysing the return signal, the desired information on the location and condition can be obtained. Similar to GPR, this method also relies on the di-electric properties of the soil surrounding the pipe to monitor the moisture content of the soil.

The ideal application requires a bifilar transmission line to be installed alongside the pipe during the laying of the pipe (Cataldo et al., 2015). This allows for quick pipe condition surveys (Cataldo et al., 2014) and can easily be modified to allow for continuous, real-time monitoring for the entire life of the infrastructure (Cataldo et al., 2015). Another major advantage of this system is that it functions independently of the operating condition of the pipe and does not require high water pressure to effectively pinpoint leaks (Cataldo et al., 2012).

It has been shown that this method can also be applied to existing conductive pipes by placing a conductive wire on the ground surface directly above the pipe (Cataldo et al., 2012). The pipe and the wire on the ground surface act as the sensing element, requiring the pipe to be electrically continuous. This system is also efficient, considering that a pipe length of up to 300 m can be surveyed with one single measurement, which amounts to approximately 6 km of pipe per day (Cataldo et al., 2014).

2.5.9.2 Limitations

The biggest limitation to this technique is that, for it to function optimally, the bifilar transmission line needs to be installed during the initial laying of the pipe. The real-time monitoring capability is therefore not available for existing pipes. Furthermore, if applied to existing pipes, the pipes must be continuously conductive.

2.5.10 Electrical resistivity tomography

2.5.10.1 Description

With electrical resistivity tomography, the electrical resistivity of the soil is measured by injecting current into the ground with electrodes and measuring the potential difference between the electrodes (Cataldo et al., 2014). The resistivity is simply calculated by Ohm's law and is then mapped to illustrate the variation of resistivity in the soil surrounding the pipe. The potential leaks are then pinpointed by identifying areas of low resistivity, which indicate moist soils or water-filled cavities.

2.5.10.2 Limitations

A disadvantage of this method is that it requires electrodes to be inserted into the ground, which can be time-consuming, depending on the condition of the ground. Furthermore, the results are easily distorted by other anomalies in the ground that influence the resistivity (Cataldo et al., 2014).

2.5.11 Magnetic flux leakage detection

2.5.11.1 Description

Magnetic flux leakage detection, as an inline inspection method, is one of the oldest methods of ferrous pipe inspection (Orazem, 2014), and is very accurate for determining any changes in pipe wall thickness and for detecting corrosion pits.

Large magnets fitted on a carrying device induce a saturated magnetic field, resulting in a magnetic flux distribution in the pipe wall. In perfect pipes, the magnetic flux field will be homogeneous, but damaged areas cause abrupt reductions in magnetic permeability, increasing the resistance to flux, and therefore causing the flux to change direction. Flux leakage therefore occurs at the pipe defects, where the material is thinner and incapable of carrying all the magnetic flux. The flux leakage can then be detected to pinpoint the location of the defect.

The method is commercially available for inline pipe inspections. Magnets and sensors are fitted to a carrying device that positions them at a constant distance from the inside wall of the pipe. This unit, commonly referred to as a smart pig, is then guided through the length of the pipe to carry out the inspection (Orazem, 2014).

Most magnetic flux leakage techniques require direct contact with a cleaned, unlined pipe surface for efficient functioning, as well as to avoid damage to the pipe lining (Liu et al., 2012). New advancements, however, allow this method to function effectively without pipe wall contact, allowing for the accurate assessment of epoxy-lined and even cement mortar-lined pipelines. The high effectiveness of this method for identifying pipe defects has been verified for large mortar-lined steel pipes up to 2 m in diameter (Hannaford and Melia, 2010).

2.5.11.2 Limitations

This method remains a time-consuming exercise, and requires the pipe to be out of operation for the entire duration of the inspection. In a cited case study, the surveying of a pipe 2 m in diameter and 12 km in length required a 10-week downtime period (Hannaford and Melia, 2010). Furthermore, for this method to be effective, the pipe must first be emptied and cleaned thoroughly (Hao et al., 2012). It can only be used for ferrous pipe inspections, and a pigging station is required for this equipment to be inserted into the pipe. This method has also been found to be unreliable for detecting short and shallow defects.

2.5.12 Remote field eddy current technique

2.5.12.1 Description

The remote field eddy current technique (RFET) is another direct, inline inspection method. A transmitter coil is energised by a low-frequency, alternating current and produces a magnetic field in the pipe wall. Flux lines from the magnetic field generate voltage across the pipe wall, which in turn generates eddy currents. A receiving coil positioned at a certain distance from the transmitter coil then senses the alternating magnetic fields created by the eddy currents.

Figure 2.18: RFET setup (Innospection, n.d.)

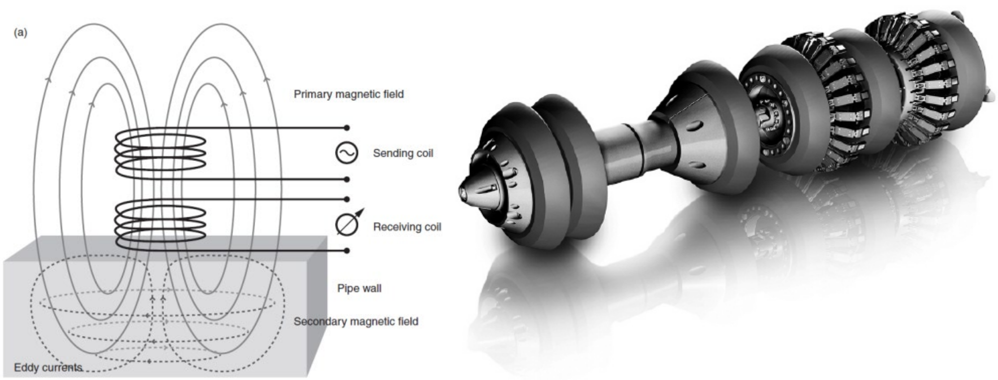

Figure 2.19: RFET flow diagram (Orazem and Tribollet, 2008) and commercially available carrying device

The receiver coil records the phase, as well as the voltage amplitude of the incoming signal. The phase is used to identify the defect depth, while the signal amplitude can be analysed to estimate the defect volume.

Commercial tools are available for the inline inspection of pipes up to 700 mm (Pipeline Inspection and Condition Analysis Corporation, n.d.). The tools, known as hydroscopes or hydra snakes, consist of a carrying device, a transmitting coil and a receiver coil. These devices can operate in wet or dry conditions and are either pulled through the pipe with a cable, or are pumped through the system.

One advantage of this method is that no intimate contact with the pipe wall is required, allowing the system to function effectively, even if the pipe is lined or covered slightly with sludge or sand.

The broadband electromagnetic technique is a similar method to the conventional RFET method discussed above, except that a broad range of frequencies between 50 Hz and 50 kHz (Liu and Kleiner, 2013) is transmitted instead of a single frequency. The advantage of this method is faster inspection speeds. Although commercially available, this method is not common.

The remote field eddy current (RFEC)/transformer coupling (TC) technique functions on a similar principle, but was developed for pre-stressed concrete pipes (PCP) to identify the locations of broken wires in the concrete pipe walls. It is one of the most common methods of condition assessment for PCP (Prinsloo et al., 2011). A system called the PipeDiver is commercially available to perform this exact function. It is a flexible, untethered and buoyant device that travels the length of the pipe using the flow of the water inside the live pipe.

2.5.12.2 Limitations

The RFET method can only be applied to ferrite pipes, while the RFEC/TC technique is only suitable for pre-stressed concrete pipes. Both techniques require a pigging station for the device to be launched.

Another drawback of this technique is the low strength and low frequencies (10 Hz to 1 kHz) at which this method is effective, resulting in a slow inspection speed, although newer technology allows for surveying speeds of between 5 m and 15 m a minute (Pipeline Inspection and Condition Analysis Corporation, n.d.).

This technique is easily influenced by conductive debris or external electrical noise. The technique is therefore highly dependent on the skills and experience of the operator to distinguish potential pipe defects from this noise (Liu et al., 2012). Furthermore, although the method detects internal and external flaws with equal effectiveness, it cannot distinguish between internal and external defects.

2.5.13 Sahara system

2.5.13.1 Description

This system is an inline detection technique that uses acoustic hydrophones in combination with a CCTV camera to simultaneously identify leak locations and inspect the internal condition of the pipe. Leak locations and rough estimates of the leak sizes are identified from the distinct noises of leaks detected by the apparatus.

It makes use of a tethered device that is fitted with a parachute, which uses the flow of the live pipeline to pull the system through the entire length of the pipe.

One of the main advantages of the system is its compact size when the parachute is in the collapsed position, enabling the device to travel through obstacles in the pipeline, as well as allowing for the device to be easily introduced into the pipe through small pipe openings (Prinsloo et al., 2011).

2.5.13.2 Limitations

In comparison to other inline pipe inspection methods, this method has very few limitations. A significant limitation is that the device itself is expensive, and skilled operators are required to operate it and trace it on the ground surface as it travels through the pipe.

2.5.14 Detection techniques using conservation of mass

Conservation of mass techniques require the measurement of flow into and out of the pipeline, with mass flow appearing to be the easiest and most common of these technique (Ostapkowicz, 2016). The mass flow technique can accurately determine the existence of leaks, as well as the combined intensity of all the leaks. However, it lacks the ability to locate the leaks.

The most primitive application of the mass flow technique is achieved by simply installing flow meters at the beginning and at the end of the pipeline under inspection. The difference in the flow entering and leaving the pipe indicates the amount of leakage from the system, with accuracy solely dependent on the flow meters used. Flow conditions other than steady-state conditions also negatively influence the accuracy of this method, partially due to the delay in the pipe inlet and outlet flows in respect of the pressure changes (Ostapkowicz, 2016; Turkowski and Bratek, 2007).

An adaption of this technique exists for water distribution networks and allows for identifying the approximate location of leaking pipe sections. It is known as the district meter area technique. With this approach, a network is divided into a number of sections known as DMAs. The inflow to each DMA is measured and monitored. Leakage can then be pinpointed by progressively isolating the DMAs and the pipes within the DMA networks (Rogers, 2014).

2.5.15 Negative pressure wave and gradient methods

2.5.15.1 Description

These are indirect condition monitoring techniques that can detect abrupt new leaks, such as pipe bursts. In steady-state conditions, when a burst occurs in a pipe, it will generate negative pressure waves into both the upstream and downstream direction of the pipeline. With the negative pressure wave method, the waves can be detected with sensitive sensors at either end or, preferably, at multiple locations on the pipeline. The leak location can then be calculated using the measured time of flight of the upstream and downstream wave in conjunction with the pipe wave speed. The gradient method requires multiple sensors on the pipeline, which detect the degree of attenuation of the pressure waves created by the leak. The degree of wave attenuation over distance can be graphed as straight lines that intersect at the leak location (Ostapkowicz, 2016).

2.5.15.2 Limitations

These methods can only be used to detect and locate large leaks and cannot be used to detect existing or slowly increasing leaks (Ostapkowicz, 2016).

2.5.16 Inverse transient method

2.5.16.1 Description

The inverse transient method and frequency domain techniques obtain leak information from transients with the inverse method. That is, instead of using system characteristics to determine the system's state, the known system state is used to identify system characteristics, such as leaks (Colombo et al., 2009).

Transient waves have excellent propagation properties due to their low frequency and higher energy, causing them to attenuate little over long distances (Karney et al., 2009). All pipeline features alter the transient waves to some extent, resulting in the accumulation of a vast amount of data through a single test. This data can then be analysed to reveal the approximate location and characteristics of the pipeline features (Colombo et al., 2009). Leaks, for instance, generally cause a sudden pressure drop due to the absorption of energy by the leak, and can be identified by analysing the time of flight of the wave and the characteristic wave speed of the pipeline.

With the inverse transient method, hydraulic transients with known intensity are injected into the pipeline at various locations and the dynamic transient data is recorded at predetermined points along the pipeline. A set of expected data is then generated from a computational model that simulates the same transient events in the pipeline. The input parameters and model algorithms are varied until model results are obtained that agree best with the data recorded. The model data is then compared to the set of dynamic data (Karney et al., 2009).

With accurate model fitting, deviations between the two sets of data indicate pipe defects, such as leaks. The location of the possible leak can be directly determined by identifying the location where the deviation between the two data sets occurs.

2.5.16.2 Limitations

It can become very complex and time-consuming to mathematically model a long pipe section with all its components. The resulting models often depend on a number of assumptions for pipe parameters, such as pipe wall friction (Karney et al., 2009). This method is therefore prone to model input and model structure errors by the operator (Colombo et al., 2009), such as the incorrect input of system characteristics and numerical mistakes.

A further challenge is system noise and distinguishing leak signals from signals caused by other system features (Colombo et al., 2009). Air cavities in the pipeline, for instance, cause discrepancies between the actual and modelled results (Turkowski and Bratek, 2007), often raising false alarms.

2.5.17 Frequency domain technique

2.5.17.1 Description

The frequency domain analysis technique is an alternative to the inverse transient method, and is less dependent on the accuracy of the transient model. With this method, steady, oscillatory flow is induced in the pipeline by operating a valve downstream of the pipe to a set pattern. The frequency response of the system is measured and analysed at the downstream valve for a range of frequencies. The response is then compared to a modelled frequency response for the pipe without leaks, which is numerically calculated from the known pipe characteristics (Mpesha et al., 2001; Colombo et al., 2009). Obtaining the expected frequency response at the closing valve is much simpler and requires much less computational input in comparison to the inverse transient method. The leaks and leak magnitudes are then identified from the amplitudes of the measured frequency response (Mpesha et al., 2001).

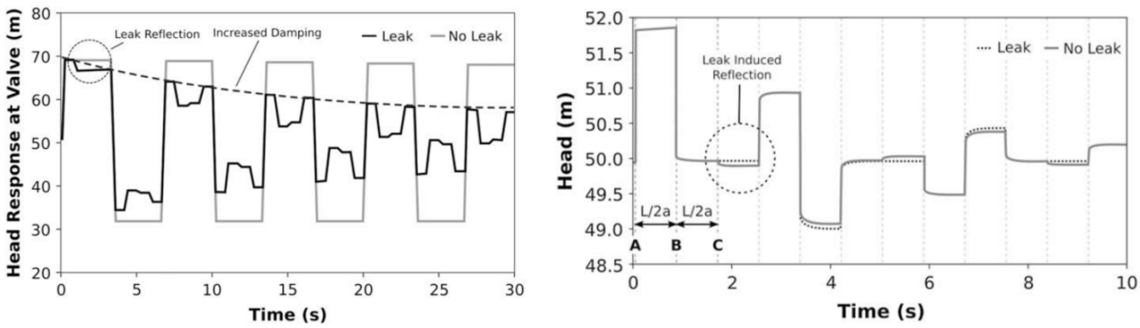

Figure 2.20: Two examples showing the comparison of transient pressure waves for the intact system and leaking system after the downstream valve is closed (Ostapkowicz, 2016)

2.5.17.2 Limitations

An advantage of the transient analysis approach is that it only causes a disruption in the operation of the pipe for a short period. The frequency response method has the additional advantage that all actions and measurements are taken at one location on the pipeline (Mpesha et al., 2001). A drawback of this method is that transient states must be created through the opening and closing of valves, in contrast to the normal operation of the plant. This leads to an increased risk of failure of the pipeline and may require the operating conditions to be constrained (Karney et al., 2009). Furthermore, this technique requires highly qualified staff due to its current complexity (Ostapkowicz, 2016).

The state of development of this technology is accurately summarised by the following statement made by Colombo et al. (2009) in the conclusion to a literature study on transient-based leak detection methods: “While all have bestowed upon the technique some measures of approval, carefully contrived hypothetical examples and heavily controlled laboratory trials with the most rudimentary systems do not yet achieve the level of validation required for a strategy that must work in complex systems under a wide range of conditions.”

A number of field tests have been carried out and are reported in literature (Colombo et al., 2009). Although these tests prove that the above methods can be successful in identifying and pinpointing leakage, this method remains too complicated and error-prone for successful commercial implementation. Significant work is still needed to develop this method into a practical leak detection method (Colombo et al., 2009; Karney et al., 2009).

CHAPTER 3: METHODOLOGY

3.1 INTRODUCTION

This chapter describes the design, construction and application of the pipe condition assessment equipment used in this study. The PCAE is based on a smaller device that has been tested on municipal distribution systems as part of another research project.

The device is based on the idea that if a pipe section filled with water is isolated from its users and the rest of the system, the only route for water to exit the pipe is through leaks that exist in the pipe. By connecting a water source and pump to the pipeline, it is possible to measure the leakage rate by measuring the inflow required to maintain a given pressure. Measuring the leakage rate at different pressures allows for the leakage flow rate, and subsequently the leakage area, to be estimated as a function of pressure.

This procedure can be used to identify existing leaks in a pipe and, if it has leakage, to estimate the leakage characteristics, which consist of the initial leak area and the head-area slope.

The next section describes the design of the PCAE, followed by the field test procedure and the required data analysis to characterise pipeline leakage.

3.2 PIPE CONDITION ASSESSMENT EQUIPMENT DESIGN

The design process was an iterative process involving multiple interim designs before deciding on the final design. This process was intended to ultimately improve the quality and functionality of the design.

The following minimum design requirements were set for the PCAE:

- It must be suitable for testing both bulk and distribution system pipelines.
- It must consist of materials that can handle up to 12 bar of pressure.
- It must be capable of measuring and accurately logging both flow rate and pressure.
- The water metering solution must be capable of measuring down to background flow rates (i.e. flow rates <250 ℓ an hour) and allow for data logging.
- The pressure transducer should allow for data logging at a frequency of 100 m/s.
- Excess air should be removed automatically.
- The full device must be mobile and robust enough to handle field environments.

Several components were incorporated into the PCAE to satisfy the aforementioned considerations. Figure 3.1 shows the process and conceptual design of the PCAE, which contains a water tank, valves, a magnetic flow meter, an inverter, a pump, uPVC pipes and a plastic-reinforced hose adaptor.

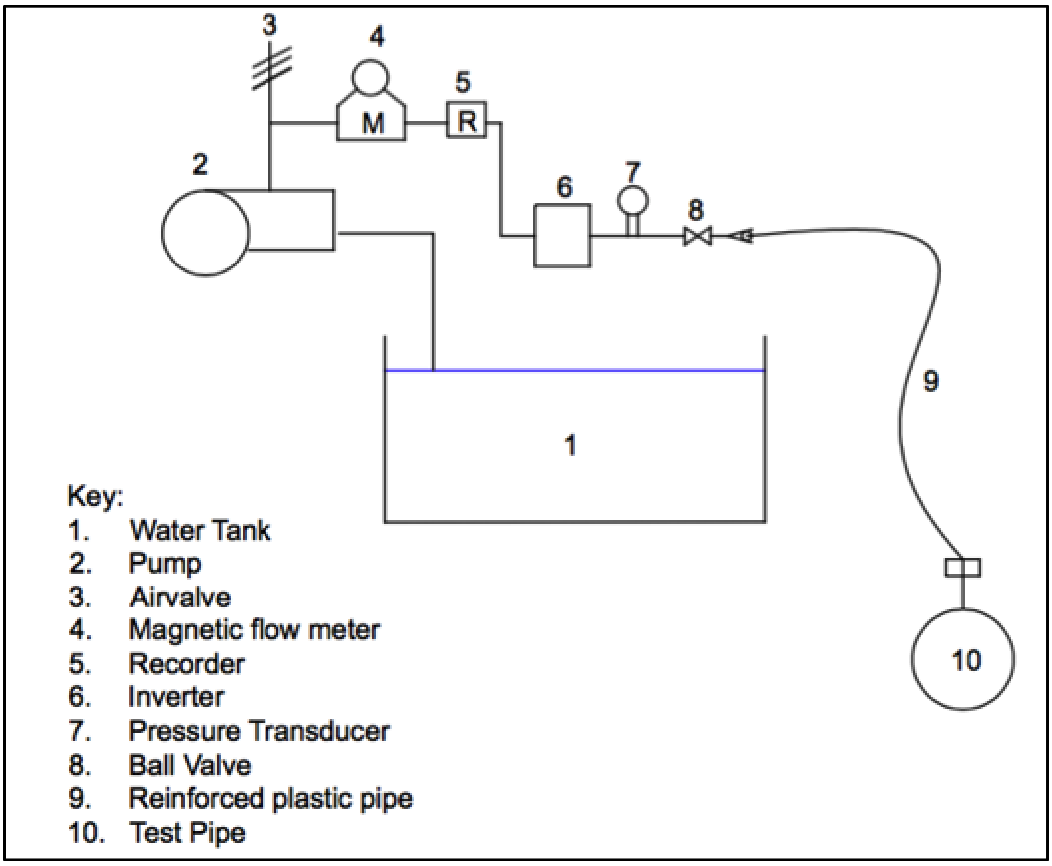

Figure 3.1: Process and component design of the system

The detailed technical description of the individual components used to construct the PCAE is discussed next.

3.2.1 Pump

The following criteria were used to select a pump for the PCAE:

- The pump should be designed for conveying water.
- The materials used to construct the pump should be compatible with water; thus, the materials should be protected against corrosion.
- The pump should be a pressure-controlled, variable-speed pump to carry out the necessary pressure tests.
- The pump's maximum pressure should not exceed the maximum allowable pressure for typical pipelines.
- The pump environment is also an important factor because the pump will be used in the field as well as in the laboratory; therefore, it should be robust and easy to transport.

The Euroflow HS18-40N-1 horizontal multistage stainless steel centrifugal pump was selected. This pump is suitable to convey water, and its materials are compatible for this application. Figure 3.2 shows this pump and its installation, where L = 440 mm, L_1 = 186 mm, L_2 = 168 mm, H = 255 mm and D = 165 mm.

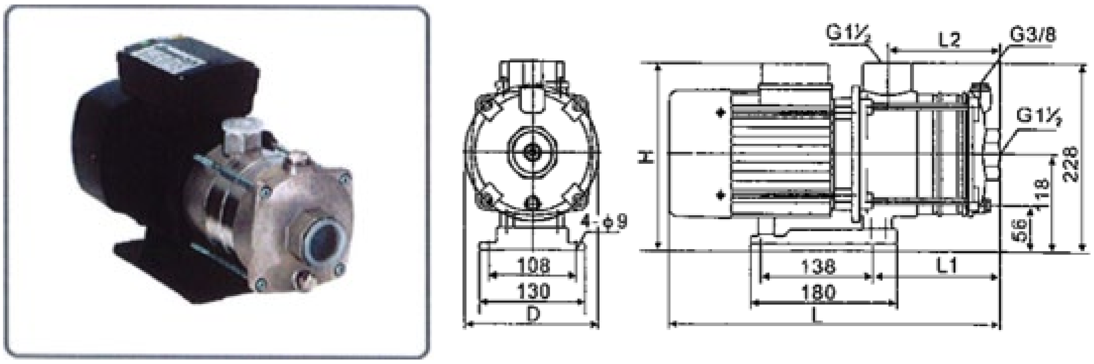

Figure 3.2: Euroflow horizontal multistage stainless steel centrifugal pump

In Figure 3.3, the performance curve of the selected pump is demonstrated by the 40N-1 pump curve. As can be seen from the 40N-1 pump curve, this pump can deliver a maximum flow rate of 16 m^3 per hour. The net positive suction head (NPSH) point for the pump is also shown in Figure 3.3, as the intercept between the 40N-1 curve and the NPSH curve.

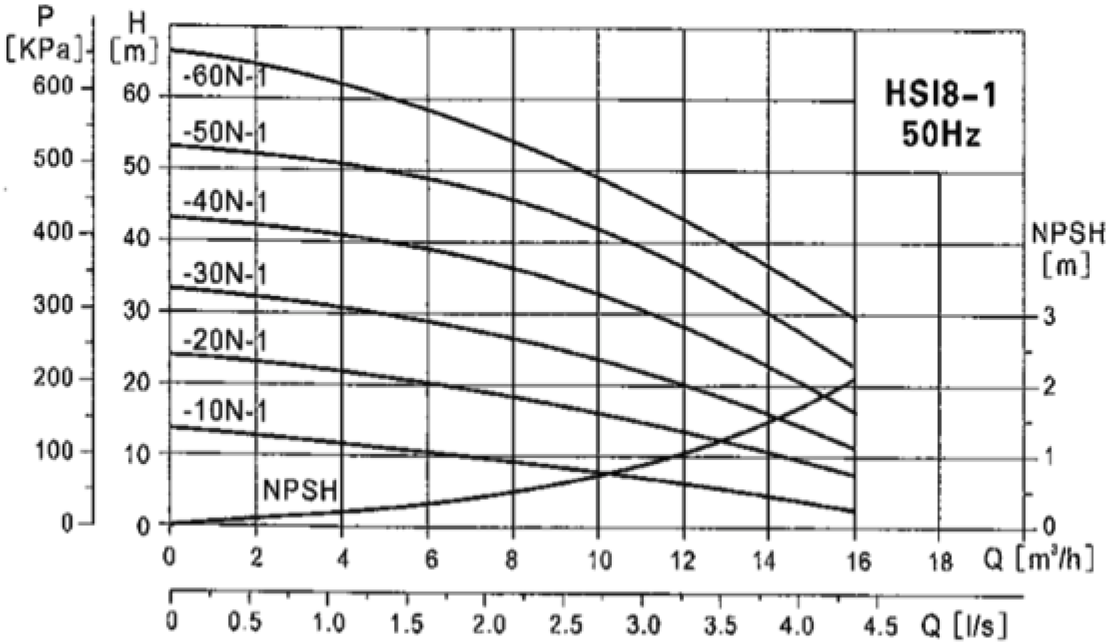

Figure 3.3: Pump performance curves of different pump models

The NPSH required for the 40N-1 pump is about 1.8 m, as can be seen from Figure 3.3. The equipment's available NPSH can be calculated using Equation 3.1 and knowing the pump inlet pressure and liquid vapour pressure

$$\boldsymbol{NPSH_{available}} = \frac{P_{inlet}}{\rho g} + \frac{v_{inlet}^2}{2g} - \frac{P_{vapour}}{\rho g}$$

Equation 3.1

where P_{inlet}, is the inlet pressure, ρ is the density of water, g is the acceleration, v_{inlet} is the inlet velocity and P_{vapour} is the vapour pressure of water at 20 ˚C, which is the assumed temperature of water in pipe systems.

Table 3.1 provides details of the performance of the pump. According to the table, the HS18-40N-1 pump model requires 1.5 kW of power to drive the motor.

Table 3.1: Performance of the pump

MODEL	Driving motor P2(kW)	Q (m^3/h)	4.0	6.0	8.0	10	12	14	16
HSI8-10N-1	0.55	H (m)	11	10	9	8	7	6	5
HSI8-20N-1	0.75		22	20	19	18	13	11	8
HSI8-30N-1	1.1		31	29	26	24	20	16	11
HSI8-40N-1	1.5		41	39	37	33	28	23	17
HSI8-50N-1	2.2		51	49	46.5	42	37	30	23
HSI8-60N-1	3.0		62	58	52	48	42	36	30

3.2.2 Inverter

The pump comes with a DAB Active driver plus an inverter, shown in Figure 3.4, that is used to control the variable speed pump. The inverter will also ensure that the pump uses the minimum necessary power to meet the pumping needs, avoiding unwanted waste and bringing significant energy savings.

Figure 3.4: Constant pressure inverter

This inverter has an integrated electronic pressure transducer, flow sensor and a non-return valve. This inverter has a 32 mm male thread inlet connection and a 32 mm female thread outlet connection.

3.2.3 Flow meter

The metering solution is a critical component of the PCAE because the potential minimum level of leakage that can be detected depends on the minimum level the flow meter can measure accurately. For this reason, electromagnetic flow meters were considered appropriate for the PCAE, due to their high accuracies.

The selected electromagnetic flow meter was required to adhere to the following criteria:

- It must measure up to the pumps' maximum operating flow rate of 16 m^3 per hour.
- It must have the lowest possible starting flow and the least possible uncertainty.
- It must have logging capabilities that allow for the flow to be logged.
- It must be robust for field application.

The ABB Process Master FEX500 electromagnetic water meter, shown in Figure 3.5, fits the above criteria and was selected for the PCAE.

Figure 3.5: Process Master FEX500 electromagnetic flow meter by ABB

The Process Master FEX500 electromagnetic flow meter has a nominal diameter of 25 mm and weighs 6.4 kg. This electromagnetic flow meter can measure flows ranging from 0.4 m^3 per hour to 24 m^3 per hour. The meter can detect low flows that are 1% of the maximum flow rate.

The ABB electromagnetic flow meters come with calibration certificates and thus do not require any further calibration. These meters, however, must be kept horizontal at all times during operations.

In order to connect the electromagnetic flow meter to the PCAE, a PVC flange, shown in Figure 3.6, was to be connected to the outer flange of the meter using a suitable bolt and nut connection. The PVC flange would then have an adapter piece that could easily be connected to the rest of the pipework.

Figure 3.6: PVC flange for the electromagnetic flow meter

3.2.4 Pressure sensor

A pressure sensor was required to log the pressure readings of the PCAE during tests. The required sensor had to adhere to the following criteria:

- It must be robust for field application.
- It must record pressures at 0.001 Hz or higher.
- It must have logging capabilities.

The ABB 2600T series analogue pressure sensor and transmitter were selected for the PCAE.

Figure 3.7: ABB pressure sensor

3.2.5 Data recorder

A logging solution was required to log the data from the electromagnetic flow meter and pressure sensor. There are different types of loggers with various levels of sophistication and interactivity. The most basic is a portable device that can connect to the flow meter or the pressure transducer to keep track of the data. For this study, an advanced data logger was required and had to meet the following criteria:

- It must be able to display the pressure and flow profiles of the PCAE during a test.
- It must be able to log and store data that can be accessed and analysed using an appropriate analysis software.

The ABB Field-mount paperless recorder SM500F, shown in Figure 3.8, was selected as a suitable logging solution. The ABB SM500F recorder has important capabilities, such as live display of the data, logging data on an SD card and, finally, the possibility of accessing and analysing the data using software.

Figure 3.8: ABB Field-mount paperless recorder SM500F

The recorder shown in Figure 3.8 has multiple electrical connections, as shown by Figure 3.9(a). The recorder itself is powered through the power supply connection, shown as G in Figure 3.9(a), containing the live, neutral and earth connection. The electromagnetic flow meter and the pressure transmitter are connected to the recorder as digital inputs.

The electromagnetic flow meter has a positive (red) and a negative (blue) wire that comes from the meter, and connects to the recorder at B3 and B4, respectively.

The pressure transmitter, on the other hand, has three connections: a positive (red), negative (blue) and a terminal (black). The positive and negative connections from the transmitter connect to the recorder at D3 and A3. The terminal connection is a single black wire from A4 to D4. Figure 3.9(b) shows the actual connections.

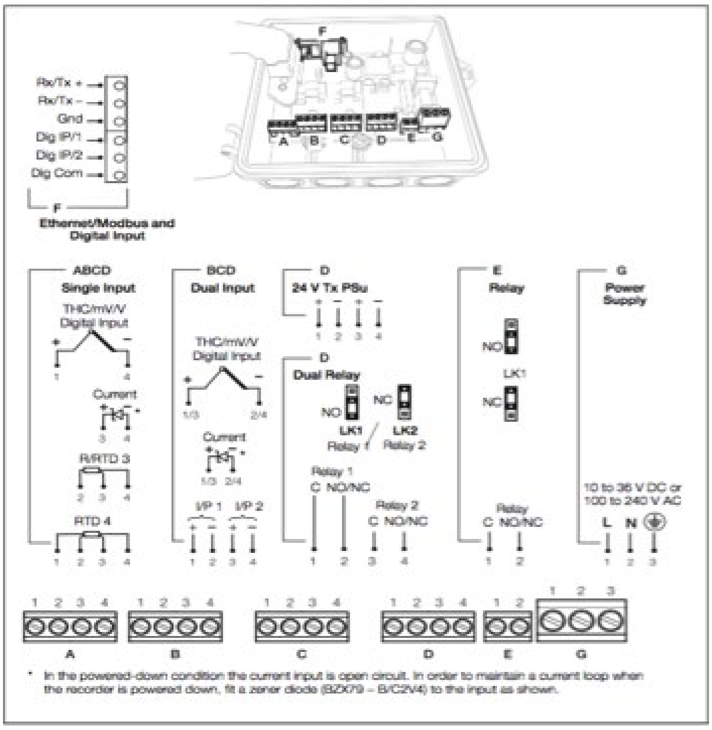

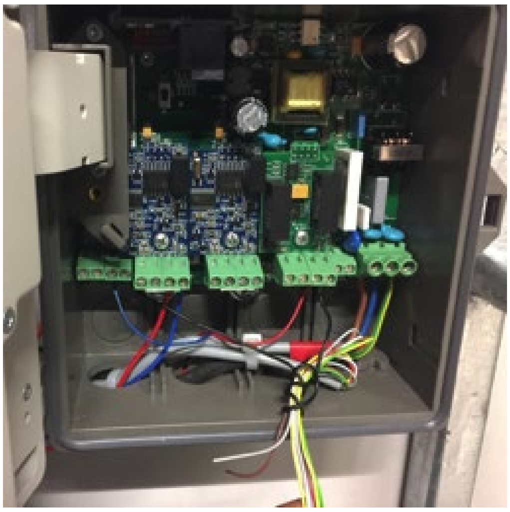

(a) **(b)**

Figure 3.9: a) Schematic view of the electrical connections; and b) the actual connections

The flow and pressure profile of the PCAE are displayed on a chart output, as shown on the screen of the recorder in Figure 3.8. At the same time, the data is stored on an SD card. The SD card can be placed in a computer's SD slot and the data can be accessed and analysed using the ABB DataManager Pro software.

3.2.6 Generator

An electricity generator will be used mainly during field testing if a power source is unavailable. To determine the size of the generator that is required, the total wattage of the maximum number of items to be run simultaneously was calculated. This was done to ensure that the required wattage to operate the PCAE never exceeds the maximum run rating of the generator.

The PCAE items that are identified for the electric power input are the pump, the inverter, the magnetic flow meter, the recorder and the pressure transducer. The total wattage of these items was calculated to be 2.4 kW. Therefore, the Ryobi RG-2700 generator was selected and fitted with an overload protection switch (see Figure 3.10).

Figure 3.10: Generator used to power the PCAE

The selected generator has a power output of 2.7 kW air-cooled. The maximum run rating, which is the maximum allowable total wattage, is 2.5 kW. It is thus capable of running the device. The generator comes with a four-stroke engine. The fuel tank takes 12 ℓ and uses unleaded petrol. The generator has a minimum run time of 10 hours. Given that each field test can take approximately one hour, a full tank can allow for at least nine tests.

3.2.7 Pipework

The PCAE was assembled using Class 12 uPVC pipes. To maintain material compatibility, all the connection pieces, fittings and bends were also uPVC. Class 12 uPVC pipes were used since they are rigid enough and can withstand the high pressures required to run the bulk system tests. In order to determine the appropriate size of the Class 12 pipes, it was necessary to calculate some parameters, including the cross-sectional area of the pipe, the flow velocity for various cross-sectional areas and the pipes' friction head losses.

Given that the PCAE's maximum flow rate will be 16 m^3 per hour, obtained from the maximum flow rate delivered by the pump, the equivalent cross-sections (A), flow velocities (v) and friction head losses (hf) can be calculated for various pipe diameter sizes (D) and lengths (L), as shown in Table 3.2.

Table 3.2: Cross-sections, velocities and friction losses for various pipe diameters

Pipe diameter (mm)	Area (m^2)	Velocity (m/s)	h_f (m/m)
20	3.1 x 10-04	14.5	26.93
30	7.1 x 10-04	6.29	3.55
40	1.3 x 10-03	3.54	0.84
50	2.0 x 10-03	2.26	0.28
60	2.8 x 10-03	1.57	0.11
70	3.8 x 10-03	1.15	0.05

From Table 3.2 the 50 mm pipe diameter was chosen because it gives an acceptable maximum flow velocity of 2.26 m/s, and a frictional head loss of 0.2 m per meter of pipe length.

3.2.8 Ball valves

Hand-operated ball valves were used for the PCAE to control the flow. Figure 3.11 shows the PVC ball valve. The reason for choosing this ball valve is the easy visual confirmation of the valve's status, for example, the handle will lie parallel in alignment with the flow when opened, and perpendicular to it when closed.

Figure 3.11: The 50 mm compact PVC ball valves

3.2.9 Constructing the device

After approval of the final concept design, the next phase of the design process was constructing the PCAE. The first step before construction was to purchase all the required apparatus that were listed. Manufacturers of the various apparatuses were contacted and approached to assist with acquiring the necessary components.

Due to the iterative nature of the design, it was often difficult to pre-empt the challenges that would be encountered with the actual construction of the PCAE. It was often necessary to solve problems as they occurred.

Another unforeseen challenge was the difficulty presented by the presence of apparatuses with varying pipe inlet/outlet diameters. This resulted in the need for a number of adaptors that would either increase or reduce the pipe diameter to make it fit accordingly. Additional adapters would make the device longer than anticipated. This was dealt with by simply reducing the length of the 50 mm uPVC pipes to maintain a reasonable size that was portable.

Figure 3.12 shows the design drawing of the PCAE and Figure 3.13 shows the actual PCAE assembly. This assembly was fitted to a trailer with a 1 000 ℓ water tank, as shown in Figure 3.14.

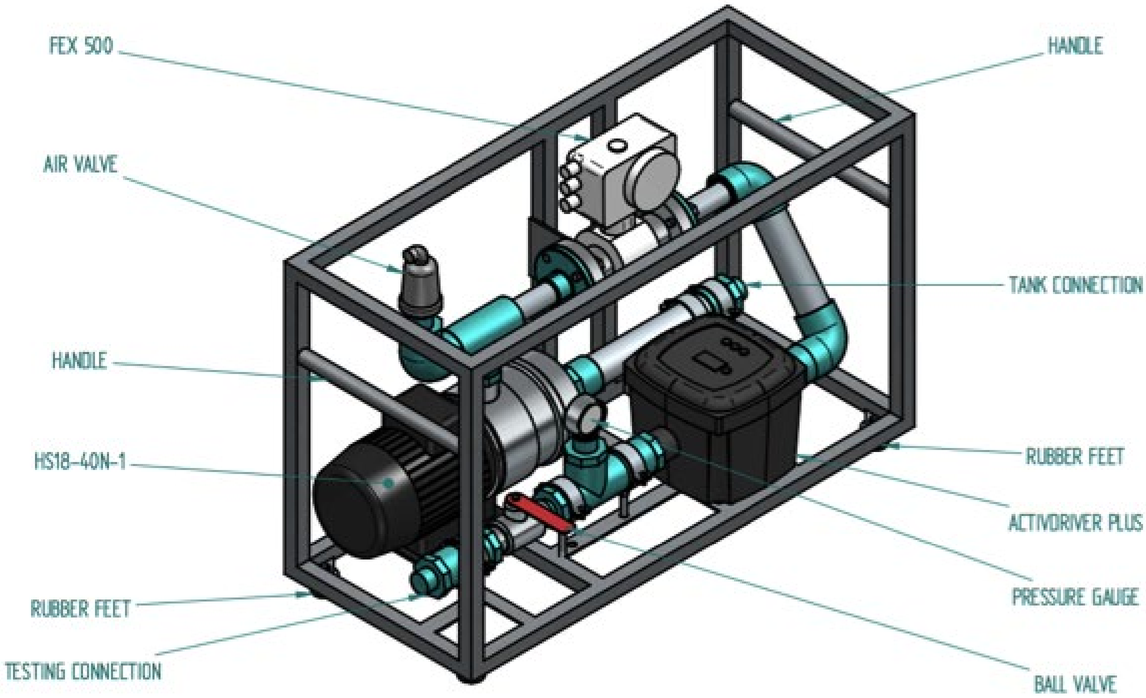

Figure 3.12: Pipe condition assessment equipment component labels

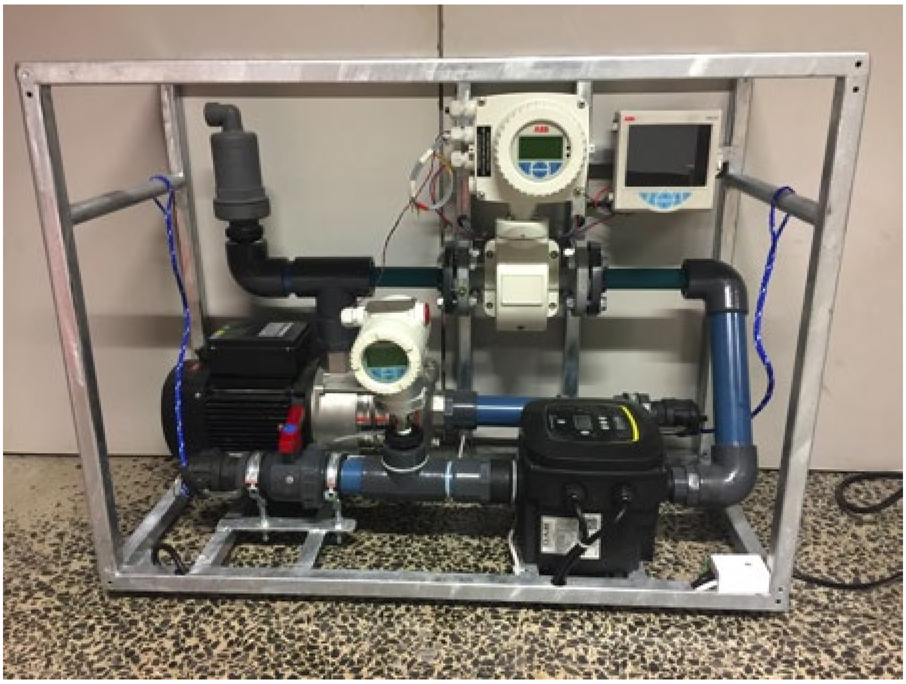

Figure 3.13: Constructed pipe condition assessment equipment

Figure 3.14: PCAE installed on a 1 000 ℓ water trailer

3.3 FIELD TEST PROCEDURE

3.3.1 Site inspection

The site inspection predominantly entails a survey of the pipeline network to be tested. As-built drawings of the pipeline network were requested before the survey was carried out. The as-built drawings were used to map and locate various pipeline infrastructure accessories that were critical to successfully carry out the tests. Notably, these pipeline accessories, for the most part, included isolation valves, fire hydrants and any alternative ideal points of connection to the pipeline.

Furthermore, any discrepancies between the as-built drawings and the associated pipeline on site were noted. Once the pipeline network had been satisfactorily surveyed, a suitable pipeline in the network was identified for testing. The selected test pipeline should adhere to the following criteria:

- It must have existing and functional isolation valves along the pipeline to isolate the pipe during the tests.
- It must have a point of connection above or below the ground that links to the pipeline and is located between the two isolation valves, e.g. a fire hydrant.
- The pipeline should be accessible by the PCAE

Each criterion listed above is important to carry out the test successfully. In particular, the pipeline connection point and the capability of isolating the pipeline are paramount, because these capabilities are critical components of the test procedure carried out when using the PCAE.

The site inspections also provide the opportunity to ensure that all the necessary equipment is available. Specifically, it is important to ensure that any connection apparatus required to connect the PCAE to the pipeline access point is arranged.

The connection points can differ from one pipeline to another. For example, along a potential stretch of pipeline, the connection may include, among others, fire hydrants, scour valves, air valves or, in some cases, a combination of these. Regardless of the connection found on site, it is important to ensure that, prior to the tests, a suitable adaptor is organised that can conveniently connect the PCAE to the pipeline connection point. In cases where multiple above-ground pipeline connection options are available, it is best to select the most convenient option.

With the assistance and consultation of the pipeline asset managers, information pertaining to the selected test pipe was gathered. This information consists of three aspects:

- Details of the pipeline's history and structural integrity
- Information regarding guidelines and specifications about how the pipeline isolation valves and access points are operated on site
- Information regarding all stakeholders who are potentially affected when the test pipe is decommissioned during the test, and sending out letters of notice to inform all affected stakeholders

3.3.2 Leak test procedure

The procedure for the condition assessment of the pipelines in the field is described in this section.

3.3.2.1 Step 1: Flush access point and initiate PCAE

Identify the most convenient connection point that links to the test pipe underground. Briefly open the connection point to allow a brief flush to clear any sediment and stagnant water in the test pipe. With the appropriate connection accessories, connect a reinforced hosepipe from the pipeline connection point to the PCAE tank connection and fill the water tank until it is full.

3.3.2.2 Step 2: Establish the operational pressure in the test pipe

To ensure that the operational pressure of the test pipe is not unknowingly exceeded, establish the pipeline's operating pressure. This is done by connecting the reinforced pipe from the pipeline connection point to the PCAE's testing connection. Open the PCAE's ball valve and allow the pressure transmitter to record the pressure in the pipeline.

3.3.2.3 Step 3: Set a minimum test pressure for the test pipe

Once the operational pressure is established, turn on the generator to power and start the PCAE's pressure-controlled, variable-speed pump. Set the PCAE's pressure-controlled, variable-speed pump to a minimum test pressure. This is done to ensure that the operating pipeline pressure is maintained at the set minimum test pressure, and never drops too low, risking introducing air in the pipeline.

3.3.2.4 Step 4: Isolation test

The isolation tests entail isolating the test pipe from the network and restricting flow. This is done by shutting the isolation valves of the test pipe, and ensuring that any offtake pipelines (e.g. service connections) that feed off the test pipe are isolated accordingly.

3.3.2.5 Step 5: Leak testing

The leak test entails a series of pressure and flow tests to assess the condition of the pipe and its isolation valves. To do this, the PCAE's pressure-controlled, variable-speed pump is set to a suitable test pressure. Subsequently, the water in the tank is pressurised back into the test pipe and the flow rate is monitored, via the recorder, until it stabilises. If the flow rate is zero, this means that there is no leak in the test pipe, and the test is stopped. However, if there is flow into the pipe, this will warrant a condition assessment investigation. A series of pressures is then set, and the corresponding stabilised flow rates are logged for the test pipe.

3.3.2.6 Step 6: Ending the test

All the network valves used to isolate the test pipe section will be open. Any offtakes that may have been closed will be opened so that the network can operate as before. Disconnect the PCAE from the test pipe connection point.

3.4 DATA ANALYSIS

3.4.1 Data recorded by the PCAE

The PCAE's recorder output produces data files containing the pressure and flow rate readings. These data files are downloaded from the recorder's storage media (the SD card), which can then be read using the ABB DataManager Pro v 1.7.3 analysis application. This application was the most suitable because of its compatibility with the ABB products installed in the PCAE.

DataManager Pro is a process data management and analysis application that is used to store and review data that is archived by an ABB ScreenMaster paperless recorder, which is mounted onto the PCAE. Figure 3.15 shows the DataManager Pro interface with its various features.

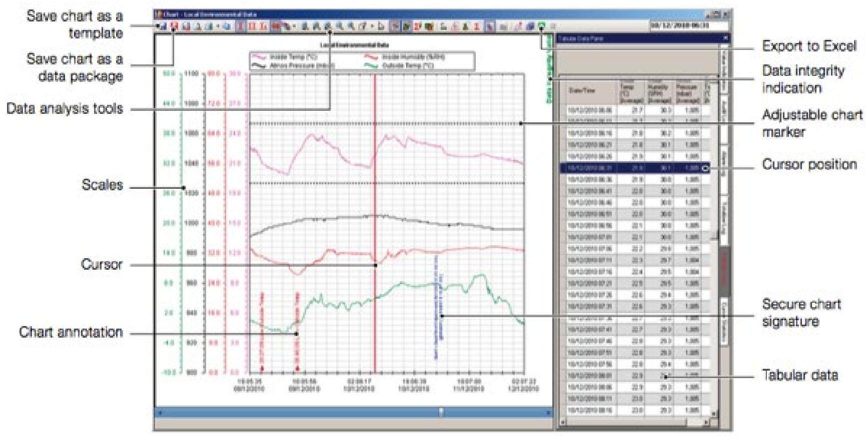

Figure 3.15: DataManager Pro chart view

Once the data has been imported, it can be viewed graphically, as shown in Figure 3.15, or exported to an MS Excel-compatible format for further analysis.

3.4.2 Data analysis calculations

Once the data is exported to an MS Excel-compatible format, a spreadsheet is generated and the following steps are performed:

3.4.2.1 Step 1: Interpretation of the data

Ensure that all the pressure and flow data units are recorded in SI unit format, i.e. m and m^3/s for the pressure and flow rate, respectively.

3.4.2.2 Step 2: Determine the actual pressure in the test pipe

Due to the fact that the pressure transmitter of the PCAE, which measures the pressure in the test pipe, is not located inside the test pipe, the recorded pressure requires some adjustment to quantify the actual pressure in the test pipe. In this case, the following pressures need to be accounted for to adjust the pressure accordingly:

- The head losses (h_f) due to the length of pipe between the pressure transmitter and the entrance to the test pipe
- Minor losses at bends, changes in diameter, valves and other components
- The static head (hs) due to the elevation difference between the PCAE and the test pipe on site

3.4.2.3 Step 3: Plot the pressure and flow rate against time

After establishing the actual pressure in the test pipe (h_{TP}), a graph portraying the flow rate (Q) and the pressure (h_{TP}) against time (t) is plotted in MS Excel. In this graph, the flow rate and pressure data are plotted on the primary and secondary y-axis, respectively, while the time is plotted on the x-axis. The primary objective of this graph is to verify that both flow and pressure stabilises and to identify the respective values at each stabilised step.

3.4.2.4 Step 4: Estimate the N1

Before the leakage exponent *N1* is estimated, a single flow rate (Q), and pressure (h_{TP}) reading for each step is determined by averaging the stabilised flow rate and pressure readings, respectively. The single flow rate (Q) and pressure (h_{TP}) reading are plotted against each other, with the flow rate on the y-axis, and the pressure on the x-axis of the graph. By fitting a power equation to the single flow rate vs the pressure data points, the *N1* value can be obtained. The power equation will have a coefficient value and an exponent value, representing the leakage coefficient (*C*) and the leakage exponent (*N1*), respectively.

3.4.2.5 Step 5: Calculate the effective leak area (C_dA)

The effective leak area (C_dA) obtained from the field test data represents the sum of all the leaks on the isolated test pipe. In other words, it demonstrates the size of all the accumulated leaks in the isolated test pipe. In mathematical terms, the effective area can be expressed as follows:

$$\sum \boldsymbol{C_d A} = \frac{\boldsymbol{Q}}{\sqrt{\boldsymbol{2\ g\ h_{TP}}}}$$

Substituting the single pressure (h_{TP}) and its corresponding flow rate (Q), the effective leak area can be calculated for each pressure step.

3.4.2.6 Step 6: Characterise leakage using the modified orifice equation parameters

The MOE leakage parameters for individual leaks consist mainly of an effective initial leak area (C_dA), and effective head-area slope (C_dm). In practice, pipelines are known to have a combination of leaks. Thus, taking into consideration the sum of all individual leaks, the MOE parameters become ΣC_dA and ΣC_dm, representing the sum of the effective leak area and the sum of the head-area slope, respectively.

If the sum of the effective leak area (ΣC_dA) is estimated at different pressures, as shown in Step 5, it follows that the sum of the effective leak area can be plotted against pressure. A linear trend line can be fitted onto the data to obtain the sum of the effective head-area slope (ΣC_dm) and the sum of the effective leak area (ΣC_dA) from the gradient and intercept terms of the equation, respectively.

CHAPTER 4: FIELD TESTS

4.1 INTRODUCTION

This chapter documents various bulk pipe condition assessment tests that were carried out using pipe condition assessment equipment.

The report then discusses a methodology that was developed to systematically analyse gravity lines with large elevation differences. Through the generation of nodes at different points on the pipeline, the extent of leakage at each node can be analysed. This creates an envelope of possibilities where leakage could potentially occur in the pipeline. Incorporating knowledge on typical failure mechanisms and their corresponding head-area slopes, the most likely leak locations may be identified. Finally, the results of various pipe condition assessment tests carried out in the field are reported in detail. In some cases, pipes were tested again after a certain period to assess any changes in their condition.

4.2 BS 8 PIPELINE – TEST 1

4.2.1 Introduction

The BS 8 test pipeline was a gravity pipeline, situated in the Caledon region, approximately 115 km from the Cape Town central business district. The pipeline was identified in consultation with the Overberg Water Board (OWB). The OWB is responsible for the operation and maintenance of the entire Overberg water pipe network.

Figure 4.1 depicts a section of the Overberg water pipe network, of which the BS 8 pipeline is a part. As can be seen, the BS 8 pipeline is an offtake pipeline that is charged from a main pipe (labelled in Figure 4.1 as S.HOOF1).

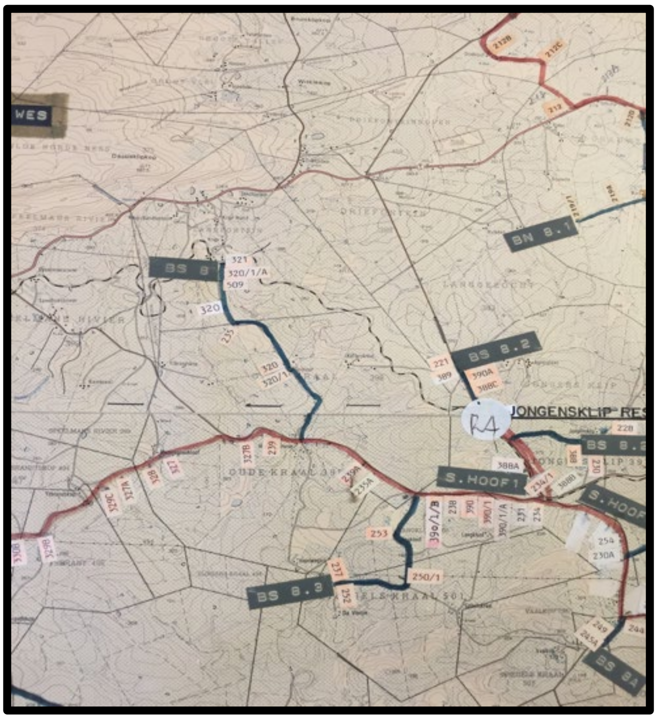

Figure 4.1: Part of the Overberg supply network that shows the BS 8 pipeline

The BS 8 pipeline comprises the following components: one isolation valve at the offtake, a closed flange at the top of the pipe, six user take-offs (mainly farmers), seven air valves and seven scour valves along the pipeline. The total length of the pipeline is approximately 5.4 km, with nominal diameters, ranging between 50 mm and 75 mm, and it has a burial depth of about 1.5 m. The pipeline is made up of various pipe material, including asbestos cement, steel and uPVC pipes.

The OWB indicated that, historically, the BS 8 pipeline has been a particularly problematic pipeline, with leakage being the major problem. In attempting to minimise the leaks, sections of the pipeline have been replaced with new uPVC pipes; hence, the pipeline is made up of mixed materials.

A data file, provided by OWB, with information about the layout and components of the BS 8 pipeline, was uploaded to Google Earth. Using the software, the BS 8 pipeline was plotted onto a satellite image of the area. Figure 4.2 depicts the satellite image layout of the BS 8 pipeline. It must be noted that the figure only shows the components necessary for the leak test performed in this study.

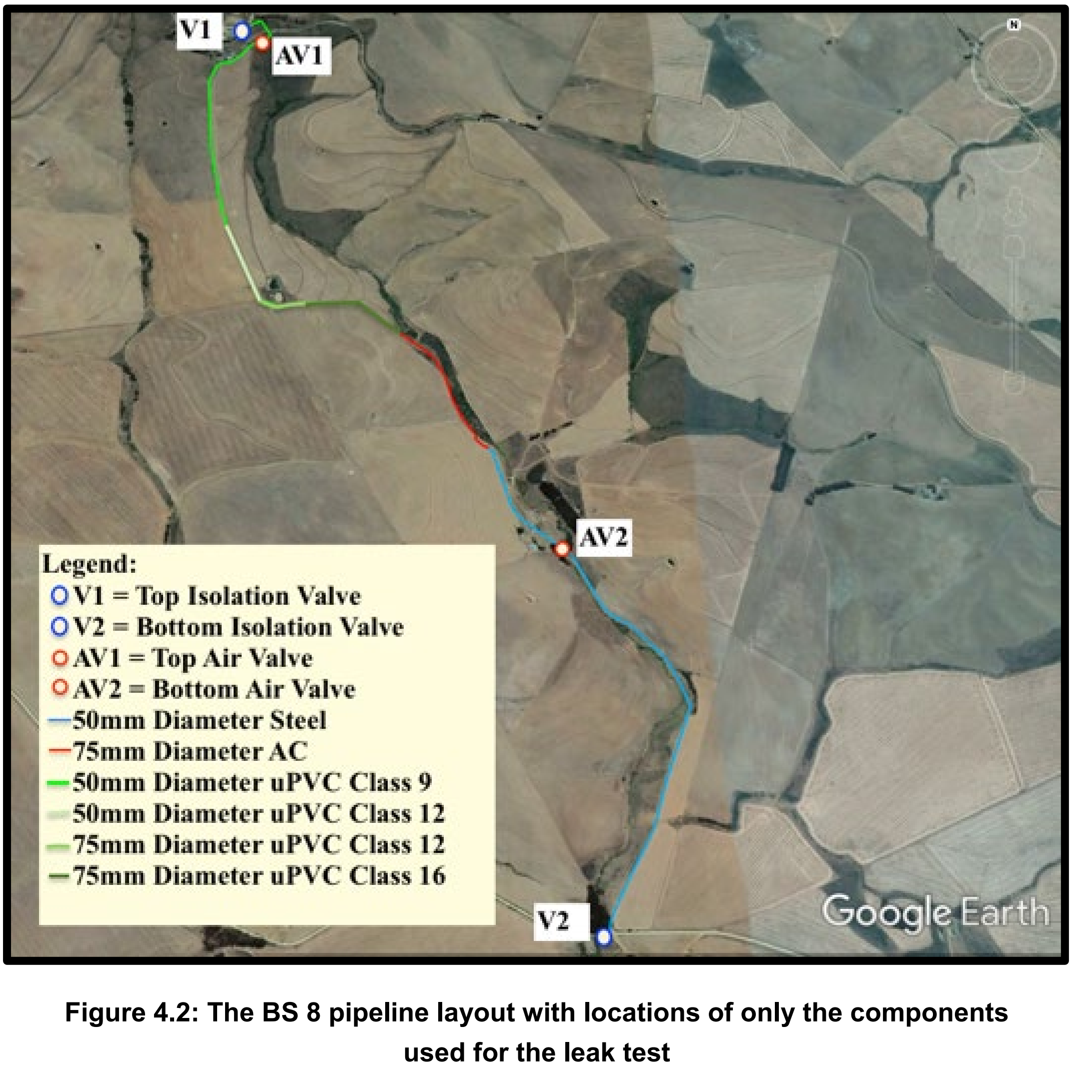

Figure 4.2: The BS 8 pipeline layout with locations of only the components used for the leak test

The overall elevation profile of the BS 8 pipeline was extracted from Google Earth.

Figure 4.3 shows the elevation profile from the bottom isolation valve (V2) to the top of the pipe. The overall elevation difference between the bottom and the top of the BS 8 pipeline was found to be approximately 190 m.

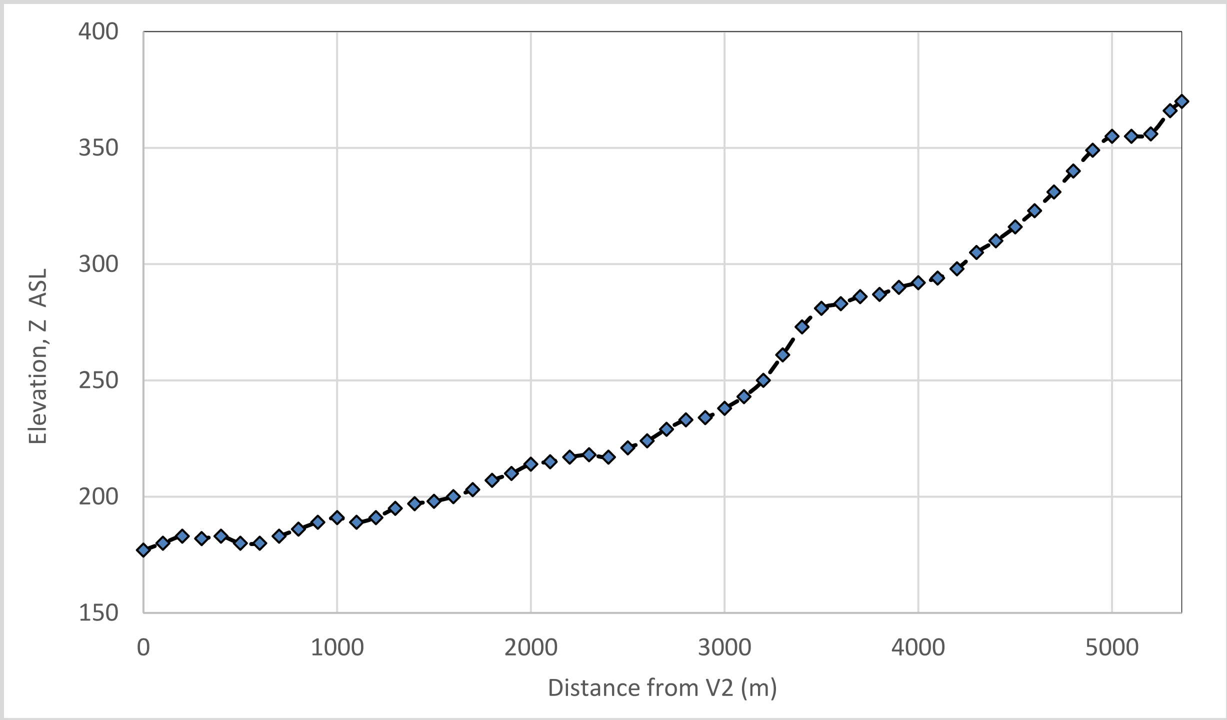

Figure 4.3: The Overberg test pipeline elevation profile

4.2.2 Procedure

The PCAE was connected to the BS 8 pipeline via an air valve. The air valve was the most convenient apparatus because of its ease of access. During the site visit, it was observed that all air valves on the BS 8 pipeline were housed in a small cylindrical concrete chamber, shown in Figure 4.4. Inside the concrete chamber, the air valve, shown in Figure 4.5(a), was connected to the BS 8 pipeline via a stop valve shown in Figure 4.5(b). The air valve and stop valve were connected to each other via a threaded connection.

Figure 4.4: The air valve's concrete chamber

(a) (b)

Figure 4.5: (a) The air valve; and (b) the BS 8 pipeline stop valve connection

When selecting the most suitable air valve connection point to connect to the PCAE, the main objective was to identify a connection point on the pipeline, such that, when the PCAE pump was activated from that connection point, the entire pipeline was pressurised. This was important to consider since the line was a gravity line and the PCAE pump could only deliver a maximum pressure head of 43 m, while the elevation head from the bottom of the BS 8 pipeline to the top was approximately 190 m. In other words, the PCAE pump would not be able to pressurise the entire pipeline if the PCAE was connected at the bottom of the BS 8 pipeline. Therefore, the most suitable connection point was at the top of the pipeline; hence, the topmost air valve (AV1 in Figure 4.2) was identified as the most suitable point to connect to the PCAE, and the PCAE was transported to its location along the BS 8 pipeline.

Prior to removing the air valve, the stop valve was closed to ensure that water does not flow from the BS 8 pipeline. The air valve was then removed and replaced with a 25 mm male-threaded Gardena quick release coupling. The quick release coupling connected the PCAE hosepipe to the BS 8 pipeline, as shown in Figure 4.6.

Figure 4.6: The PCAE hosepipe connected to the BS 8 pipeline

The operational pressure at AV1, to which the PCAE was connected, was examined and found to be about 15 m. This low pressure was expected, as this connection point was very close to the highest point on the BS 8 pipeline (see Figure 4.2). As a result of this low pressure, the water tank was filling very slowly. In order to speed up the process of filling the tank, a connection point with a higher pressure was required.

In consultation with the OWB operations team, a bottom air valve, shown as AV2 in Figure 4.2, was identified as a suitable connection point with a higher pressure. As a result of the higher pressure, the tank could be filled quicker. The PCAE was transported to AV2. Upon arrival, the air valve chamber at AV2 was opened and the stop valve closed. Thereafter, the air valve was removed and replaced with a Gardena fitting that was used to connect the hosepipe to the BS 8 pipeline.

Prior to filling the PCAE water tank, the stop valve on the pipeline was opened to flush the BS 8 pipeline. However, it should be noted that AV2 was located on the steel section of the BS 8 pipeline and, because the stop valve was initially opened too quickly, this stirred up sediments in the pipeline and made the water brown, as shown in Figure 4.7.

Figure 4.7: The colour of the water during the flushing process

After five minutes of flushing the BS 8 pipeline, it was observed that the water did not change colour and remained brown. This was brought to the attention of the OWB operations team on site. They were not particularly concerned about the colour of the water, and granted permission to continue with the test. The PCAE tank was then manually filled with the brown water from the BS 8 pipeline from the top, as shown in Figure 4.8.

Figure 4.8: The PCAE water tank being filled up at AV2

Once the tank was full, the PCAE was transported back to AV1, where the PCAE was reconnected to the BS 8 pipeline. The PCAE pump was switched on, and the leak test executed.

4.2.3 Results

4.2.3.1 Data interpretation

A graphic representation of the raw flow and pressure data, plotted against time, is shown in Figure 4.9. The flow rate represents the leakage flow rate, and the graph clearly shows that there was significant leakage on the BS 8 pipeline.

It is typically expected that the pressure and flow rate profile, over the same period of time, would show similar profile patterns. For this test, for example, both data profiles were expected to show a clear step-up and step-down pattern that is repeated for the duration of the test. However, Figure 4.9 suggests that only the pressure data showed a clear step-up and step-down pattern, while the flow rate data did not vary significantly throughout the period of the test. This was an unexpected result. However, this anomaly can be attributed to the elevation difference between the point at which the PCAE was connected to the BS 8 pipeline and the point on the pipeline where the leakage actually occurred.

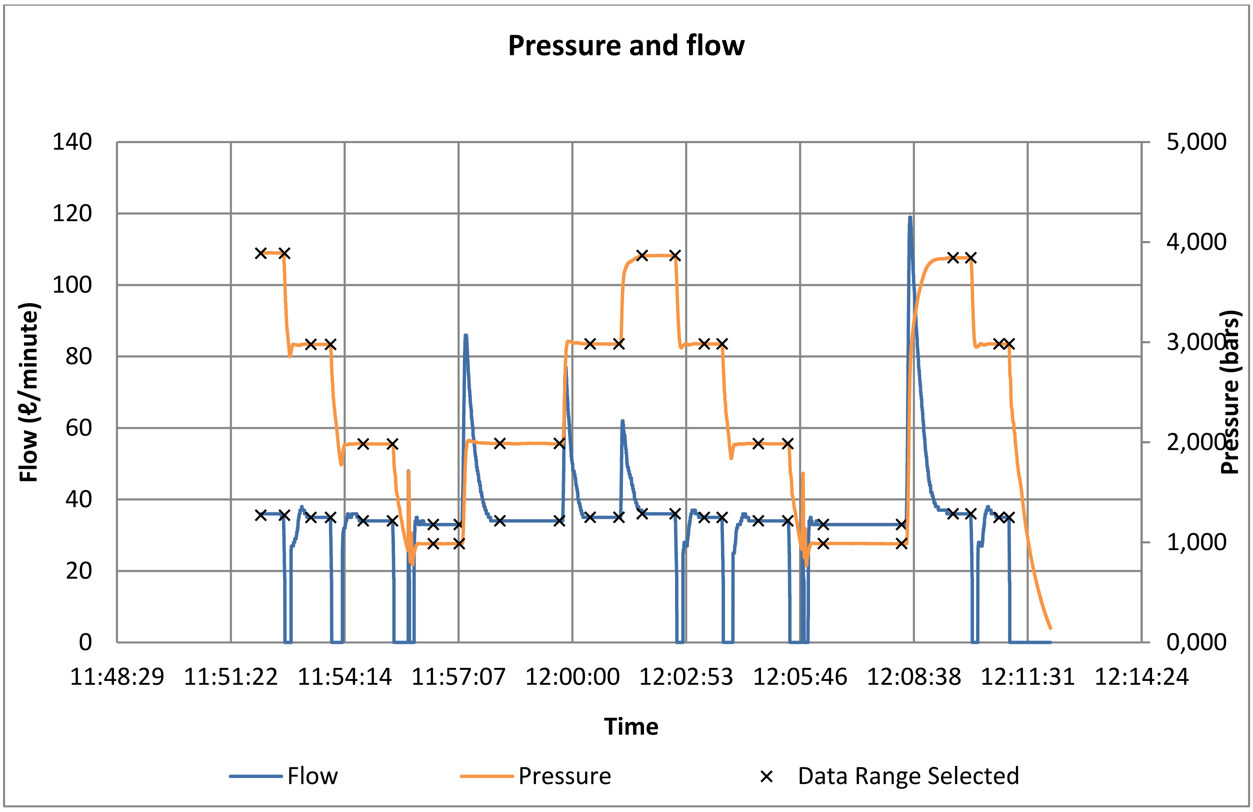

Figure 4.9: The pressure and flow profile for the Overberg test pipe

In general, it was observed, from Figure 4.9, that the pressure steps were more stable compared to the flow steps. It was also observed that the largest fluctuations in the flow steps occurred at the beginning of the step, typically when the pressure was changed or varied. For instance, when the pressure step is increased, a sudden spike in the flow rate occurs before the flow rate stabilises; and when the pressure is decreased, the reverse happens. This is because a sudden increase in pressure increases the pipe diameter and, consequently, increases the volume of water entering the pipe. A decrease in pressure, on the other hand, reduces the volume of water entering the pipe and, thus, will result in a sudden reduction in flow rate.

For this test, it was important to take into account the significant elevation difference of about 190 m between the top and the bottom of the test pipeline. This is important because, depending on where the leakage occurred in the test pipeline, the pressure readings obtained by the PCAE need to be adjusted to reflect the pressure at the point at which the leak is anticipated in the pipeline, failing which, the results could be affected. Because the pipeline is a gravity line, the pressure along the pipeline can be determined by simply adding the static head pressure due to the elevation difference to the pressure measure by the PCAE.

Since the PCAE was connected at the top of the test pipeline, the measured pressure, in Figure 4.9, represented only the pressure at the top of the test pipeline. However, considering that the location at which the leakage occurred was unknown, the measured pressure had to be adjusted for different points on the BS 8 pipeline, so that various scenarios could be analysed. For this purpose, the centre and bottom of the pipeline were additional points considered for analysis. In other words, the following three scenarios were analysed for this test:

- The first scenario considers whether the leak is near the top of the pipeline.
- The second scenario considers whether the leak is near the centre of the pipeline.
- The third scenario considers whether the leak is near the bottom of the pipeline.

It is important to note that, although the pressure must be adjusted to determine the pressure at the centre and at the bottom of the test pipeline, the measured flow rate remained the same for all scenarios. This is because the measured flow rate represents the total leakage flow rate of the entire test pipeline and, regardless of where the pressure is measured, this leakage will be the same. For each measured pressure and flow step in Figure 4.9, the selected stabilised data range was averaged to obtain a single measured pressure and flow data point. Table 4.1 shows the pressure variations for the three case scenarios and, as expected, the pressure was highest at the bottom of the test pipeline.

Table 4.1: Flow rate and pressure values for the three case scenarios

Average flow (ℓ/min)	Corrected pressure at the top (m)	Corrected pressure at the centre (m)	Corrected pressure at the bottom (m)
36	37	127	217
35	27	117	207
34	17	107	197
33	7	97	187
34	17	107	197
35	27	117	207
36	36	126	216
35	27	117	207
34	17	107	197
33	7	97	187
36	36	126	216
35	27	117	207

4.2.3.2 The N1 leakage parameters

The flow and pressure data points, from Table 4.1, were plotted on a graph for each case scenario, and a power equation was fitted to the data points, as shown in Figure 4.10. The power equation was used to determine the leakage exponent *N1* and the leakage coefficient *C* for each scenario. It can be seen that the three power equations had an R^2 greater than 0.9, suggesting that the power equation was a good fit to the data points for all three cases.

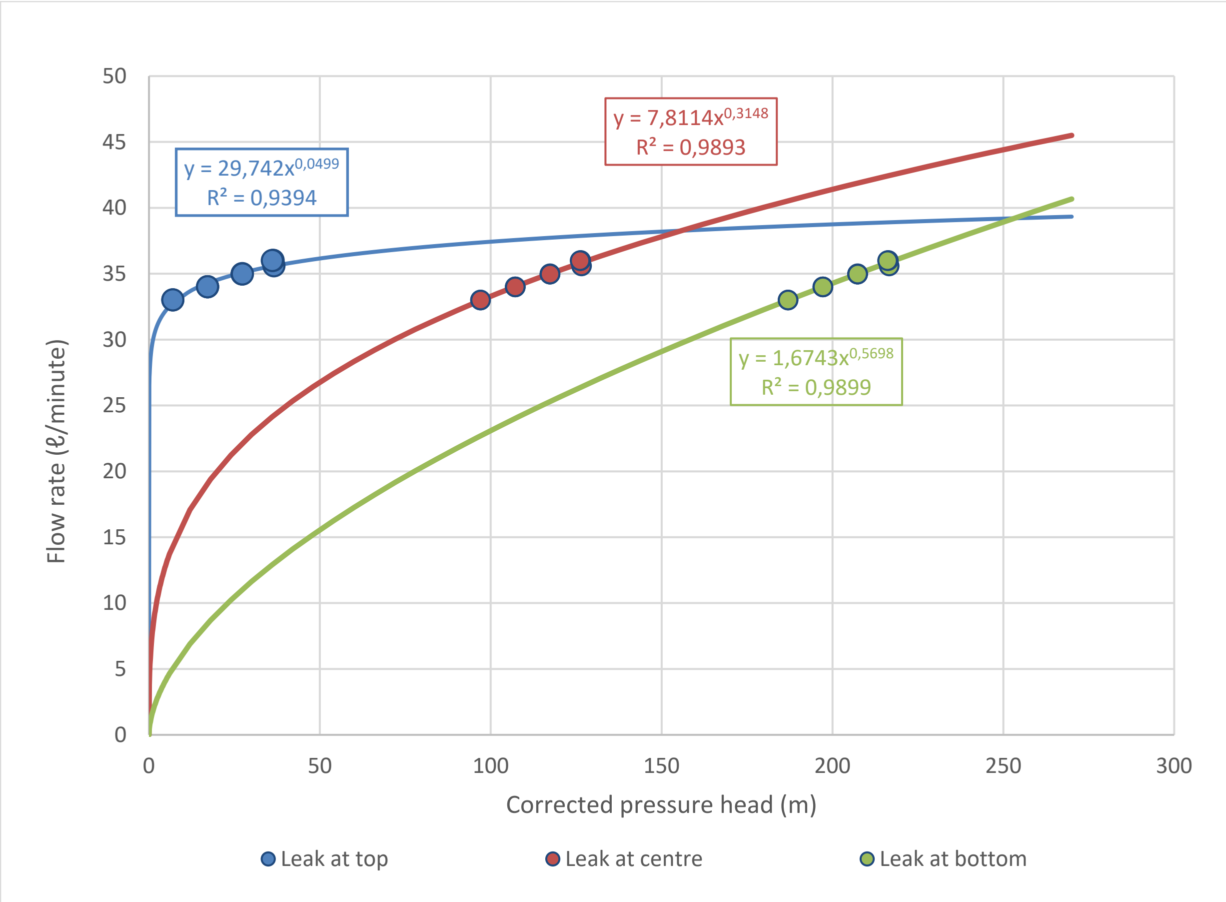

Figure 4.10: Flow rate against pressure for the three scenarios

From Figure 4.10, it can be seen that the data points with higher pressure simply shifted the flow rate data to the right-hand side of the graph. Consequently, the three scenarios presented different power equations and, therefore, different *N1* leakage parameters. The results in Figure 4.10 show that, if the leak was at the top or at the centre, the *N1* leakage exponent would be 0.0499 and 0.31, respectively, which is less than the theoretical value of 0.5. However, if the leak was at the bottom, the *N1* leakage exponent would be slightly greater than the theoretical value, at 0.57. Table 4.2 shows a summary of the *N1* leakage parameter results.

Table 4.2: The results of the *N1* leakage parameters

Scenario	*N1*	C	R^2
Leak at the top of the pipe	0.049	29.7	0.94
Leak at the centre of the pipe	0.32	7.81	0.99
Leak at the bottom of the pipe	0.56	1.67	0.99

From Table 4.2, a comparison can be made between the leakage parameter results of the three case scenarios. For the leak at the top, where the pipe material was a uPVC section, the *N1* of 0.049 was highly unlikely, as this result suggests that the leak closes with pressure, which is not common in plastic pipes in the field (Greyvenstein, 2005; Malde, 2015). For the leak at the centre, where the BS 8 pipeline consists of an asbestos cement pipe section, the *N1* of 0.32 is also unlikely for such a rigid pipe. The *N1* of less than 0.5 for the leak at the centre suggests that the leak closes as the pipe pressure increases. For the leak at the bottom, on the steel pipe section, the *N1* was slightly greater than 0.5, which is a typical *N1* result for steel pipes with round holes (Ferrante et al., 2014). Based on this, the most likely result was the result found for the leak at the bottom of the pipe.

4.2.3.3 Modified orifice equation leakage parameters

In order to determine the MOE leakage parameters, the effective initial leak area (C_dA_0) and effective head-area slope (C_dm) for each case scenario had to be determined. This was done by determining the effective leak areas (C_dA) at each pressure step using the orifice equation. Table 4.3 shows the results of the effective leak areas for each case scenario, i.e. if the leak was at the top, at the centre or at the bottom of the BS 8 pipeline.

Table 4.3: The effective area (C_dA) against pressure (h) for the three scenarios

Corrected pressure at the top (m)	Corrected pressure at the centre (m)	Corrected pressure at the bottom (m)	Effective area at the top (mm^2)	Effective area at the centre (mm^2)	Effective area at the bottom (mm^2)
37	127	217	22	12	9.10
27	117	207	25	12	9.14
17	107	197	31	12	9.11
7	97	187	47	13	9.08
17	107	197	31	12	9.11
27	117	207	25	12	9.15
36	126	216	22	12	9.21
27	117	207	25	12	9.14
17	107	197	31	12	9.11
7	97	187	47	13	9.08
36	126	216	23	12	9.21
27	117	207	25	12	9.14

The effective leak area and pressure data points, from Table 4.3, were plotted on a graph for each case scenario. A linear equation was fitted to the data points, as can be seen in Figure 4.11.

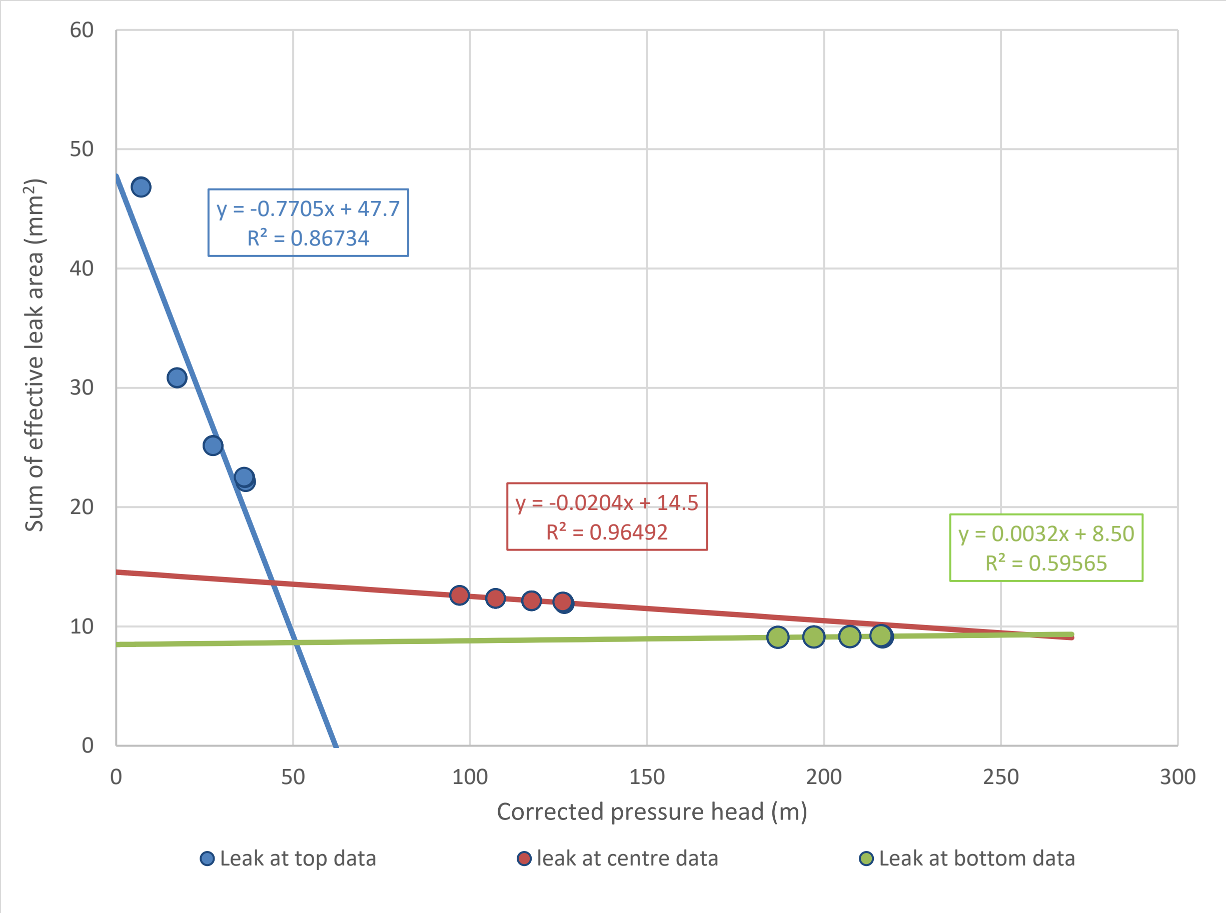

Figure 4.11: Modified orifice equation leakage parameters

Figure 4.11 shows how the effective leak area varies with the pressure head for the three scenarios, i.e. for leaks at the top, centre and bottom. The effective leak area changes differently for all three scenarios: the leak at the top and the centre portrayed a negative head-area slope of -0.77 mm^2/m and -0.02 mm^2/m, respectively, and, therefore, the leak area contracted as pressure increased; while the leak at the bottom portrayed a small positive head-area slope of 0.0032 mm^2/m and, therefore, the leak area expanded ever so slightly with increasing pressure.

It was also clear that the initial leak areas (C_dA_0), for all three scenarios were different. The leak at the top had the largest initial leak area of 47 mm^2, followed by the leak at the centre, with a C_dA_0 of 14.5 mm^2. The leak at the bottom had the smallest initial leak area of 8.50 mm^2.

Table 4.4 summarises the MOE leakage parameter results for the three case scenarios.

Table 4.4: Results of the modified orifice equation leakage parameter

Scenario	$\sum C_dA_0$ (mm^2)	$\sum C_dm$ (mm^2/m)
Leak at the top of the pipe	47.7	-0.77
Leak at the centre of the pipe	14.5	-0.02
Leak at the bottom of the pipe	8.50	0.0032

Table 4.4 compares the MOE leakage parameters for the three case scenarios. For the leak at the top, the result obtained suggested that the uPVC section of the BS 8 pipeline had a circumferential crack, which was unlikely to occur because the uPVC pipes were relatively new installations.

For the leak at the centre, the results obtained suggested that the asbestos cement section of the BS 8 pipeline had a circumferential crack, which resulted in the negative head-area slope. This is inconsistent with typical failures reported to occur in asbestos cement pipes, which commonly display longitudinal cracks (Greyvenstein, 2005).

Finally, for the leak at the bottom, the results obtained suggested that the steel section of the BS 8 pipeline had small round holes. This is consistent with small corrosion holes that have been reported to occur in metallic pipes, such as steel. The small positive head-area slope is also consistent with findings from experimental and modelling studies (Cassa and Van Zyl, 2014; Malde, 2015; Nsanzubuhoro and Van Zyl, 2016) that have investigated the leak behaviour of round holes.

4.2.3.4 The N1 and modified orifice equations

The *N1* equation and the MOE's flow prediction, for each case scenario, was determined to compare the equations to the data. Table 4.5 shows the *N1* equation and the MOE for the three scenarios. It is important to note that the leakage parameters obtained in Chapter 4.2.3.2 and Chapter 4.2.3.3 were used to formulate these equations.

Table 4.5: The N1 and modified orifice equation for the three case scenarios

Scenario	N1 equation *(ℓ/minute)*	MOE *(60 x 10^{-3} ℓ/minute)*
Leak at the top	$Q = 29.7\ h^{0.049}$	$Q = \sqrt{2g}(47.7h^{0.5} - 0.77h^{1.5})$
Leak at the centre	$Q = 7.81\ h^{0.36}$	$Q = \sqrt{2g}(14.5h^{0.5} - 0.02h^{1.5})$
Leak at the bottom	$Q = 1.67\ h^{0.56}$	$Q = \sqrt{2g}(8.50h^{0.5} + 0.0032h^{1.5})$

Using the equations in Table 4.5, the flow rates were generated for various pressure heads, ranging from 0 m to 270 m. The flow rates for the *N1* equation and the MOE were then plotted with the data to see how well the equations fitted the data. Figure 4.2 shows the *N1* equation and the MOE alongside the data points for the three scenarios.

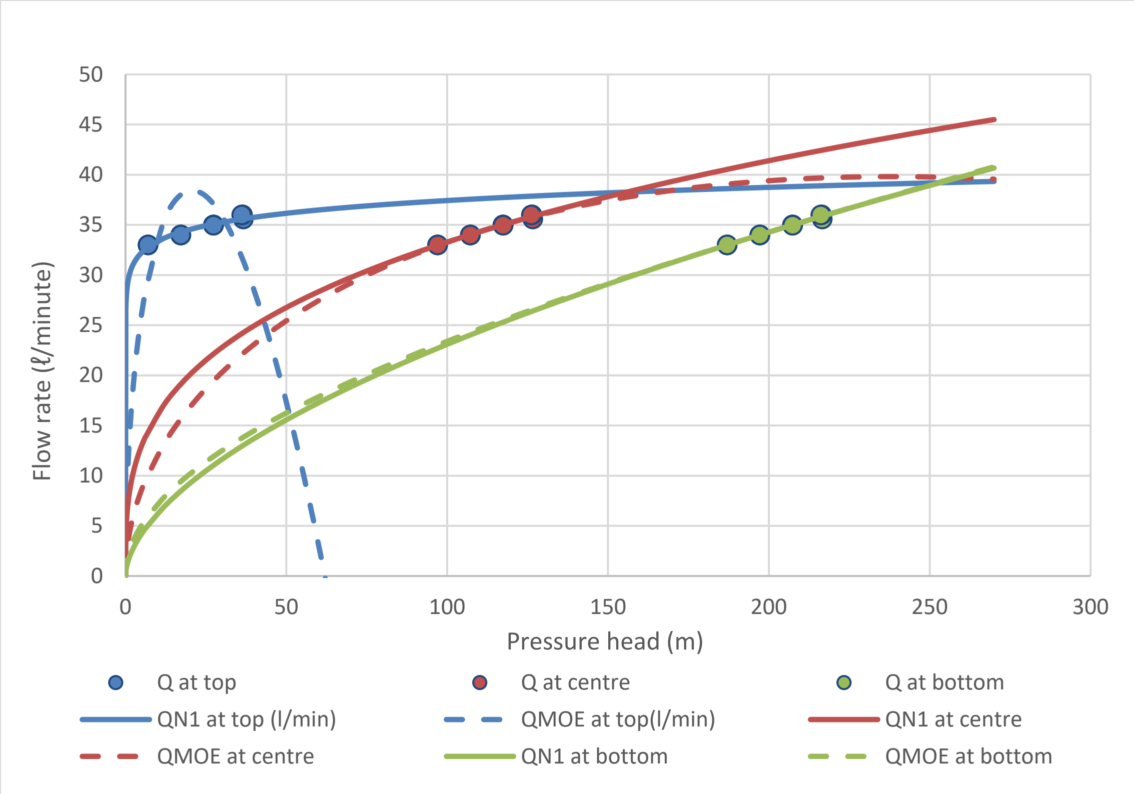

Figure 4.12: Comparison of the *N1* and modified orifice equation

From Figure 4.12, it can be seen that, for each case scenario, the *N1* equation and the MOE's predicted flows are different for the examined pressure range.

For the leak at the bottom, the *N1* equation and the MOE are almost identical and fit the data points well. This can be attributed to the nature of the leak: since it is a round hole with a very small head-area slope, it can be assumed that only the first term of the MOE contributes significantly. A close look at the first term of the MOE, for the leak at the bottom, clearly shows that its form is very similar to the *N1* equation obtained for the leak at the bottom, with a 12% difference in their leakage exponents.

For the leak at the centre, the *N1* equation and the MOE predicted the data points well. However, differences were seen, especially at lower and higher pressures of the measured data. The N1 equation predicts a higher flow rate at lower pressure (Van Zyl et al., 2017). For the leak at the centre, it was observed that the *N1* equation and the MOE fitted the data points well. However, at pressures below 90 m and above 130 m, the *N1* equation predicted higher flows, compared to the MOE. It can also be seen that the flow predicted by the MOE reaches a peak and starts reducing with pressure. This can be attributed to the negative head-area slope that indicates that the leak closes with increasing pressure.

For the leak at the top, it was observed that the *N1* equation and the MOE showed the largest differences. For this scenario, only the *N1* equation fitted the data points. The MOE showed a negative parabolic relationship between the predicted flow and pressure. This relationship can be attributed to the large negative head-area slope that resulted in the second term of the MOE, which accounts for the varying leak area being dominant. This finding was consistent with the theoretical discussion about the behaviour of leak openings with negative head-area slopes and positive initial leak areas (Van Zyl et al., 2017).

4.2.4 Actual leak condition

The OWB team had scheduled a pipe replacement for the steel section of the BS 8 pipeline. This replacement was triggered by a stream that had emerged near this section of the BS 8 pipeline. This pipe replacement was due to take place two weeks after the condition assessment was done, using the PCAE. The total length of steel pipe that was replaced was approximately 100 m.

The OWB revealed that small round holes were found on the top of the steel pipe. This finding was consistent with the results of the condition assessment leak test. The detected leakage on the steel section of the BS 8 pipeline could, therefore, be characterised as follows:

Table 4.6: Characteristics of the leakage detected on the steel section of the BS 8 pipeline

Characteristic	Leakage parameter	Units
Initial leak area	8.50	mm^2
Head-area slope	3.2×10^{-3}	mm^2/m
Leakage exponent N1	0.56	
Leakage coefficient C	1.67	

The total size of the leaks was 8.50 mm^2 and the leaks expanded by 3.2 mm^2/m of pressure head. It was therefore not very sensitive to pressure. The *N1* leakage exponent was 0.56, also suggesting that the leak was not very sensitive to pressure. The obtained leakage parameters were consistent with a round hole leak, potentially due to corrosion on the steel pipe.

4.3 BS 8 PIPELINE – TEST 2

4.3.1 Introduction

A second test was conducted on the same BS 8 pipeline in the Overberg region. The second test was done after a section of the steel pipe had been replaced. This section will discuss the test procedure of the second tests and the field test results that were obtained. The results of the second tests will be compared to the results obtained in the first test to assess whether the extent of the leakage had improved or become worse after the steel section had been replaced.

4.3.2 Procedure

The first step was to fill the PCAE water tank. Unlike Test 1, where the tank was filled via a bottom air valve connection on the BS 8 pipeline, for Test 2, the tank was filled via a reservoir. Figure 4.13 shows the location of the reservoir in the Overberg network, labelled R4 in the figure. This reservoir is the Jongensklip Reservoir and stores water from the main pipe (S. Hoof), through which the BS 8 pipeline is charged. The stored water in the reservoir is then gravitated back to the main pipe via the BS 8.2 pipeline.

Figure 4.13: Location of the Jongensklip Reservior

Figure 4.14 shows the Jongensklip Reservoir on site. The reservoir had a tap connection. A hosepipe was connected to the tap, and was directed into the water tank, as depicted in Figure 4.15. The tap from the reservoir was opened until the tank was full.

Figure 4.14: Jongensklip Reservoir

Figure 4.15: Filling the PCAE water tank using a hosepipe connected to the tap reservoir

Once the tank was full, the PCAE was transported to the point on the BS 8 pipeline where it would be connected for the condition assessment test. As in Test 1, the most suitable point of connection for Test 2 was the topmost air valve, for reasons similar to those highlighted in Chapter 4.2.2. Figure 4.16 shows the location of the topmost air valve (AV1) on the BS 8 pipeline layout.

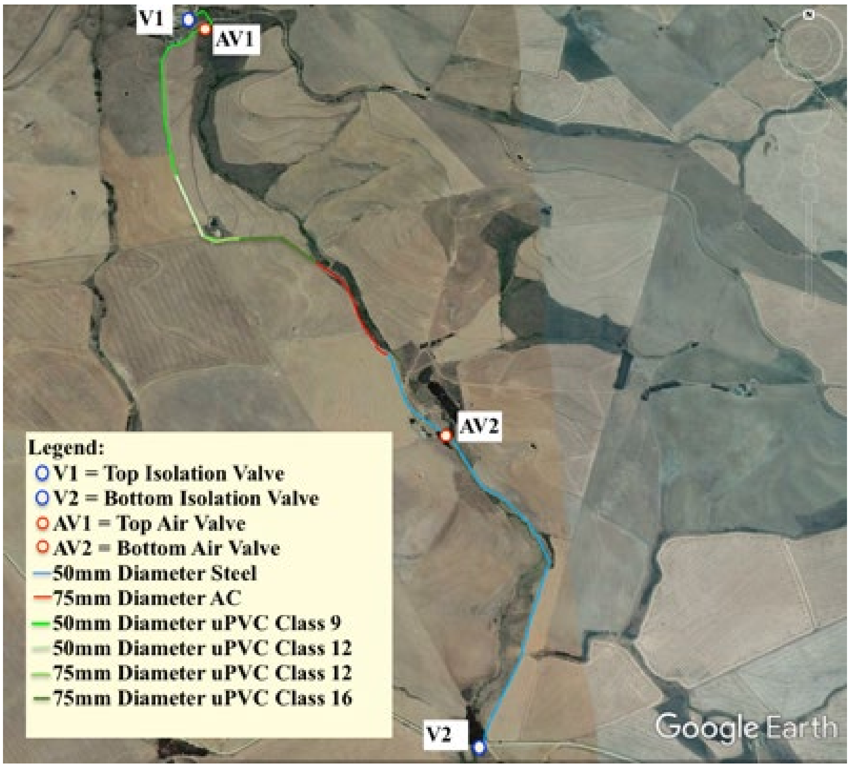

Figure 4.16: AV1 where the PCAE was connected for the leak test

After removing the air valve at AV1 and connecting the 50 mm delivery hosepipe, it was observed that no water was flowing from the BS 8 pipeline. Water was expected to flow directly from the BS 8 pipeline once the shut-off valve at the connection point was fully opened. However, this was not the case.

After investigating various possibilities as to why no water was flowing from the BS 8 pipeline, it was discovered that the OWB operations team assisting on site had isolated the BS 8 pipeline about 20 minutes prior to the research team's arrival. This prolonged pipe isolation period had some implication on the pipeline, as the water in the pipeline had already started draining. Subsequently, there was no water at the top of the pipe (AV1) where the PCAE was connected.

In order to resolve this problem, the bottom isolation valve (V2 in Figure 4.16) was opened to allow the BS 8 pipeline to be recharged. It was not known how long it would take to recharge the pipe, so the shut-off valve at the point of connection was left open while the pipeline recharged to monitor when the pipeline was sufficiently charged.

After the BS 8 pipeline was sufficiently charged, the PCAE was connected to the connection point to carry out the leak test. Prior to carrying out the leak test, the BS 8 pipeline was isolated again by closing the bottom isolation valve.

4.3.3 Results

4.3.3.1 Data interpretation

The isolated BS 8 pipeline was analysed as one system with the PCAE connected to it, as depicted in Figure 4.17. In the figure, the BS 8 pipeline is shown with its various pipe materials. Nodes were assigned to every connection point, as well as any change in pipe material and pipe diameter on the BS 8 pipeline. Table 4.7 shows a summary of the elevations for all the nodes.

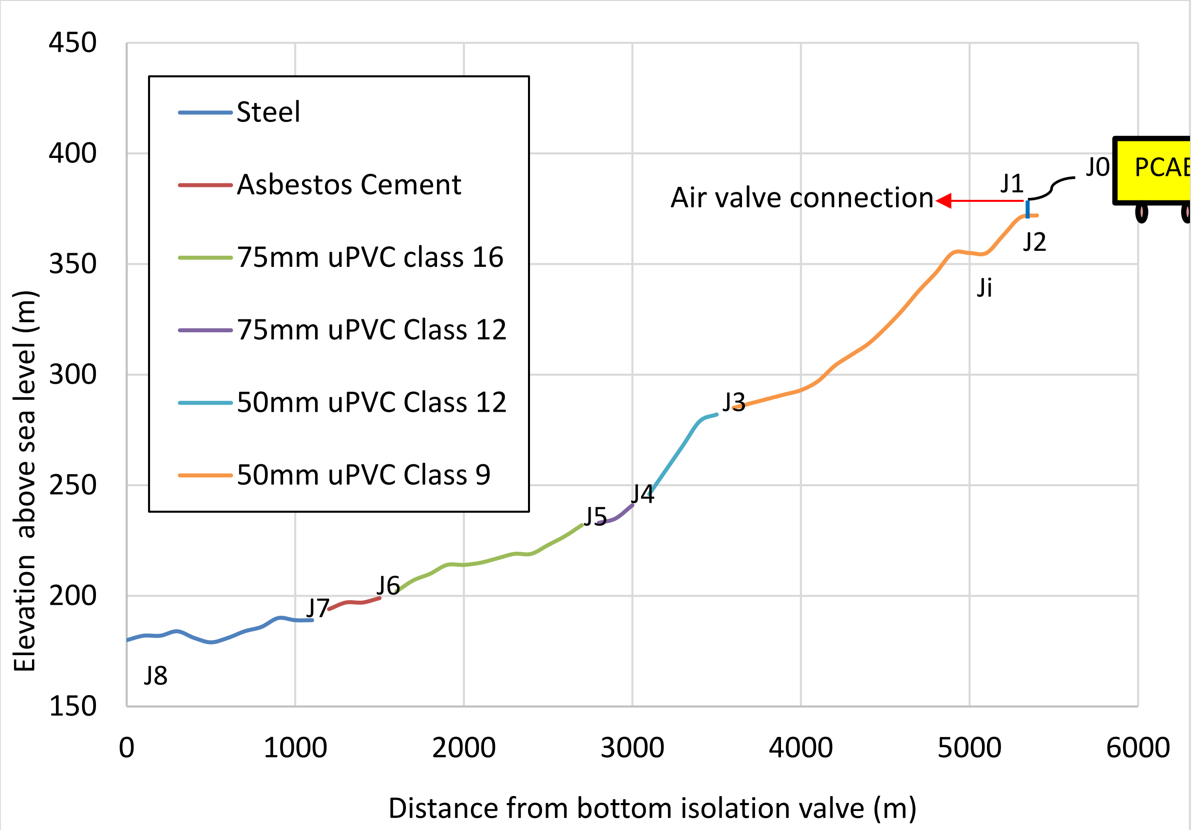

Figure 4.17: The elevation profile of the BS 8 pipeline with its various pipe material and diameters

Table 4.7: Node elevations

Node	Elevation (m)
J0	373
J1	371.5
J2	370
J3	303
J4	283
J5	275
J6	234
J7	204
J8	180

Figure 4.18 gives a graphic representation of the raw data flow and pressure recorded by the PCAE at the connection point. It can be seen from the figure that, when the flow rate and pressure both stabilised, the pressure was reduced twice and, thereafter, increased. The results show that a very large leak was present in the pipe with a flow rate as high as 190 ℓ/minute (11.4 m^3/h) at a device pressure of only 2 bar. Due to the large leakage in the pipeline, five steps were achieved for the test before the tank was emptied.

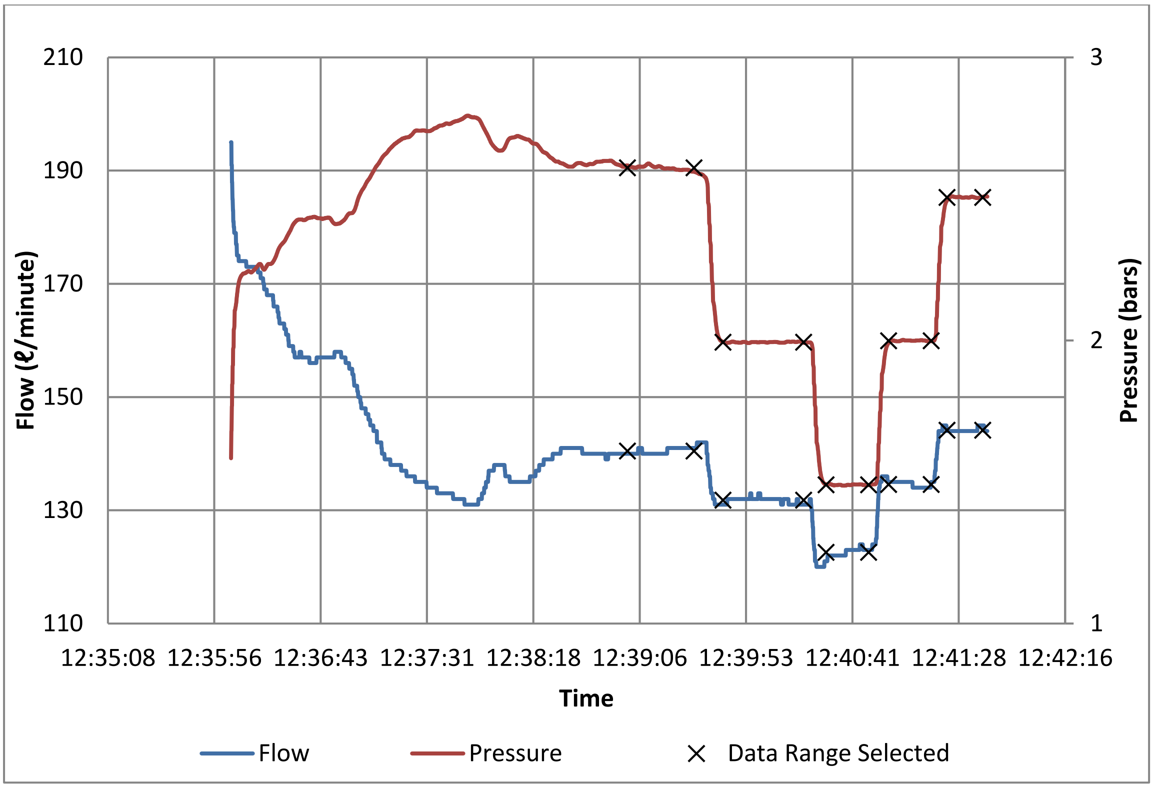

Figure 4.18: Flow and pressure profile

The graphic representation of the data was then used to identify stabilised levels of flow and pressure. The pressure and flow data range selected is indicated by the markers in Figure 4.18. The flow and pressure data for each node was determined.

The flow and pressure data obtained for nodes J1, J2 and Ji (See Figure 4.17) were the only data set used for this analysis. This was because the pressures at Node J3 to Node J8 were found to be negative. The negative pressures were as a result of the high friction head losses experienced on the pipe section between Node J2 and Node J3 containing a uPVC Class 9 pipe with a diameter of 50 mm. The negative pressures suggested that a leak could not physically occur at this point. For this reason, an intermediate point upstream of Node J3 with positive pressures was required for the analysis; hence the introduction of Node Ji, which was located about 200 m downstream of Node J2. Table 4.8 shows the results of the flow and pressure at nodes J1, J2 and Ji.

Table 4.8: The results of flow and pressure at nodes J1, J2 and Ji

Q (m^3/s)	h_{J1} (m)	h_{J2} (m)	h_{Ji} (m)
2.34E-03	27.59	26.92	69.70
2.20E-03	21.36	20.94	64.40
2.04E-03	16.29	16.12	60.25
2.24E-03	21.40	20.90	64.15
2.40E-03	26.49	25.71	68.20

4.3.3.2 The N1 leakage parameters

Figure 4.19 shows the flow and pressure data plotted for nodes J1, J2 and Ji. It can be seen that the *N1* values for nodes J1 and J2 were very similar, at 0.29 and 0.3, respectively. Even though these *N1* values were unrealistic, it was clear from these results that the *N1* value was increasing in the downstream direction. Considering that Node Ji was located downstream of Node J2, the N1 value was expected to be higher, as can be seen in Figure 4.19, which shows an *N1* value of 1 for Node Ji. This result is consistent with the behaviour of plastic pipes and could therefore potentially present the most realistic leak on the pipeline.

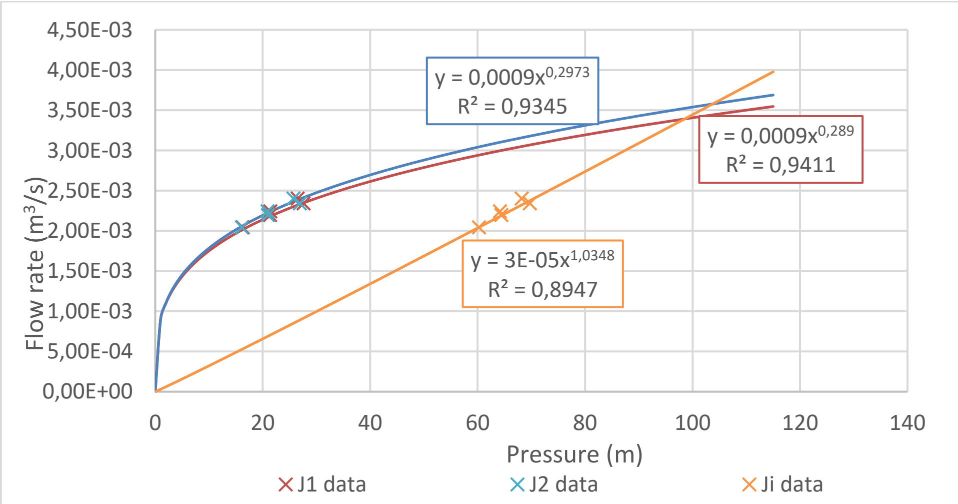

Figure 4.19: Flow and pressure data for nodes J1, J2 and Ji

A summary of the *N1* leakage parameters is provided in Table 4.9.

Table 4.9: Summary of the N1 leakage parameters found for the BS 8 pipeline Test 2

Node	N1 leakage exponent	Leakage coefficient
J1	0.29	9×10^{-4}
J2	0.3	9×10^{-4}
Ji	1	3×10^{-5}

4.3.3.3 Modified orifice equation

The effective area against the pressure head data for nodes J1, J2 and Ji are plotted in Figure 4.20. It can be seen that nodes J1 and J2 had very similar results, both portraying a negative head-area slope of -1.1 mm^2/m and -1.0 mm^2/m, respectively, suggesting that the leaks at these nodes were closing with increasing pressure. On the other hand, the leak at Node Ji, had a positive head-area slope of 0.5 mm^2/m, suggesting that the leak increases with increasing pressure.

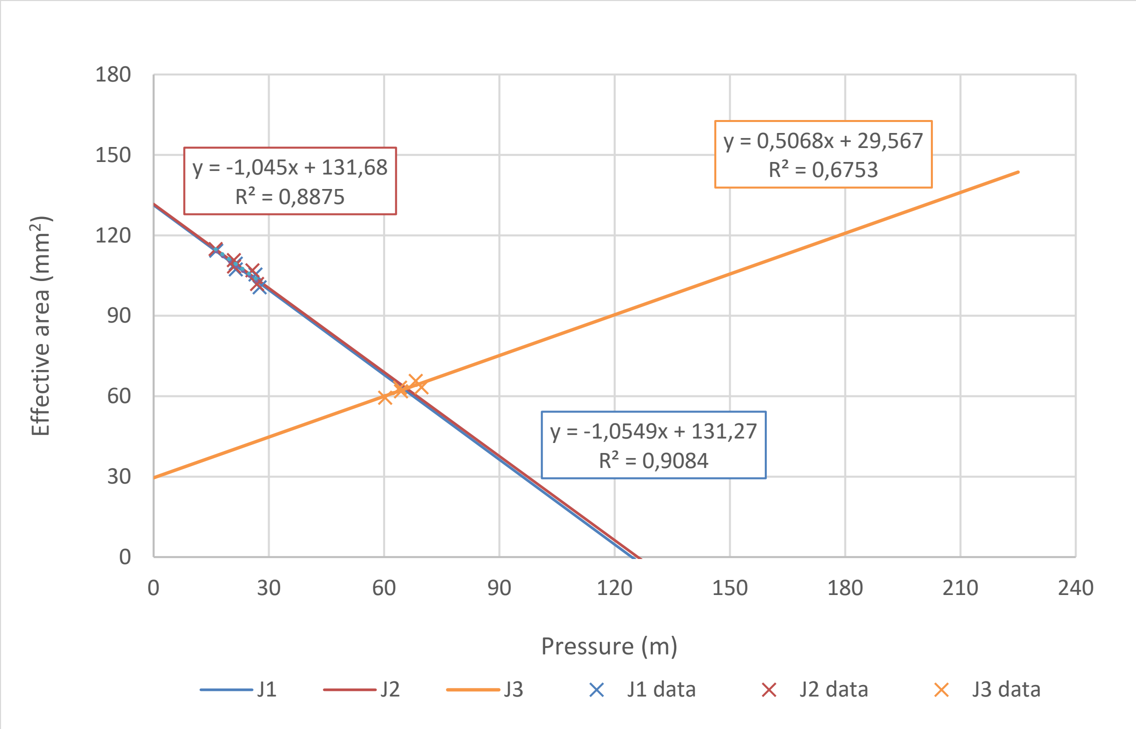

Figure 4.20: Effective area against the pressure head for nodes J1, J2 and Ji

4.3.4 Comparison of BS 8 pipeline tests 1 and 2

Table 4.10 shows a summary of Leak Test 1 and Leak Test 2 carried out on the BS 8 pipeline. The table shows that the leakage characteristics were different for the two tests. The results of Leakage Test 1 showed that the leak was from a round hole on the steel section of the BS 8 pipeline that was 50 mm diameter. This was found to be correct.

Leakage Test 2, which was done after a section of the steel pipe had been replaced, showed that a large new leak had occurred on the pipe, most likely in the middle or upper parts of the uPVC pipe section.

Table 4.10: Comparison of results from Test 1 and Test 2 of the BS 8 pipeline

Leak characteristics	Test 1	Test 2
Section on the pipe	Steel	uPVC
Effective leak area (mm^2)	8.5	29.567
Effective head-area slope (mm^2/m)	3.2×10^{-3}	0.5
N1	0.56	1
Leak type	Round hole	Longitudinal crack

4.4 WINGFIELD PIPELINE – TEST 1

4.4.1 Introduction

The test pipeline examined at the Wingfield military base was a bulk asbestos cement pipeline. Figure 4.21 shows the layout of the Wingfield pipeline, spanning from valve V1 to valve V4. The Wingfield pipeline is 1 000 m in length, with a nominal diameter of 300 and a pipeline depth below ground level of 1 m.

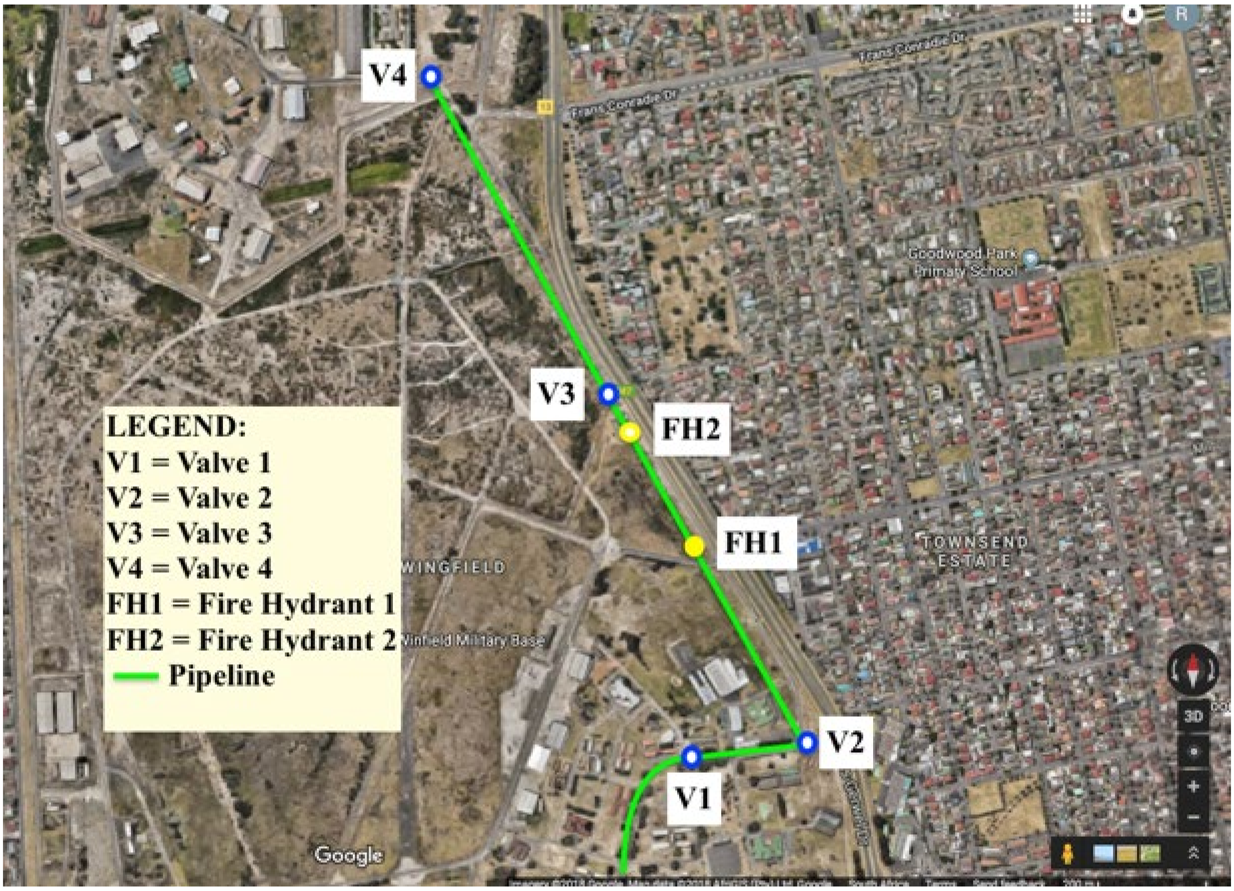

Figure 4.21: Wingfield pipeline layout

Figure 4.22 shows the elevation of the Wingfield test pipe from V2 to V4. Figure 4.21 shows that the overall elevation did not vary much for the test pipe.

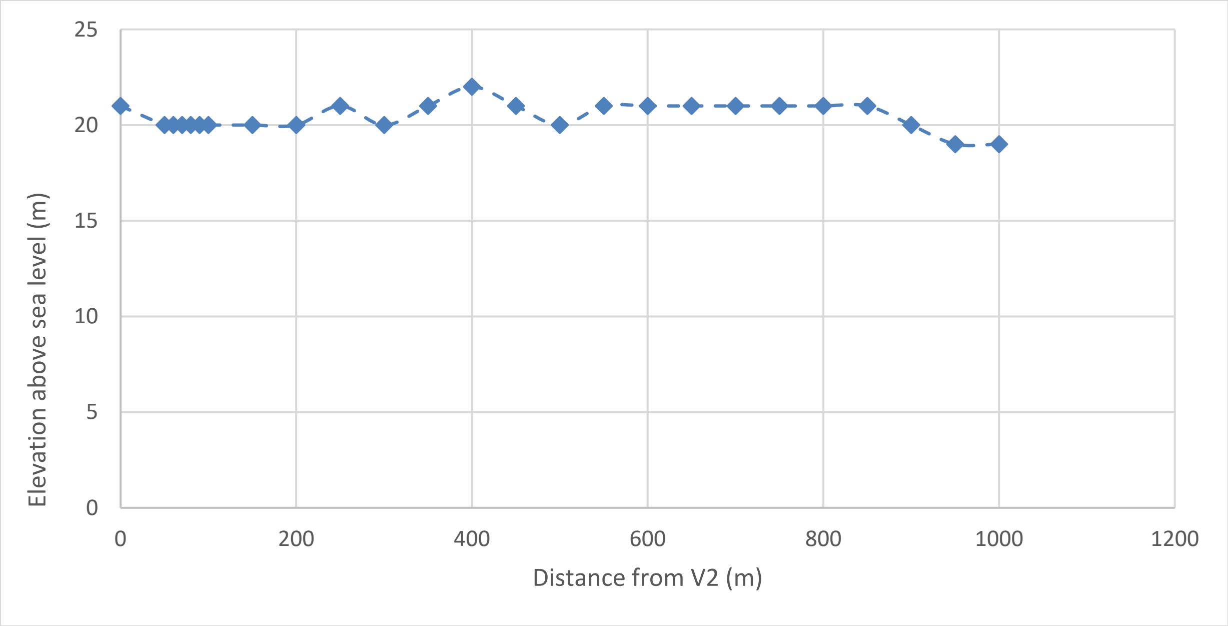

Figure 4.22: Elevation profile from valve V2 to valve V4

The test pipe was identified in consultation with a consulting company, Re-Solve, which, at the time of the tests, was doing water demand and leakage management on several sites of the Department of Public Works, of which the Wingfield military base was one.

The identified Wingfield pipeline was empty as it was not in use at the time of the tests. Consequently, prior to commencing the tests, the test pipe had to be charged with water. This meant that valve V1, in Figure 4.21, had to be opened fully to allow water from the Wingfield pipe network to charge the entire test pipe. After about 10 minutes, the test pipe was fully charged with water.

4.4.2 Procedure

The above-ground fire hydrant, located between valves V2 and V4, was identified as the most convenient connection point for the test pipe. A 50 mm reinforced hosepipe was connected to the fire hydrant, as shown in Figure 4.23.

Figure 4.23: Black 50 mm hosepipe being connected to the fire hydrant

After successfully connecting the hosepipe to the fire hydrant, the hydrant was flushed briefly to clear sediments and any stagnant water in the hydrant's pipe. The flushing process entailed briefly opening the fire hydrant and allowing water from the test pipe to flow through the hydrant and be discharged through the outlet of the hosepipe, shown in Figure 4.24. The figure also shows the colour of the water immediately after the fire hydrant was flushed.

Figure 4.24: Colour of the water during flushing

The hydrant remained open until the water from the test pipe cleared, as shown in Figure 4.25. Once the water was clear, the hosepipe outlet was connected to the PCAE tank and the tank was filled with clear water.

Figure 4.25: Clear water after flushing

Once the tank was filled, the tank valve was closed and the hosepipe was disconnected from the tank and connected to the PCAE. This meant that water was now flowing directly into the PCAE. However, due to the non-return valve in the inverter, water could not flow past the inverter. Thus, there was a pressure build-up, which was indicated on the inverter's display panel. The pressure continued to increase until a maximum pressure was reached, which stabilised, and was recorded as the operational pressure in the test pipe.

Once the PCAE recorder had logged the operational pressure, the PCAE variable speed pump was activated and set to suitable test pressures. Two tests were done:

- The first test involved isolating valves V2 and V3 (see Figure 4.21).
- The second test involved isolating valves V2 and V4 (see Figure 4.21).

For each test, after the pipeline had been isolated, and the leak tests were executed.

4.4.3 Results

4.4.3.1 Data interpretation

The first test involved isolating the pipeline by closing valves V2 and V3, which displayed no leaks . No leakage flow rate was detected and the pressure profile was constant. As a result of this result, the second test was carried out, where the pipeline was isolated between valves V2 and V4.

The raw flow and pressure data obtained from the second test is plotted in Figure 4.26. While the pressure curve is smooth, the flow curve displayed local scatter at the start of the step and then, eventually, stabilised. The stabilised data range, selected for analysis, is shown by the markers in Figure 4.26.

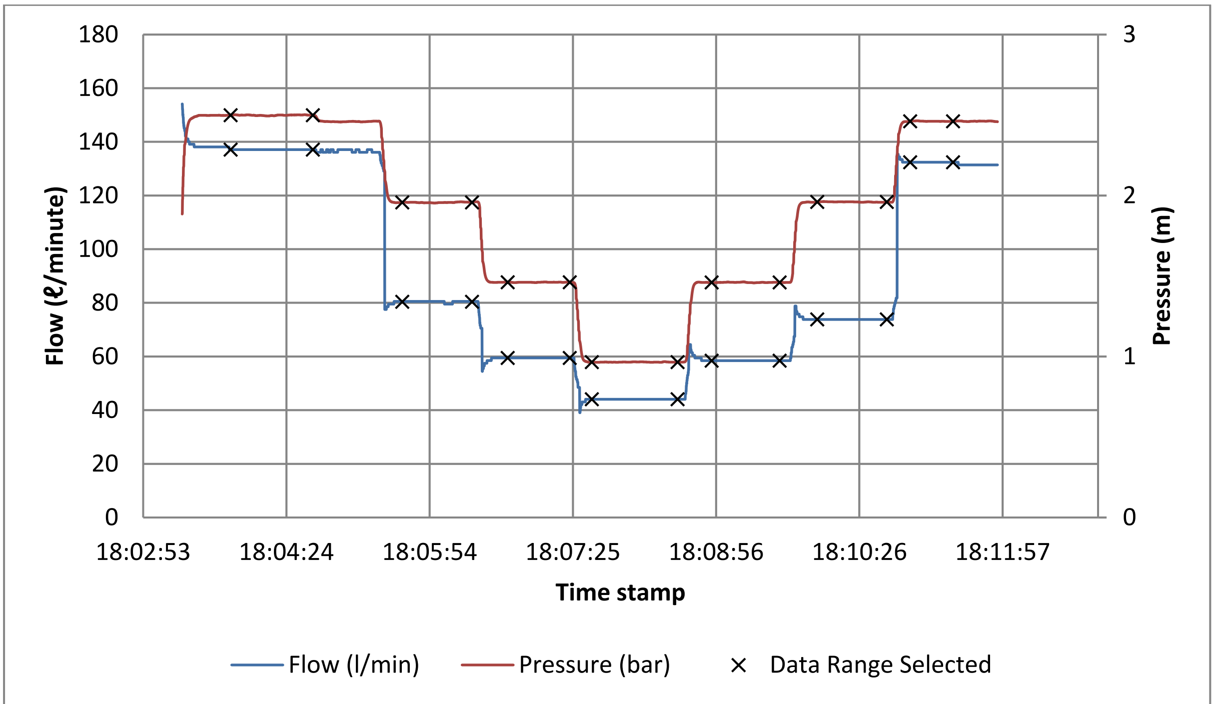

Figure 4.26: Flow against pressure raw data for the Wingfield test pipe

Using the stabilised flow and pressure data points, the average flow and pressure for each step was calculated. Table 4.11 proceeds to show the average pressure and flow values obtained for each step. From Table 4.11, it can be seen that, for each step, the average measured pressure ($h_{measured}$) and flow ($Q_{measured}$) were converted to SI units, from bar and ℓ/minute, to m and m^3/s, respectively. Additionally, the measured pressure head ($h_{measured}$) has been corrected to give the actual pressure in the test pipe ($h_{correct}$), which takes the friction losses (h_f) and the static head difference (h_s) between the test pipe and the PCAE into account.

Table 4.11: The averaged pressure and flow for each step test

Step	h measured (bar)	h measured (m)	h_f (m)	h_s (m)	$h_{correct}$ (m)	$Q_{measured}$ (ℓ/minute)	$Q_{measured}$ (m^3/s)
1.	2.5	25.50	4.11E-01	1.3	23.79	136.6	2.28E-03
2.	2	20.40	1.41E-01	1.3	18.96	80	1.33E-03
3.	1.5	15.30	7.59E-02	1.3	13.92	58.71	9.79E-04
4.	1	10.20	4.16E-02	1.3	8.86	43.44	7.24E-04
5.	1.5	15.30	7.38E-02	1.3	13.93	57.87	9.65E-04
6.	2	20.40	1.18E-01	1.3	18.98	73.3	1.22E-03
7.	2.5	25.50	3.77E-01	1.3	23.82	130.8	2.18E-03

4.4.3.2 The N1 leakage parameters

The measured flow rate ($Q_{measured}$) and the corrected pressure head were plotted against one another, as shown in Figure 4.27. A power equation was then fitted through the data points to determine the *N1* leakage parameters: the *N1* leakage exponent and the leakage coefficient (*C*).

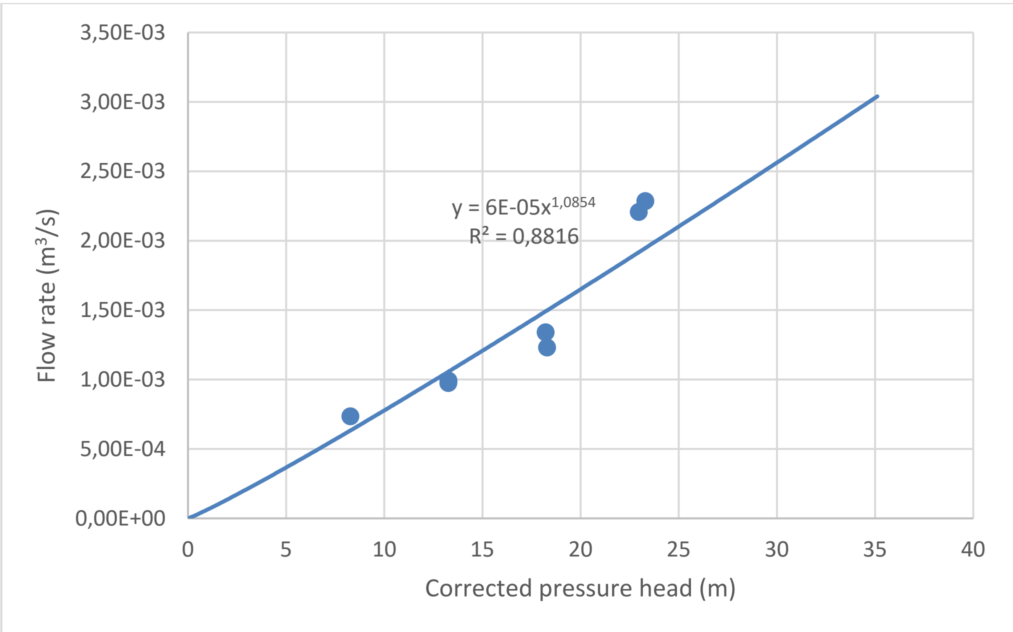

Figure 4.27: The flow and pressure head for the varying pump speeds

Figure 4.27 shows that there was an increase in flow with an increase in the pressure head. When taking a closer look at the result in Figure 4.27, it was observed that the two steps at the high pressures did not fit well with the power equation fitted to the data. As a result of this observation, two power equations were fitted to the data points. One power equation was fitted at the lower pressure data points, and the other was fitted to the higher pressure data points. Figure 4.28 shows two power equations fitted to the pressure and flow data set.

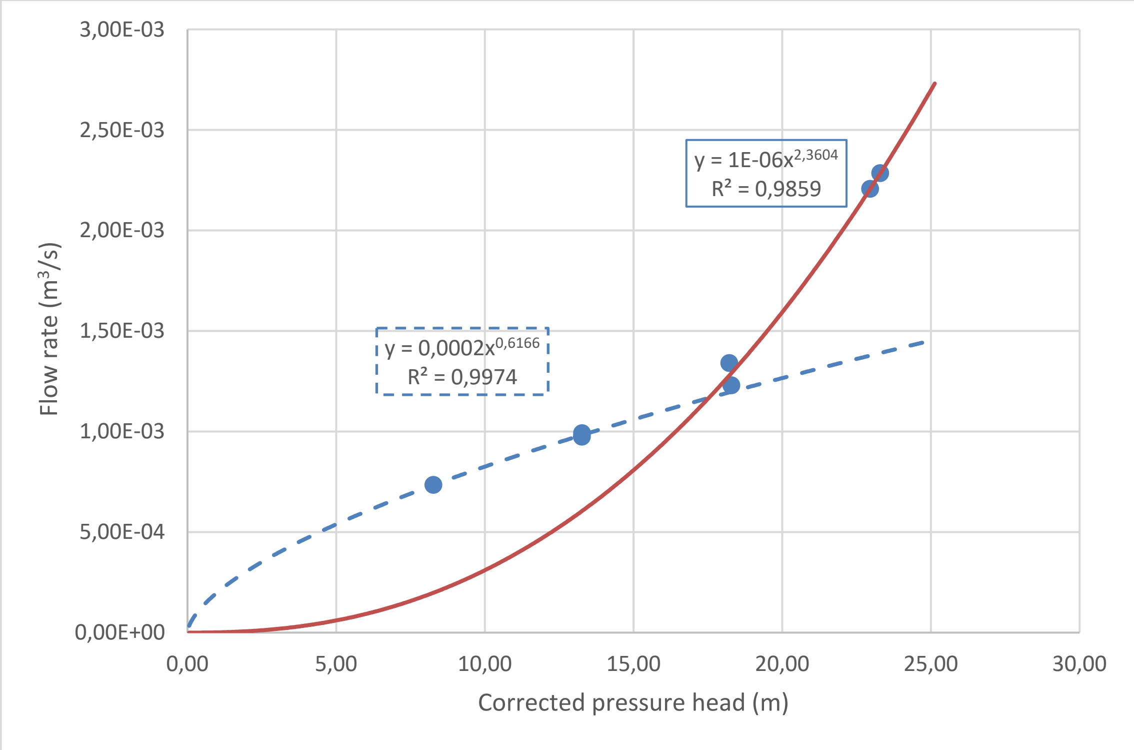

Figure 4.28: Flow against pressure data with two power equations

In Figure 4.28, the two curves fitted the data very well, with an R^2 greater than 0.9. This result suggested that two mechanisms could be used to describe the overall leakage in the pipeline. The first process starts to occur at the lower pressures (dotted curve), while the second process starts to occur at the higher pressures (solid curve).

The *N1* value obtained for the process occurring at the lower pressures was 0.6, suggesting that this process occurred on a rigid section of the pipe system, such as the pipe itself. The *N1* value obtained for the process that transpired at the higher pressures was 2.3, suggesting that this process was happening on a component of the pipe system that was very sensitive to pressure, e.g. a rubber seal. Table 4.12 provides a summary of the *N1* leakage parameters for the two processes.

Table 4.12: Summary of the *N1* leakage parameters

N1 leakage parameter	Leak on pipe	Leak on seal
N1	0.6	2.36
C	2×10^{-4}	1×10^{-6}
R^2	0.99	0.98

4.4.3.3 Modified orifice equation

In order to check the MOE leakage parameters; the effective leak area (C_dA_0) and the effective head-area slope (C_dm) for the leak were determined. The effective leak area was then plotted against the pressure head in Figure 4.29.

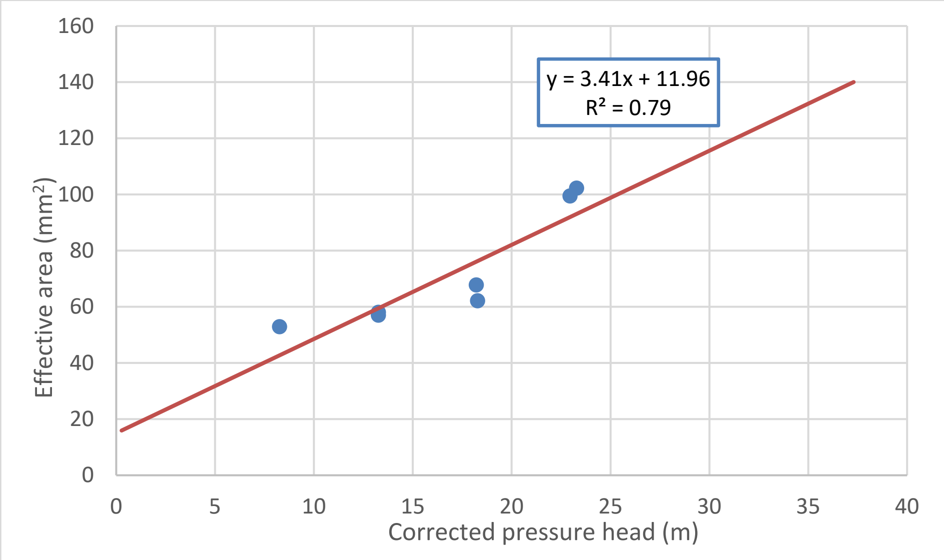

Figure 4.29: Effective area against pressure head for the Wingfield Test 1

A linear line was fitted to the data set and used to obtain the effective leak area (C_dA_0) and the effective head-area slope (C_dm). The effective initial leak area, which was given by the intercept of the line, was found to be 11.96 mm. The effective head-area slope, which was given by the gradient of the line, was found to be 3.41 mm^2/m.

A closer look at Figure 4.29 reveals that the data points at the higher pressure did not fit very well to the overall linearity of the other points. This observation warranted further investigation as to whether two distinct mechanism played a role, with one mechanism already having an effect at the lower pressures, and the other being induced at the higher pressures.

In order to investigate this further, two linear lines were plotted as shown in Figure 4.30. One line was plotted through the data set at the lower pressures, representing the characteristics of the first mechanism, and the other line was plotted at the higher pressures of the data set, representing the characteristics of the second mechanism.

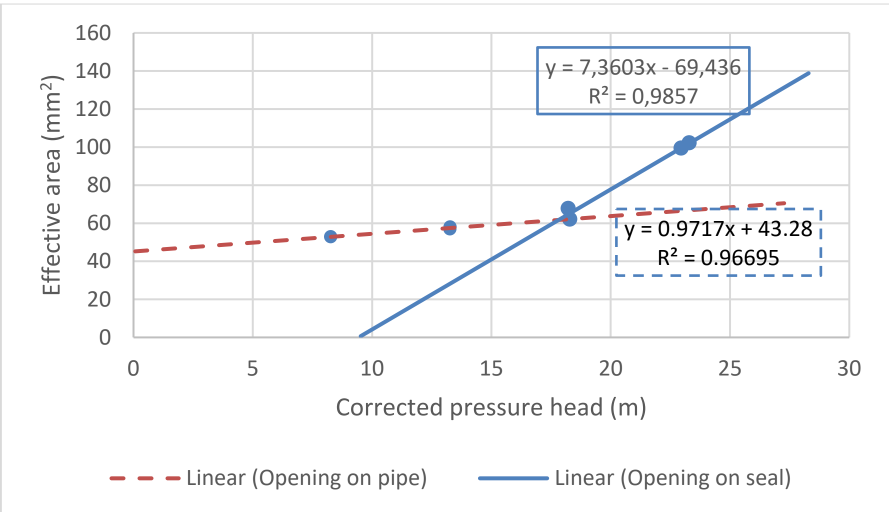

Figure 4.30: Effective area against pressure for the Wingfield pipeline

From Figure 4.30, it can be seen that the first mechanism has an effective initial leak area of 43 mm^2 and an effective head-area slope of 0.97 mm^2/m. This is consistent with a longitudinal crack, which is the typical failure mechanism of asbestos cement pipes, as shown in Figure 4.31.

Figure 4.31: Typical failure mechanisms in asbestos cement pipes (Greyvenstein, 2004)

The second mechanism, which is a combination of the first mechanism and another mechanism, resulted in an effective initial leak area of 69.44 mm^2 and an effective head-area slope of 7.36 mm^2/m. The pressure head at the intercept of the two linear lines in Figure 4.30 could potentially indicate the pressure at which the second mechanism starts to have an effect on the behaviour of the leak. From the image shown in Figure 4.31, it is anticipated that the first process is a longitudinal crack, which opens up with pressure. When a certain pressure is reached, the opening in the crack interferes with the seal, and hence the second mechanism.

4.5 WINGFIELD PIPELINE – TEST 2

4.5.1 Introduction

A second test was conducted on the Wingfield asbestos cement pipeline exactly three months after the first leak test was done. According to the consultants in charge of the Wingfield pipeline on site, the pipeline was isolated and had never been in operation since the last leak test. Prior to carrying out the second leak test, it was requested that the pipeline be recharged overnight so that the pipe could be full on the day of the test.

4.5.2 Procedure

The PCAE was transported to the Wingfield site. The first step was to connect the PCAE by means of a 50 mm rubber hosepipe. The hosepipe was connected to an above-ground fire hydrant located at FH1 in Figure 4.32.

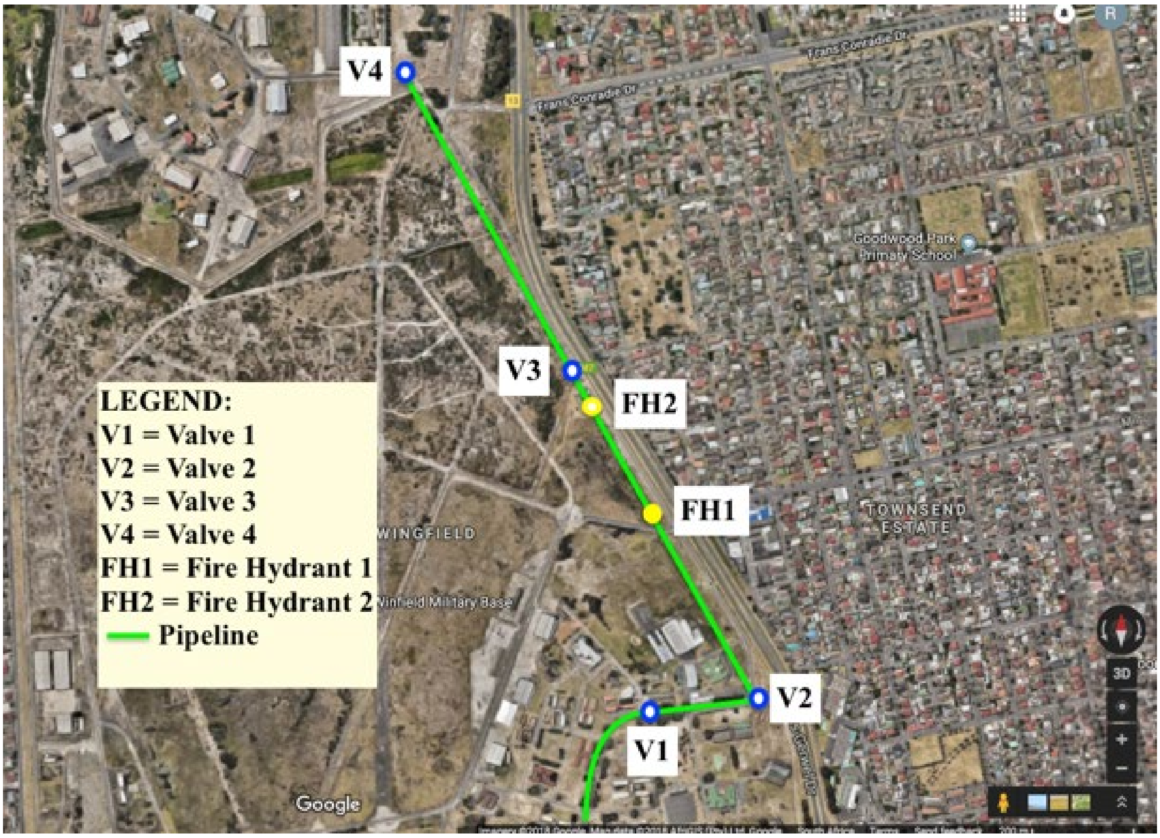

Figure 4.32: Wingfield pipeline layout

Figure 4.33 shows the condition of the hydrant stand pipe to which the PCAE was connected. It can be seen from the figure that the hydrant pipe was severely corroded. Nonetheless, the test continued.

Figure 4.33: Fire hydrant connection

After connecting the hosepipe to the hydrant, the hydrant valve was opened to flush out any sediments. Immediately after opening the hydrant, the hydrant pipe failed through a burst on the steel pipe feeding the hydrant. This failure may have occurred for two reasons: firstly, because the hydrant valve was opened too quickly and the sudden shock induced in the system caused the failure; secondly, because the hydrant pipe was already severely corroded, the integrity of the pipe wall was extremely compromised and any sudden pressure in the pipe would cause the pipe to fail. Figure 4.34 shows the corroded hydrant after the burst. It can be seen that the hydrant head did not fail, but the hydrant pipe wall disintegrated. For this reason, the test was discontinued and another one scheduled after the hydrant pipe had been replaced.

Figure 4.34: Failed fire hydrant pipe

4.6 WINGFIELD PIPELINE – TEST 3

4.6.1 Introduction

A third leak test was conducted on the Wingfield asbestos cement pipeline after the hydrant pipe that had burst during the second leak test had been replaced. Figure 4.35 shows the new hydrant pipe that was installed at FH1 in Figure 4.36.

Figure 4.35: The replaced fire hydrant pipe with the hydrant head

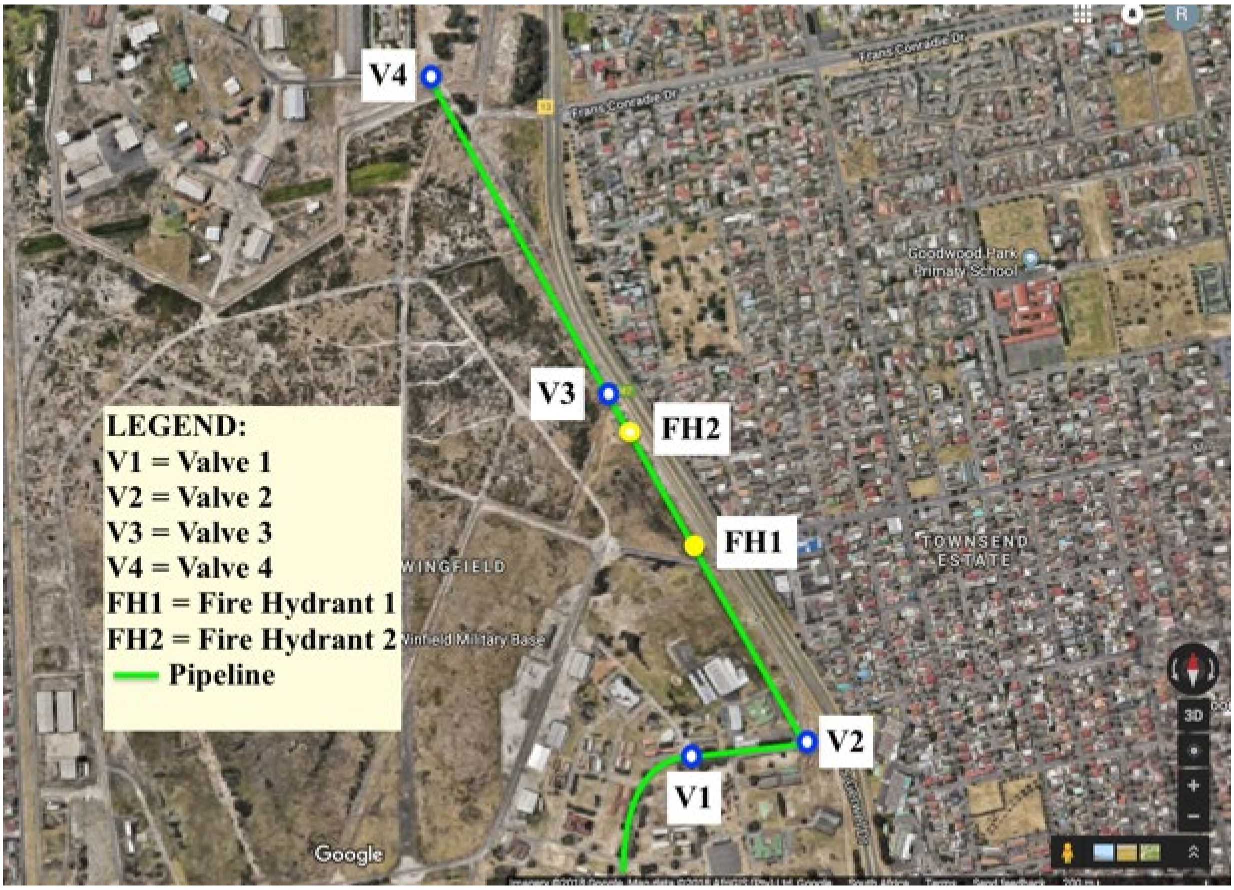

Figure 4.36: Wingfield pipeline layout

4.6.2 Procedure

The first step was to connect the PCAE to the pipeline. The fire hydrant was identified as the most suitable connection point to the pipeline. The fire hydrant at FH1 in Figure 4.36 was selected because it was the same connection used to connect the PCAE and the pipeline during the first and second leak tests. However, it was discovered on site that the replaced fire hydrant head, installed at FH1, was not compatible with the PCAE rubber hosepipe connection fitting. Consequently, the PCAE could not be connected at this hydrant. Thus, an alternative connection point along the pipeline had to be identified.

The alternative connection point was the second fire hydrant on the pipeline, located at FH2 in Figure 4.36. The fire hydrant at FH2 did not have a hydrant head and was found covered, as shown in Figure 4.37. A spanner was used to remove the cover. The contractor organised a hydrant head that matched the fire hydrant pipe, as well as the PCAE connection fitting.

Figure 4.37: Covered fire hydrant

Figure 4.38: Installed fire hydrant head with the PCAE hosepipe connected

After connecting the PCAE hosepipe to the fire hydrant, as depicted in Figure 4.38, the fire hydrant was opened to flush any sediments in the pipeline. After the water cleared, the PCAE water tank was filled with water from the pipeline until the water tank was full.

After filling the tank, the pipeline was isolated by shutting off valves V2 and V4. After the pipeline was isolated, the PCAE variable speed pump was activated and the leak test executed.

4.6.3 Results

The raw flow and pressure data obtained from this test was plotted against time, as shown in Figure 4.39. It is clear from the figure that the pipe had deteriorated substantially after the previous test and that it had a very large leak of around 190 ℓ/minute (11.4 m^3/h). As shown in the figure, it was not possible to stabilise the flow and pressure values. Consequently, in an attempt to vary the pressure, the pressure steps were not held long enough to stabilise it.

This leak could not be analysed any further due to the unstable flow and pressure results. Subsequently, the leakage characteristics were not determined. The researchers were of the view that, should more allowance have been made for the pressure to stabilise, at least two steps could have been achieved, and the leakage could have been characterised.

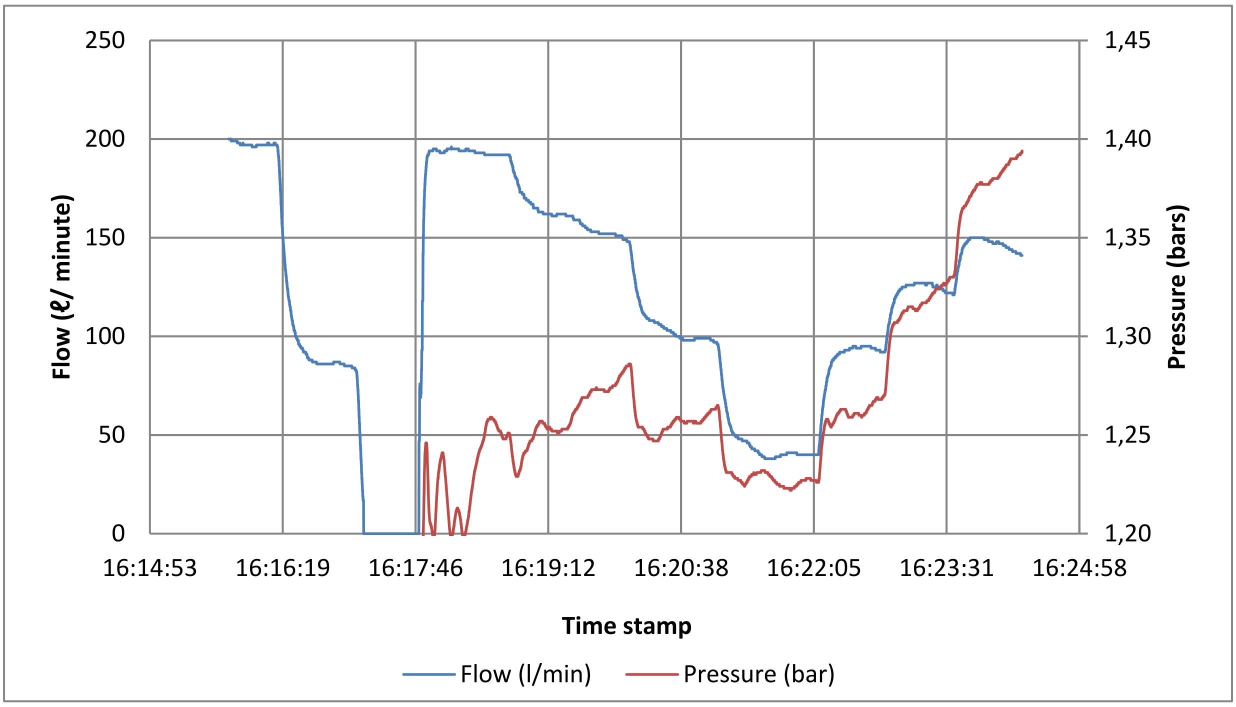

Figure 4.39: Flow and pressure raw data for Wingfield Test 3

4.7 UNIVERSITY OF CAPE TOWN PIPELINE

4.7.1 Introduction

The examined asbestos cement pipeline at the University of Cape Town (UCT) (the UCT test pipe) runs along the northwestern corner of the Ring Road, as illustrated in Figure 4.40, where the blue line indicates its layout. The UCT pipeline is 160 m in length, with a nominal diameter of 200.

This UCT pipeline was identified in consultation with the University's maintenance team, who are tasked with managing and maintaining all pipelines within the campus area. This pipeline was selected as the most feasible option, as it had the least interruptions to supply.

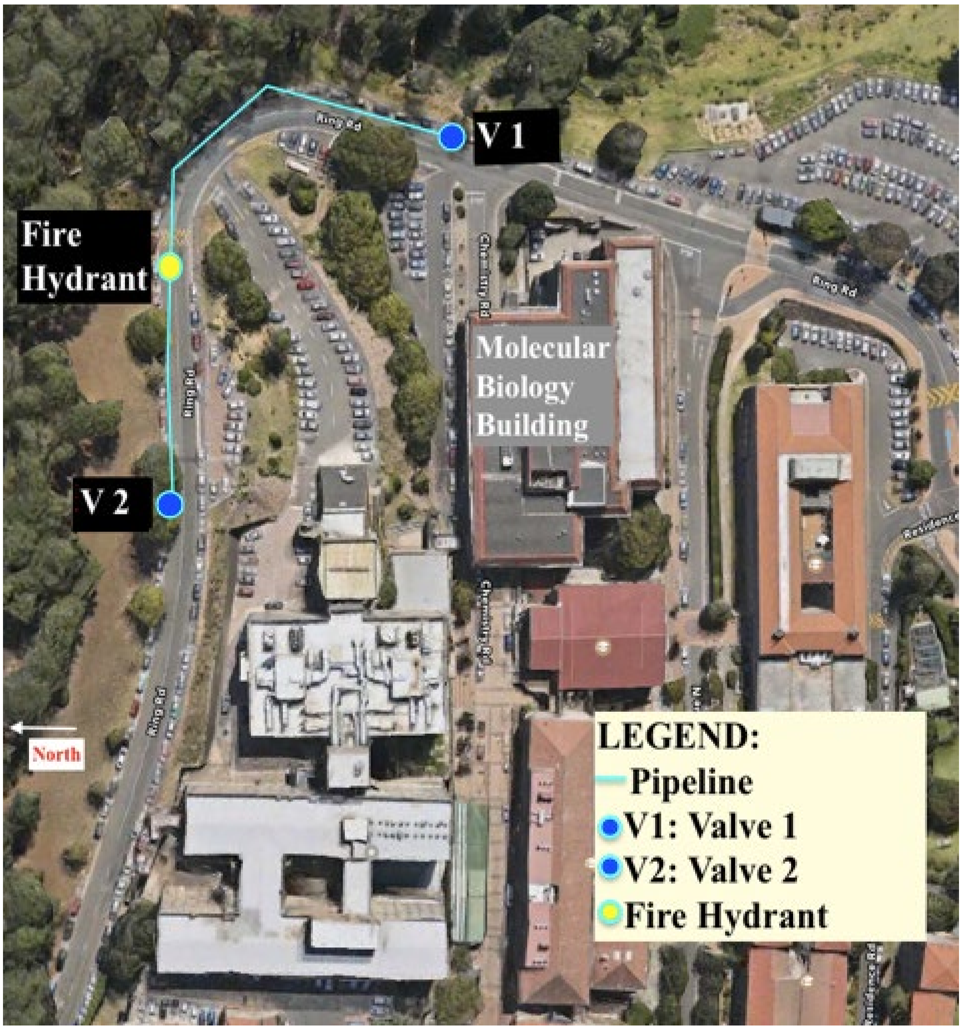

Figure 4.40: University of Cape Town pipeline layout procedure

Two isolation valves, V1 and V2, shown in Figure 4.40, were identified as suitable valves for the isolation test. The PCAE was connected to the UCT test pipe via an underground fire hydrant, as depicted in Figure 4.41. The only building that was to be isolated during the test was the Molecular Biology Building.

Figure 4.41: Underground fire hydrant connection

After successfully connecting the pipe to the fire hydrant, the fire hydrant was opened, briefly, to flush the test pipe. After the water had cleared, the tank was filled with water from the test pipe. Once the tank was filled, the operation pressure in the pipe was checked and the pressure-controlled variable speed pump started. Valves V1 and V2 were closed to isolate the test pipe. The pump was then set to suitable test pressures and the corresponding flow was checked. The results of this test are presented in the next section.

4.7.2 Results

4.7.2.1 Data interpretation

Figure 4.42 depicts the graph of the data recorded for the UCT test pipe. The graph output clearly shows that no flow rate was detected for this test. This implied one of two possibilities: firstly, that there was no leak in the test pipe; secondly, that the leak flow rate was too small to be detected by the flow meter. Further analysis of this data would inform which of the two possibilities was playing a role.

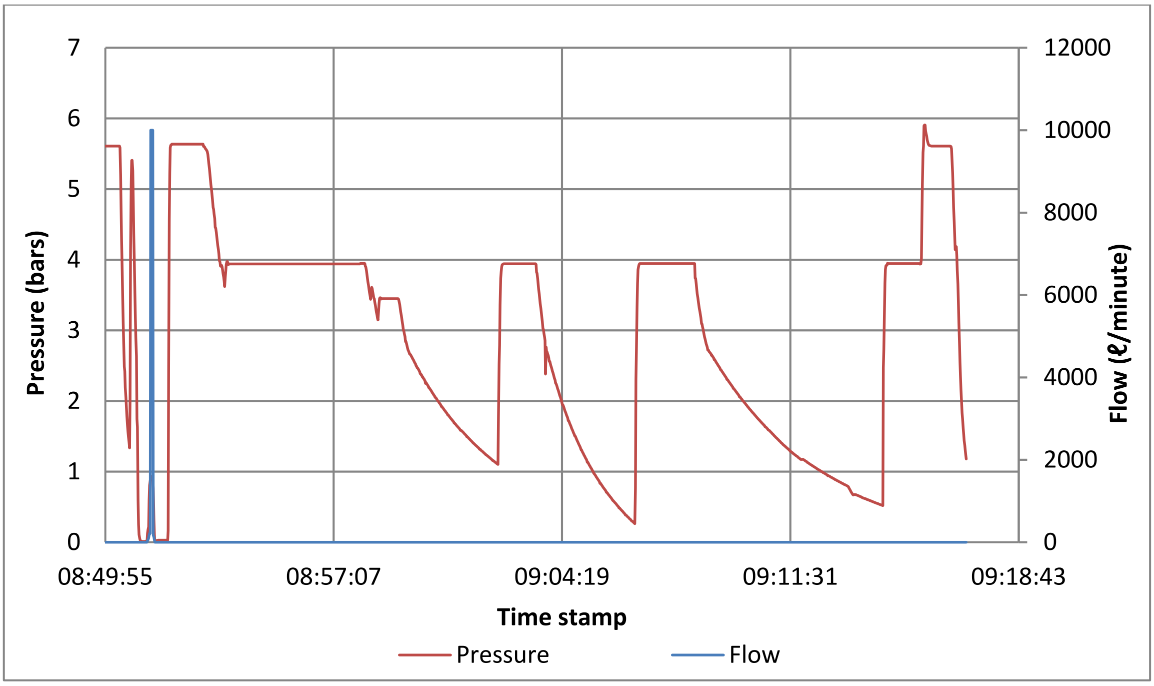

Figure 4.42: Raw data output from the UCT pipeline test

As can be seen in Figure 4.42, the starting pressure detected was 58 m, representing the operational pressure of the test pipe. As soon as valves V1 and V2 were shut, a sudden drop in pressure was observed. The pressure in the test pipe dropped to 4 bar or 40 m, which was the set point pressure of the PCAE variable speed pump. This pressure was maintained in the test pipe for as long as the PCAE variable speed pump was on. When the PCAE variable speed pump was switched off, as can be seen just before 09:00, the pressure dropped until it reached about 1.2 bar. This drop in pressure that occurred while the pipe was isolated suggested that a leak existed in the pipeline.

This pressure drop test was repeated three times. Each time, the variable speed pump was set to 40 m, resulting in the test pipe pressure rising to 40 m. Thereafter, the pump was switched off and the pressure dropped below the set point pressure of 40 m. It can also be seen that the pressure returned to the operational pressure of 58 m once the valves were opened again.

It was concluded that the pipe had a leak, but that it was too small to register on the flow meter. The minimum flow rate that the meter can register is 0.4 m^3/h (0.11 ℓ/s). Thus, a leakage flow of 0.2 m^3/h (0.055 ℓ/s) was assumed.

4.8 SIMON VERMOOTEN TO MURRAYFIELD RESERVOIR PIPELINE

4.8.1 Introduction

The Simon Vermooten to Murrayfield Reservoir steel bulk pipeline (the SVM pipeline) connects a main pipe on Simon Vermooten Road to the Murrayfield Reservoir. The pipeline is 1 460m in length, with a diameter of 500 mm.

The SVM pipeline layout is shown in Figure 4.43. Starting at isolation valve V1, it consistently rises, following the road, via an intermediate isolation valve (V2) to the final isolation valve (V3). The pipeline is pressurised by gravity to 17 bar downstream of isolation valve V1. The elevation difference between valves V1 and V3 is approximately 90 m.

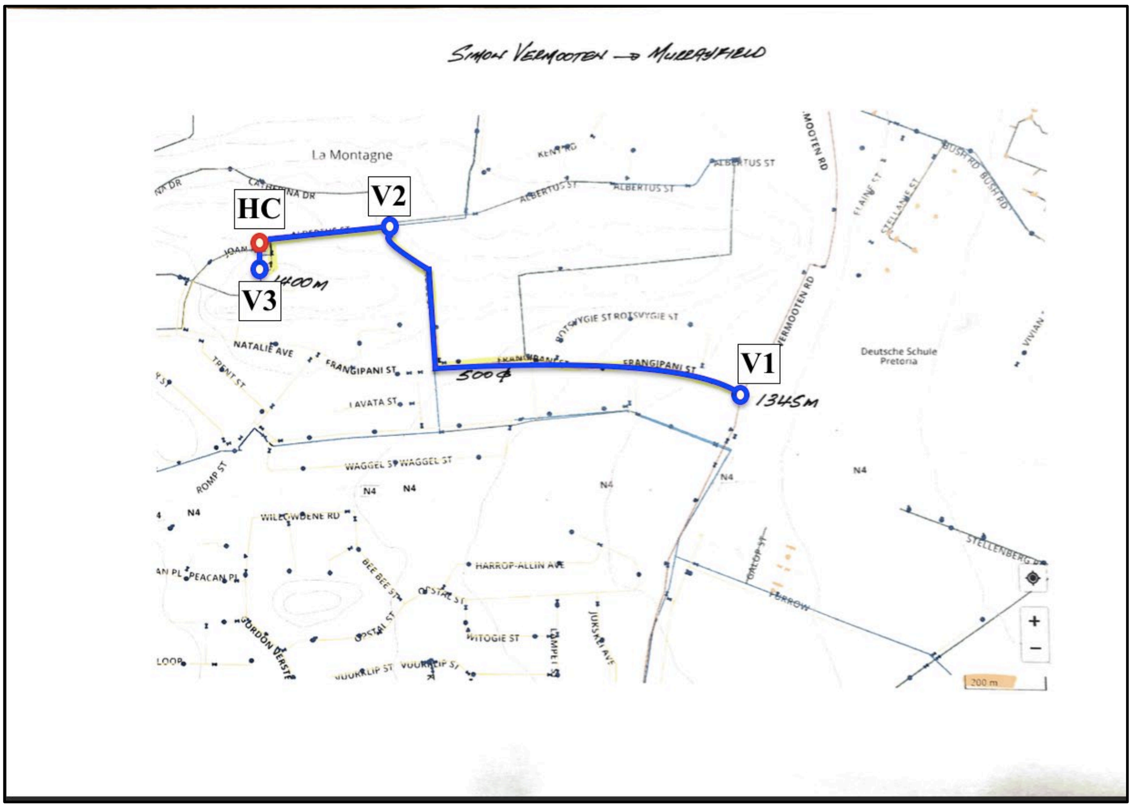

Figure 4.43: Layout of the SVM pipeline with the location of the valves

A Google Earth image of the reservoir configuration, where isolation valve V3 and the connection point are located, is shown in Figure 4.44.

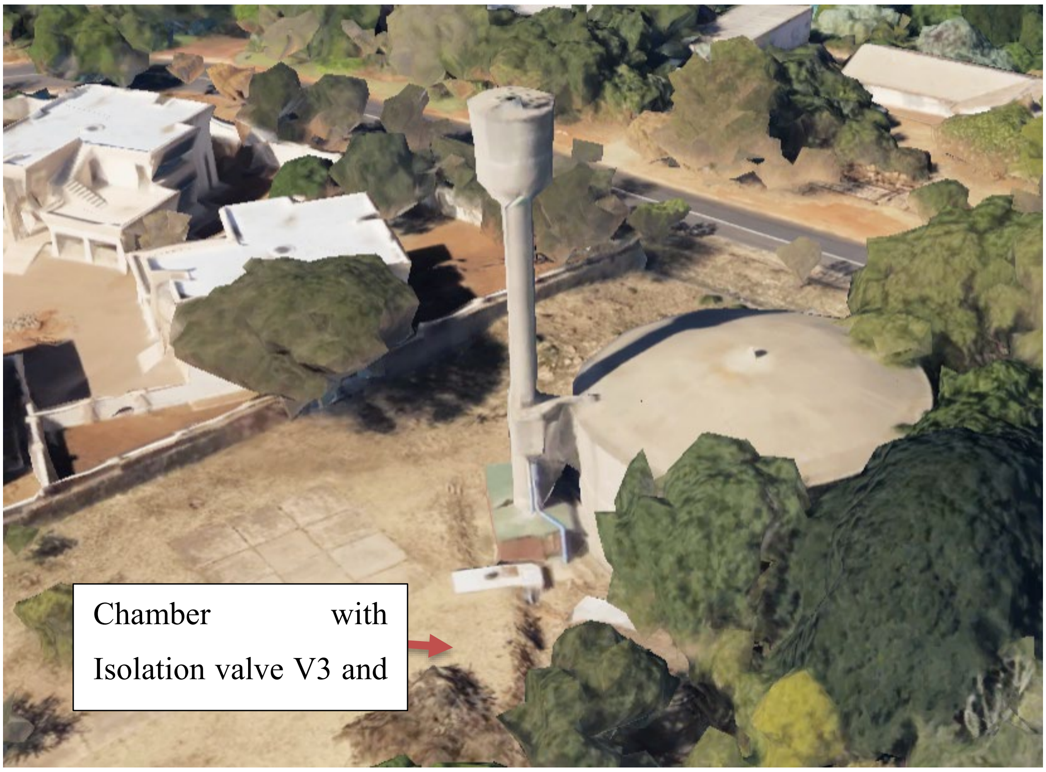

Figure 4.44: Google Earth image of reservoir configuration

4.8.2 Procedure

The operations team arrived on site after already having closed isolation valve V1. The team members were instructed to open the valve again, so that the pipeline can operate as normal. This was important since the PCAE water tank was not yet filled.

After valve V1 had been opened, a suitable connection point to the pipeline was identified. The most suitable connection point turned out to be a stop valve located in the chamber that housed isolation valve V3. Figure 4.44 shows the location of the concrete chamber. The PCAE water tank was then filled with a hosepipe that was connected to the stop valve.

The pressure before isolating the SVM pipeline was measured to be around 7.7 bar. The operations team then closed valves V2 and V3. The SVM pipe was then connected to the testing equipment, and a pressure of approximately 7.7 bar was measured again. This was an indication that valve V2 was not isolating properly.

The operations team then opened valve V2 and closed valve V1. In an attempt to depressurise the SVM pipeline, the hosepipe that was connected to the connection point was allowed to run freely. The flow decreased up to a certain point, after which a constant flow was observed to continue flowing from the hose, as shown in Figure 4.45. This was a significant flow and was presumed to be due to isolation valve V1 not sealing properly.

Figure 4.45: Constant flow observed after valve V1 was closed

The operations team proceeded to close valve V2 as well. The flow from the hosepipe decreased further, but a significant flow remained, presumably indicating that valve V2 was also not sealing properly. The hosepipe was then reconnected to the testing equipment and the pressure was measured. The measured pressure started at 3.5 bar and consistently increased to roughly 8 bar, after which the pressure remained consistent. This pressure was similar to that measured before the isolation valves were closed. As a result of the high pressure measured in the SVM pipeline, which exceeded the capacity of the testing equipment, the test could not be conducted.

4.8.3 Results

No results were obtained for this test. However, it was discovered that the isolation valves of the SVM pipeline to the supply line did not seal. Subsequently, the pressure in the pipeline equalised the supply pressure after isolation.

4.9 LYNNWOOD ROAD TO KOEDOESNEK RESERVOIR PIPELINE

4.9.1 Introduction

The Lynnwood Road to Koedoesnek Reservoir iron bulk pipeline (the LK pipeline) connected the main pipe on Lynnwood Road to the Koedoesnek Reservoir. The reservoir supplies a section of the City of Tshwane. The pipeline was 707 m in length with a diameter of 500 mm.

The LK pipeline layout is shown in Figure 4.46, starting at the isolation valve (V1), which was pressurised by gravity to a pressure of at least 10 bar. The pipeline then consistently rises to the final isolation valve (V2) just before the Koedoesnek Reservoir, which is on a hill. The elevation difference between valves V1 and V2 was approximately 50 m. The PCAE device was in the chamber that housed valve V2.

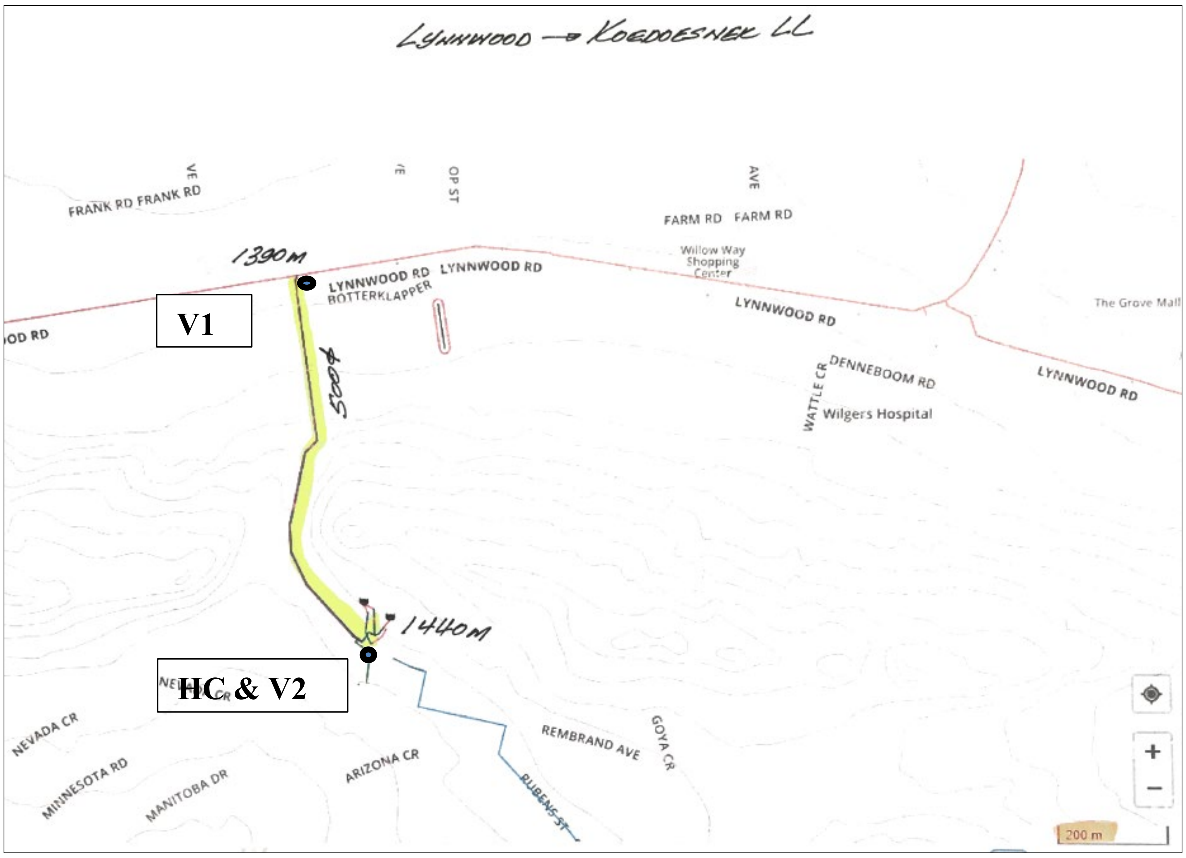

Figure 4.46: Layout of the Lynnwood Road to Koedoesnek Reservoir pipeline with the location of the valves

A Google Earth image of the site of the Koedoesnek Reservoir and the chamber housing valve V1 is shown in Figure 4.47. By isolating valve V1, the pipeline was isolated from the main source supplying the pipeline.

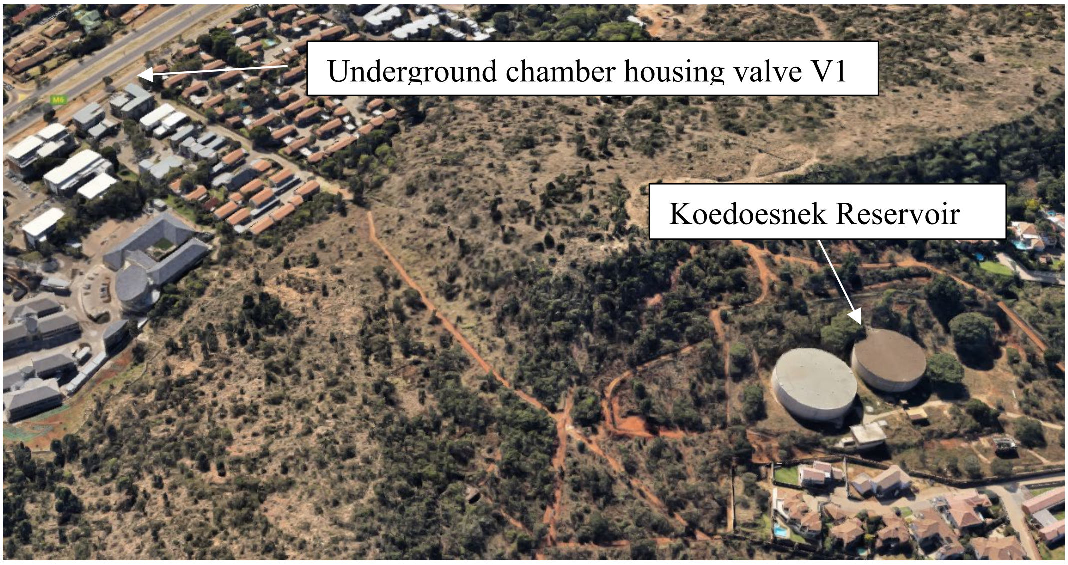

Figure 4.47: Location of the chamber housing valve V1 and the Koedoesnek Reservoir

Figure 4.48 shows a Google Earth close-up configuration of the Koedoesnek Reservoir and the chamber with the pressure-regulating valves and isolation valve V2. The chamber has three pressure-regulating valves and an isolation valve (V2) just downstream of the pressure-regulating valves and upstream of the reservoir.

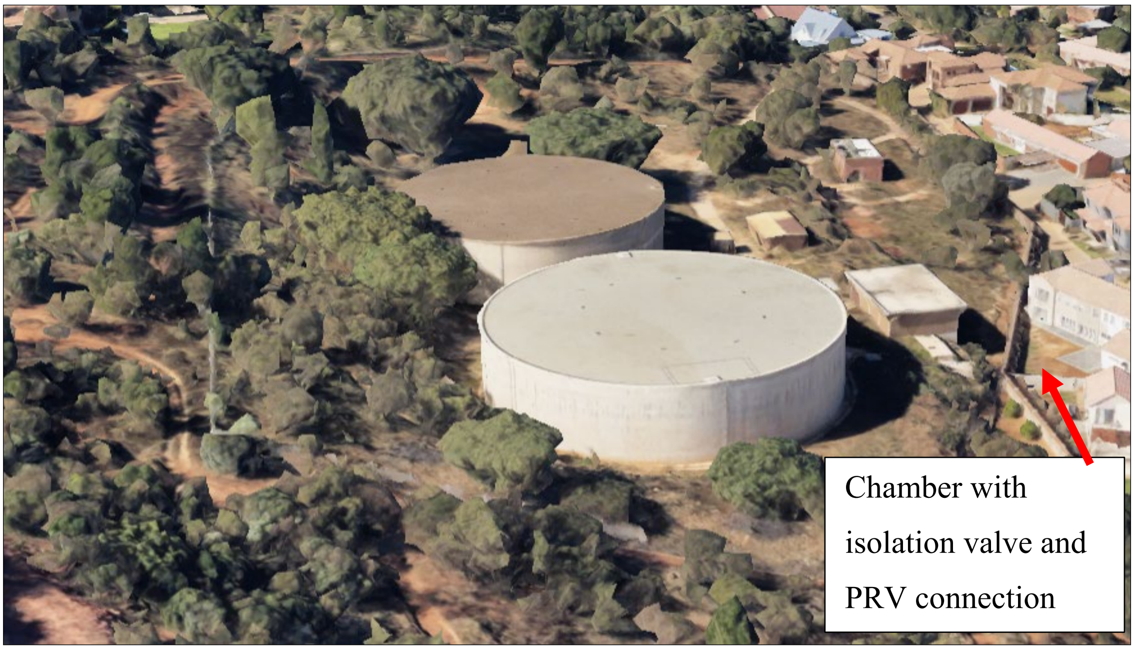

Figure 4.48: Reservoir configuration

4.9.2 Procedure

The PCAE device was connected to one of the pressure-regulating valves at the Koedoesnek Reservoir chamber. The pressure-regulating valve had a connection stop valve point, as shown in Figure 4.49.

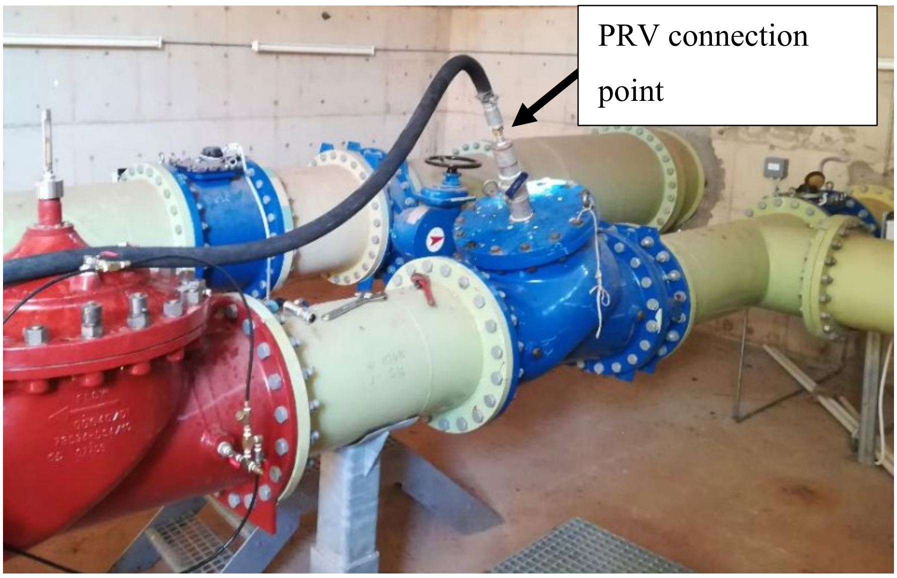

Figure 4.49: Connection of testing equipment

The PCAE trailer was pushed into the loading bay of the chamber for the PCAE's hosepipe to reach the water tank, as illustrated in Figure 4.50.

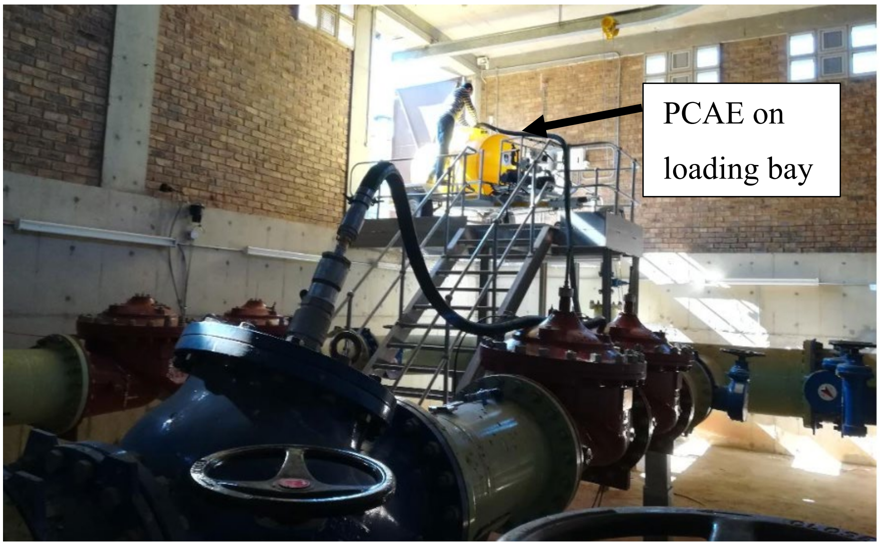

Figure 4.50: PCAE setup, with trailer in loading bay

The tank was filled by opening the stop valve at the connection point. The flow into the tank was observed to be strong and unobstructed. Once the tank was full, the stop valve was closed. The next step was to isolate the LK pipeline by closing valves V1 and V2, shown in Figure 4.46.

The first valve to be isolated was valve V1, which was housed in a concrete chamber. Upon arrival at the chamber, it was noticed that valve V1 was submerged in water because the chamber was flooded. Arrangements were made with a team from the Tshwane Metropolitan Municipality to pump the water out of the chamber. This process took about an hour. After the chamber was emptied, valve V1 was closed. A leak on a coupling was identified to be responsible for the flooded chamber. The leak was, however, on the supply side of the isolation valve and not on the LK pipeline that was tested. The isolation valve (V1) appeared to seal effectively. The next valve to be isolated was valve V1, which also appeared to seal effectively.

After isolating the pipeline, it was evident that the LK pipeline was already depressurising. A slight suction of air into the rubber hose, which was still connected to the LK pipeline, was observed, suggesting that the pipeline was isolated.

The hosepipe was then connected to the PCAE and the pump was activated at maximum pressure. The pressure was then dropped at increments of 0.5 bar up to 1.5 bar, and the flow was allowed to stabilise for each pressure step. Thereafter, the pressure was increased at increments of 0.5 bar.

4.9.3 Results

4.9.3.1 Data analysis process

The LK pipeline was analysed as a pipeline rising from the bottom isolation valve V1 on the delivery line to the reservoir, as shown in Figure 4.52. The maximum vertical difference between the bottom and the top of the pipeline was 90 m and the horizontal distance from the bottom isolation valve to the top of the pipe was evaluated to be 706 m.

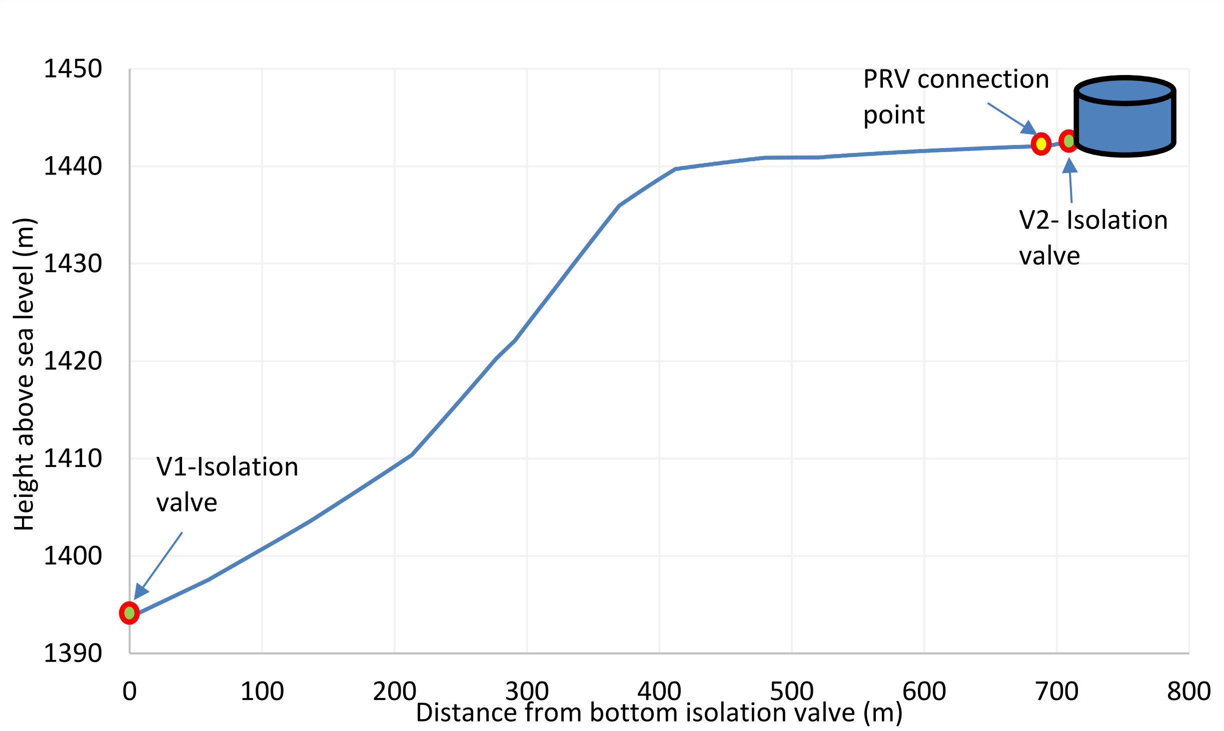

Figure 4.51: Elevation profile of the LK pipeline

Nodes were assigned at various points along the pipeline, as shown in Figure 4.52. Nodes 0 to 1 represented the hosepipe connecting the PCAE to the LK pipeline. Nodes 1 to 2 represented the stop valve on the pressure-regulating valve onto which the PCAE hosepipe was connected to access the pipeline. Nodes 2 to 4 are points along the pipeline, of which Node 2 represents the highest point. Node 3 is an intermediate node, and Node 4 is a node at the bottom of the pipeline.

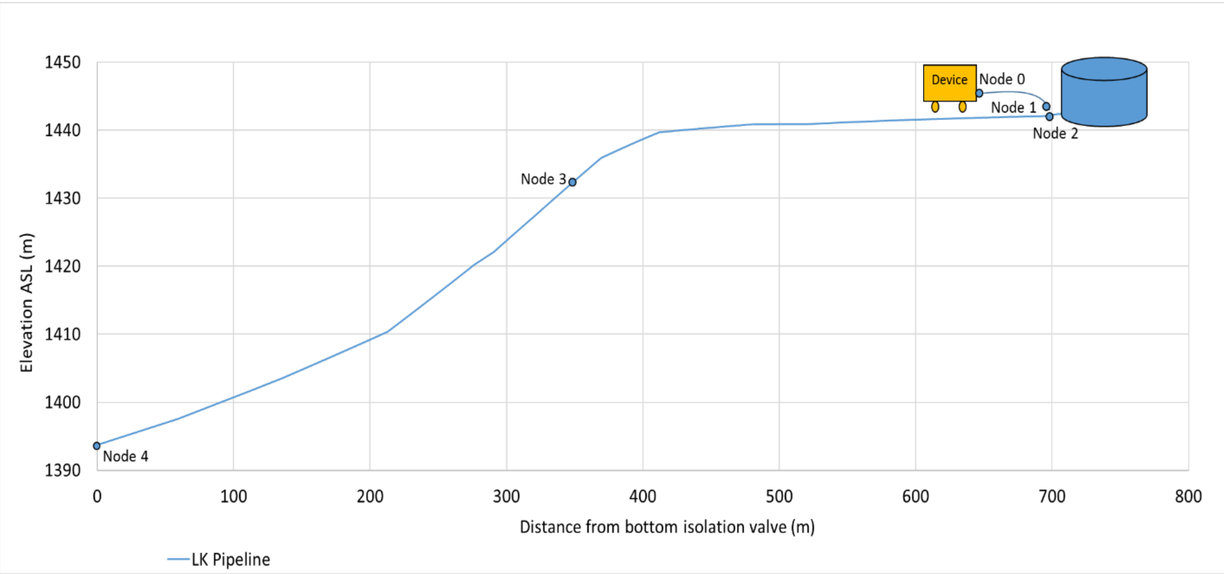

Figure 4.52: Elevation profile with nodes

4.9.3.2 *Data interpretation*

The raw flow and pressure data obtained from the PCAE recorder is plotted against time in Figure 4.53. The pressure before the isolation valve (V1) on the delivery line was more than 10 bar. The fact that the pressure could be controlled demonstrates that the isolation valves sealed properly. As can be seen from Figure 4.53, the pressure was dropped at increments of 0.5 bar, and a flow rate was detected, suggesting that a leak existed in the pipeline. The leakage flow rate was then allowed to stabilise before another pressure increment was set.

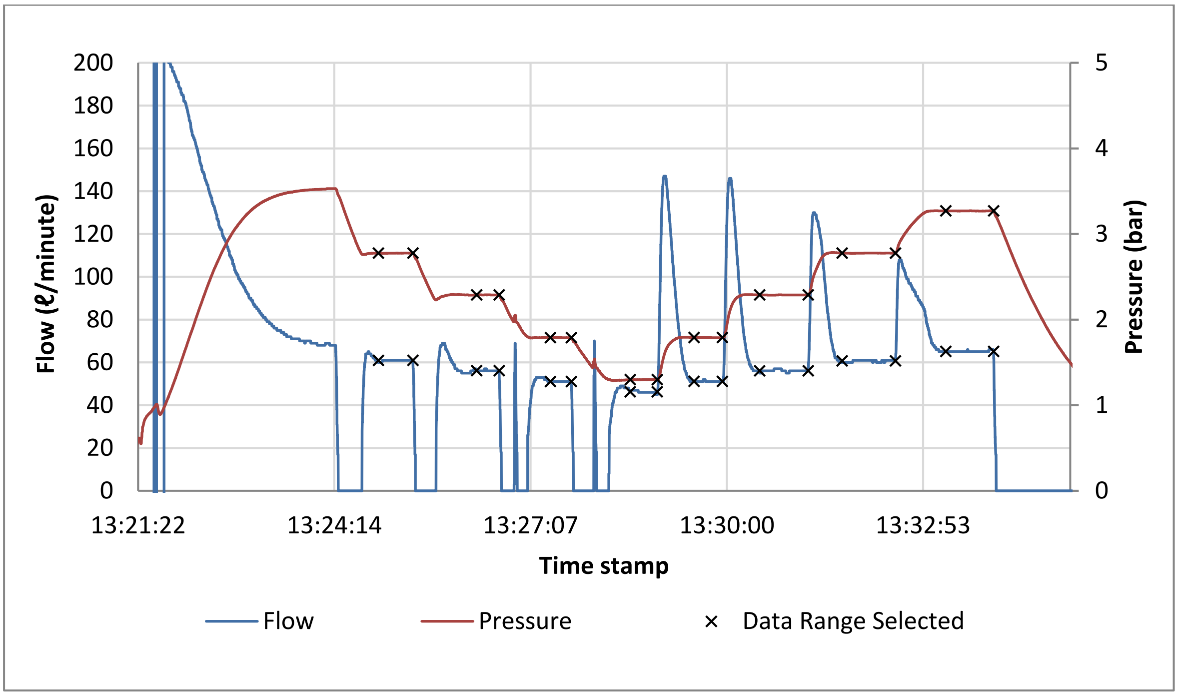

Figure 4.53: Pressure and flow data

A clear relationship between the leakage flow rate and pressure was evident in the data. The graph shows a step-down and step-up pattern repeated for both data sets. The stabilised data range of each step was used for further analysis. The selected stabilised range of the pressure and flow rate is shown by the cross markers.

The pressure and flow data in Figure 4.54 represents the data measured by the device's pressure sensor and magnetic flow meter. The pressure was adjusted for the various nodes to obtain the actual pressure at each node. The flow rate was presumed to be the same throughout the pipeline as a consequence of the conservation of mass. Table 4.13 shows a summary of the adjusted pressures for each node.

Table 4.13: The averaged stabilised flow and pressure data for each node

Flow rate, Q	h at Node 0	h at Node 1	h at Node 2	h at Node 3	h at Node 4
1.01E-03	28.31	30.07	30.64	35.45	74.79
9.35E-04	23.34	25.11	25.71	30.52	69.86
8.50E-04	18.24	20.03	20.67	25.48	64.82

Flow rate, Q	h at Node 0	h at Node 1	h at Node 2	h at Node 3	h at Node 4
7.71E-04	13.24	15.04	15.70	20.51	59.85
8.51E-04	18.26	20.04	20.68	25.49	64.83
9.34E-04	23.33	25.10	25.71	30.52	69.86
1.01E-03	28.32	30.08	30.65	35.46	74.80
1.09E-03	33.35	35.09	35.63	40.44	79.78

It can be seen from Table 4.13 that the highest pressures occurred at Node 4, followed by Node 3, then Node 2 and finally Node 1, with the smallest pressure at Node 0. The highest pressure occurred at Node 4 because this was the lowest node on the pipeline. The average pressure difference between the measured pressure and the pressure at Node 4 was approximately 46 m.

Since the objective of the analysis was to evaluate the leakage characteristics on the pipeline, only nodes 2, 3 and 4 were analysed further.

4.9.3.3 Power equation leakage parameters

Figure 4.54 shows the graph of the flow rate plotted against the pressure head for nodes 2, 3 and 4 on the test pipeline. A power equation was fitted to the data for each node. It can be seen that the power equation fits all data well. The data was then used as a basis for calculating the N1 leakage parameters, namely the leakage exponent, $N1$, and the leakage coefficient, C.

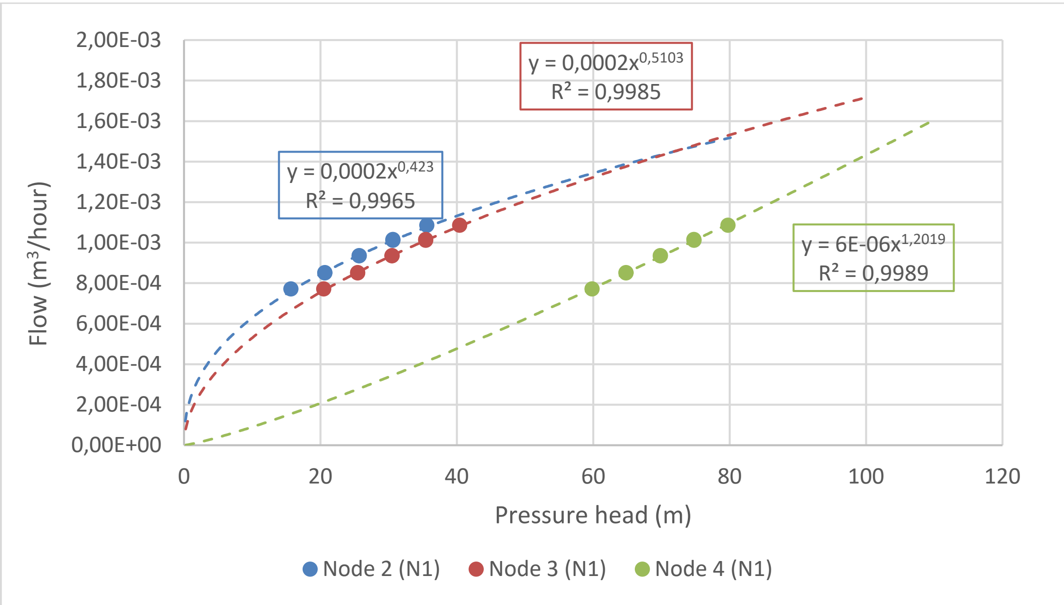

Figure 4.54: Flow and pressure data for nodes 2, 3 and 4

The results in Figure 4.54 show some variation in the leakage exponent, with the leakage exponent generally increasing with decreasing elevation. It can be seen that Node 2, at the highest elevation, had the smallest leakage exponent of 0.42, while Node 4, at the bottom of the pipeline, had the highest leakage exponent of 1.20. Node 3, the intermediate node, was found to have a leakage exponent of 0.51, which lies between 0.42 and 1.20. The results of the N1 leakage parameters for nodes 2, 3 and 4 are summarised in Table 4.14.

Table 4.14: N1 leakage parameters for nodes 2, 3 and 4

Node	Leakage coefficient, C	Leakage exponent, N1
2	2×10^{-4}	0.42
3	2×10^{-4}	0.51
4	6×10^{-6}	1.20

In practice, rigid pipes, such as the steel that was tested, are typically assumed to have N1 values of 0.5, as illustrated by the result obtained for Node 3. However, rigid pipes with extensive corrosion may have greater N1 values, such as the result found at Node 4, suggesting that the pipeline could be experiencing some moderate to extensive corrosion damage at this node (Greyvenstein and Van Zyl, 2005). On the other hand, the leakage exponent result that was substantially less than 0.5, found at Node 2, is an unlikely result for a rigid pipe, and could thus be an indication that there is no leak at this node.

4.9.3.4 Modified orifice equation parameters

The effective leak area (C_dA) was plotted against the pressure head as shown in Figure 4.55. A straight line was fitted to the data to obtain the effective head-area slope (C_dm) and the effective initial leak area (C_dA_0) from the gradient and intercept terms of the equation, respectively. It can be seen that the linear equation fits the data points very well, with an R^2 of 0.99.

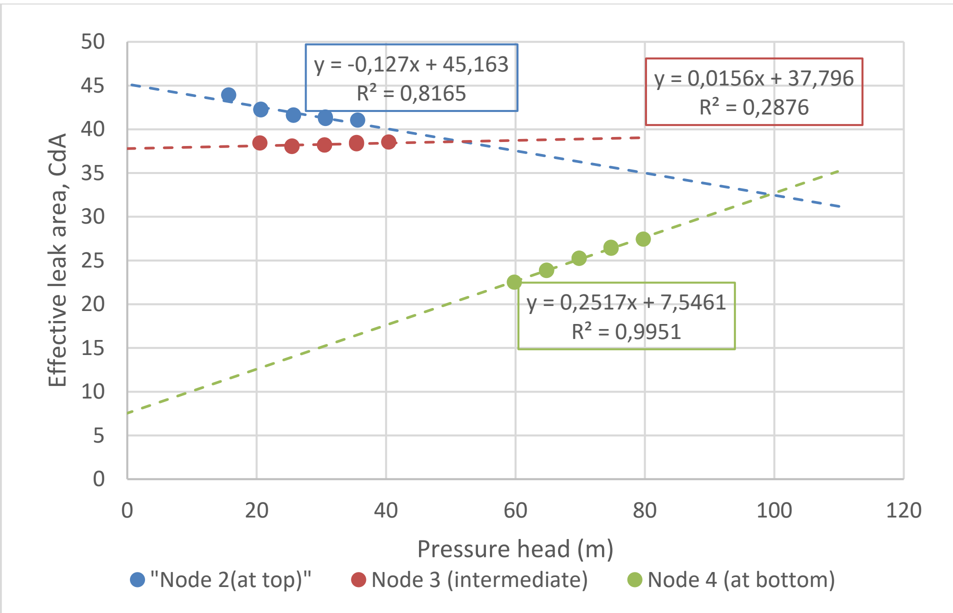

Figure 4.55: Effective leak area against pressure

The results in Figure 4.55 show that the MOE leakage parameters varied for the three nodes investigated. It can be seen that Node 2 displayed a negative effective head-area slope, suggesting that the leak area decreased with increasing pressure. Nodes 3 and 4 both displayed a positive effective head-area slope, suggesting that the leak area increased with increasing pressure. The MOE results for the pipeline are summarised in Table 4.15.

Table 4.15: Results of the modified orifice equation leakage parameters

Node	Effective Initial leakage area	Effective head-area slope	Leak characteristic
2.	45.16	-0.13	Circumferential crack
3.	37.80	0.0156	Round hole
4.	7.55	0.25	Longitudinal crack

The results shown in Table 4.15 show that if all the leakage occurred at Node 2, the leak could be characterised as a circumferential crack with an effective initial crack area of 45.16 mm^2 that reduces by 0.13 mm^2/m of pressure subjected to the pipeline. This leak type is unlikely to occur on a steel pipeline. Typical failure modes for steel pipes have predominantly been found to be corrosion failure, and in some cases longitudinal cracks, but hardly ever circumferential cracks (Greyvenstein and Van Zyl, 2005).

The results obtained for Node 3 show that if the leakage occurred at Node 3, the leak could be characterised as a round hole leak that may occur due to corrosion. This is mainly due to the small head-area slope of 0.015 mm^2/m of pressure subjected to the pipeline. The initial leak area of the round hole was estimated to be 37.80 mm^2.

Finally, the results for Node 4 show that if the leakage occurred at Node 4, the leak type could be characterised as a longitudinal crack, with an initial crack area of 7.55 mm^2, which expands by 0.25 mm^2/m of pressure subjected to the pipe. This result is characteristic of a longitudinal crack because of the positive head-area slope that is greater than 0.1 mm^2/m (Malde, 2015).

4.10 GARSFONTEIN TO PARKMORE HIGH-LEVEL RESERVOIR PIPELINE

4.10.1 Introduction

The Garsfontein to Parkmore High-level Reservoir steel bulk pipeline (the GP pipeline) was pressurised by the national bulk water supplier, Rand Water, to a pressure of at least 6 bar. The pipeline was 2 640 m in length, with a pipe diameter of 406 mm.

The layout of the GP pipeline is shown in Figure 4.56, starting at the isolation valve (V1) located near the Garsfontein Reservoir site. The pipeline dips 60 m down through a narrow valley and then rises to the Parkmore High-level Reservoir. The final isolation valves, V2, V3 and V4, are located approximately 40 m upstream of the Parkmore High-level Reservoir. The pipeline is pressurised by a Rand Water line to a pressure of at least 6 bar.

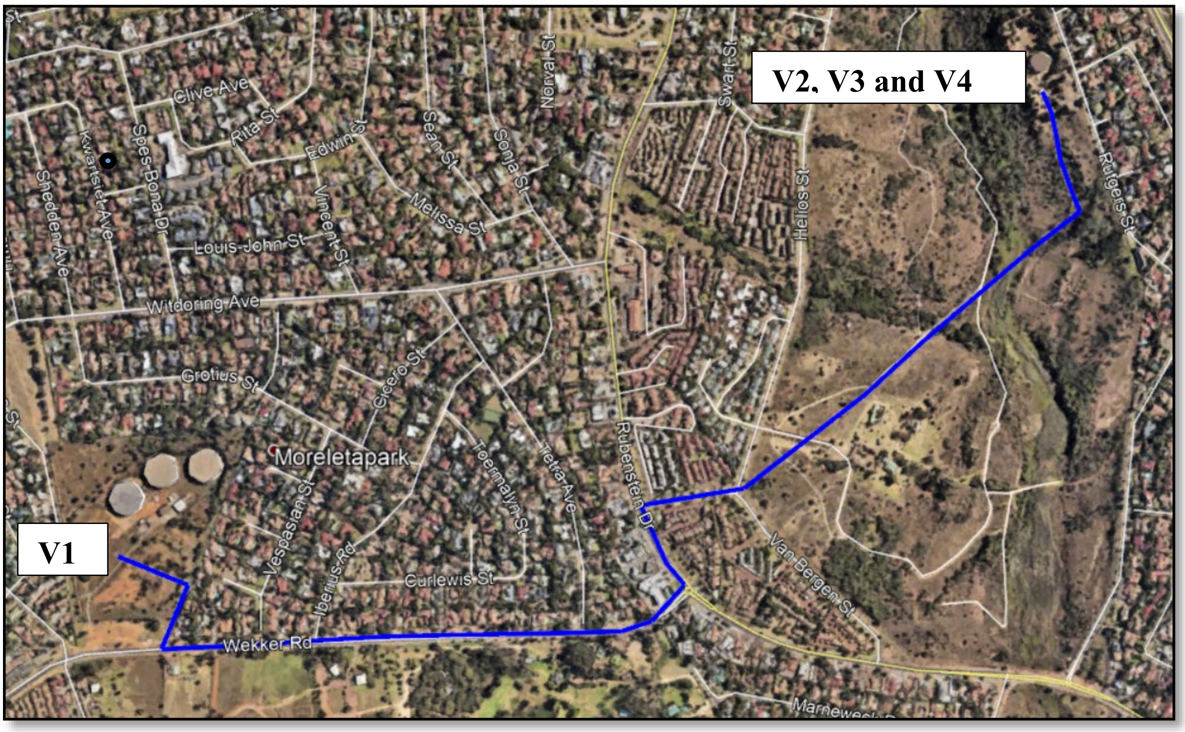

Figure 4.56: Pipeline route starting at V1 (5 bar+) and ending at V2 (5 bar+)

A Google Earth image of the Garsfontein Reservoir site configuration is shown in Figure 4.57, with the location of isolation valve V1, a pressure-regulating valve housed in an underground concrete chamber. By isolating this pressure-regulating valve, the pipeline was isolated from the main source supplying the pipeline.

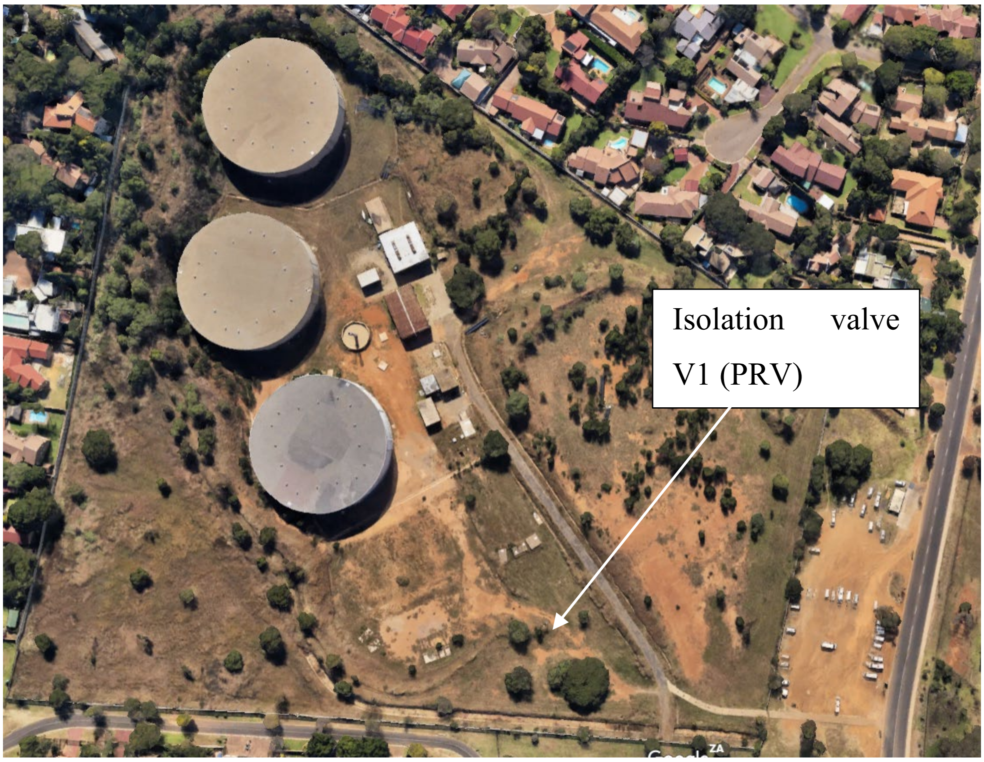

Figure 4.57: Garsfontein Reservoir setup

Figure 4.58 shows the Google Earth image of the Parkmore High-level Reservoir, with the location of the chamber that house isolation valves V2, V3 and V4. This chamber was also where the device was connected.

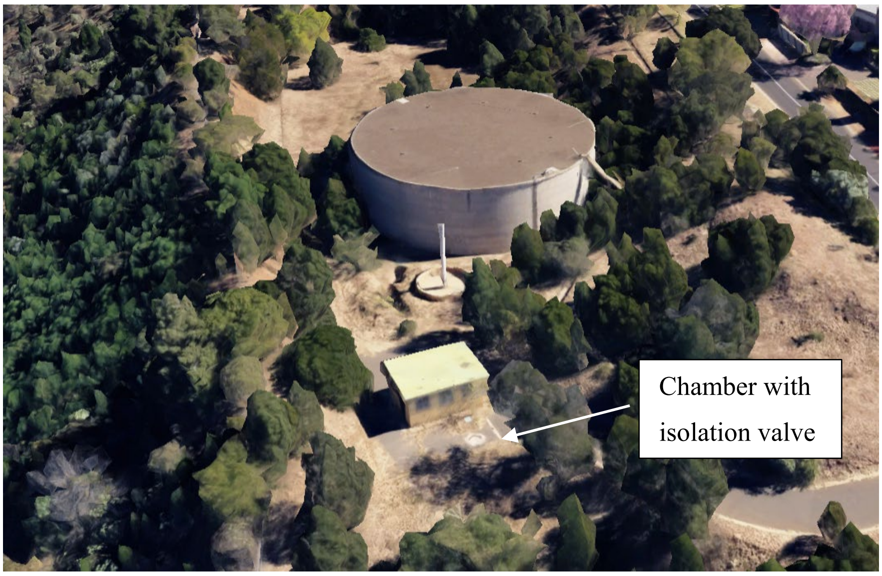

Figure 4.58: High-level Reservoir configuration

Figure 4.59 shows the setup in the chamber housing valves V2, V3 and V4. From Figure 4.59, it can be seen that isolation valve V2 was a gate valve, V3 was a pressure-regulating valve and V4 was another gate valve. Some apparatuses were installed on the pipeline. These included a flow meter and two off-takes supplying a distribution network from the reservoir.

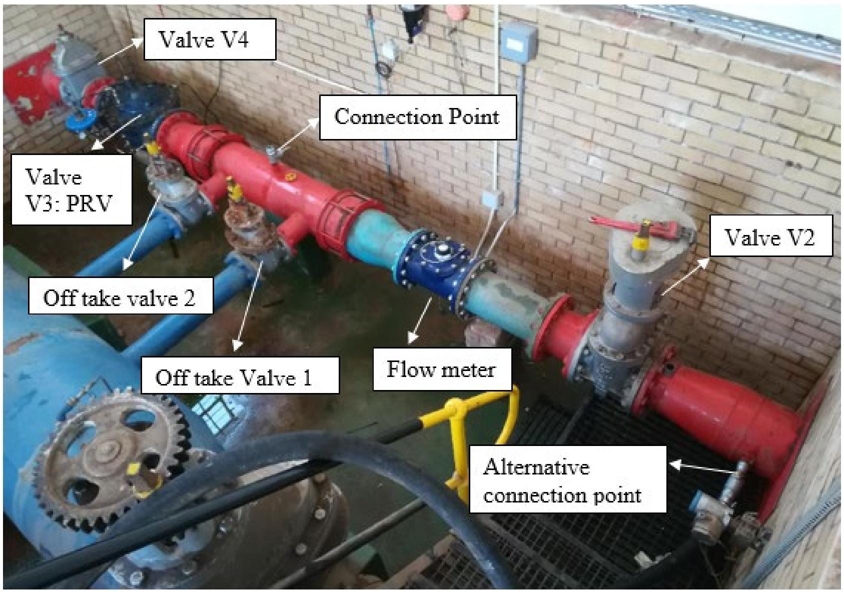

Figure 4.59: Chamber housing valves V2, V3 and V4 and other components

4.10.2 Procedure

The tests began at the Garsfontein Reservoir, where the operator closed isolation valve V1 (a pressure-regulating valve). According to the operator, the pressure-regulating valve closed effectively and no sign of leakage through the valve was observed or heard.

The PCAE device was connected to the GP pipeline via the 25 mm threaded connection that had been installed on the main pipe, as shown in Figure 4.60. The PCAE water tank was then filled. After filling the tank, isolation valve V4 (also shown in Figure 4.60) was closed. The two valves on the respective offtake valves were already closed on arrival. These two offtake valves had apparently never been operated, and the operational team was certain that they did not leak.

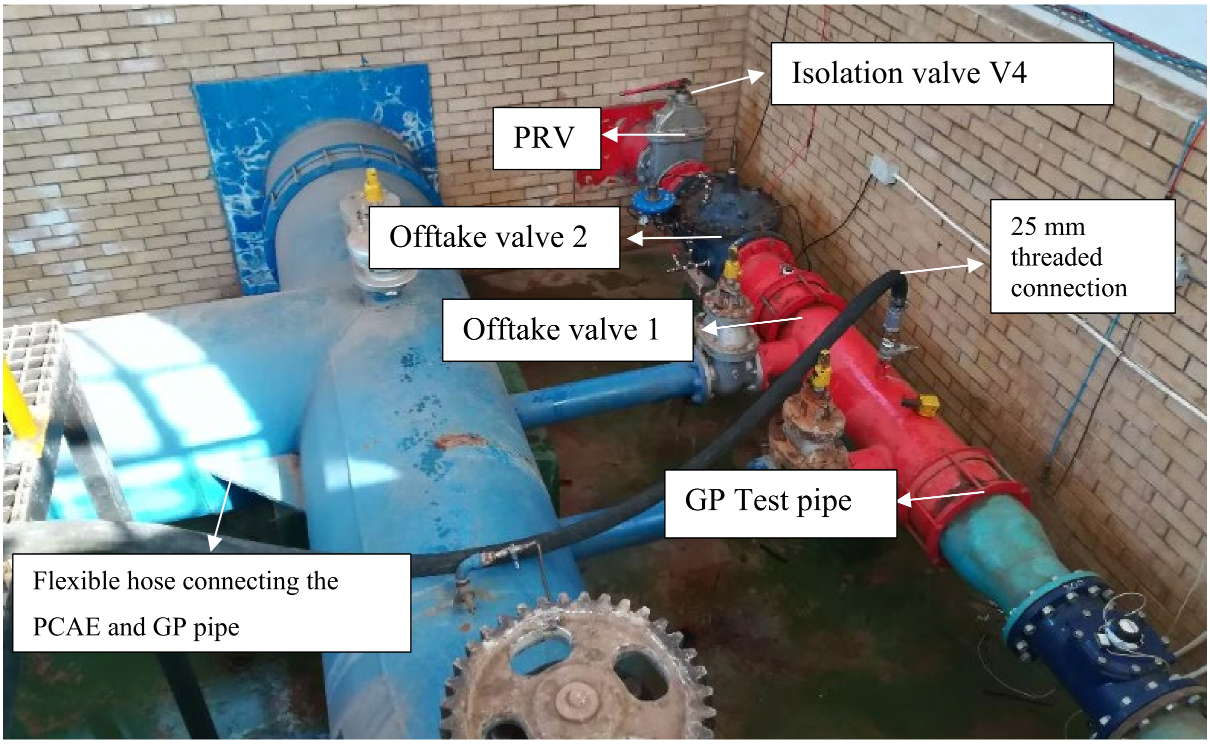

Figure 4.60: Connection of testing equipment

After isolating the GP pipeline, it appeared as if air was being sucked into the flexible hose, indicating that the GP pipeline was draining. Consequently, it was assumed that the isolation valves V1 and V4 sealed the GP pipeline effectively.

The variable speed pump was then activated to pressurise the GP pipeline and the first leak test commenced. The pump was set to the maximum pressure, which went up to 3.1 bar, as shown in Figure 4.61. After that, the pressure was dropped at increments of 0.5 bar from 3.1 bar to 1.2 bar and then increased again incrementally by 0.5 bar.

A very clear leak was detected, which appeared to be pressure dependent, as the flow rate pattern was consistent with the pressure pattern. The PCAE water tank eventually emptied after about 15 minutes of testing.

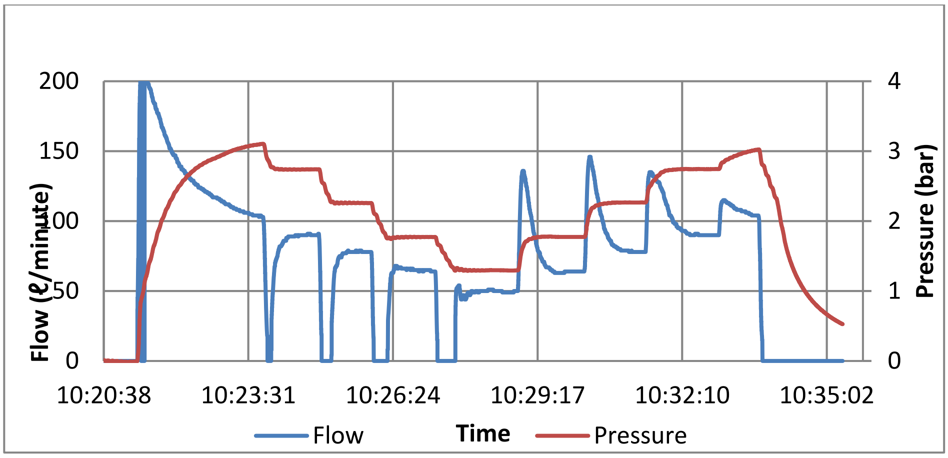

Figure 4.61: Pressure and flow profile data

It was decided to repeat the test. Valve V4 was opened again to fill the PCAE water tank, and then closed after the tank was full. The test was repeated, approximately 20 minutes later. It was immediately evident that the leakage was drastically reduced with very different results from the first test, as shown in Figure 4.62. The flow and pressure did not stabilise very well.

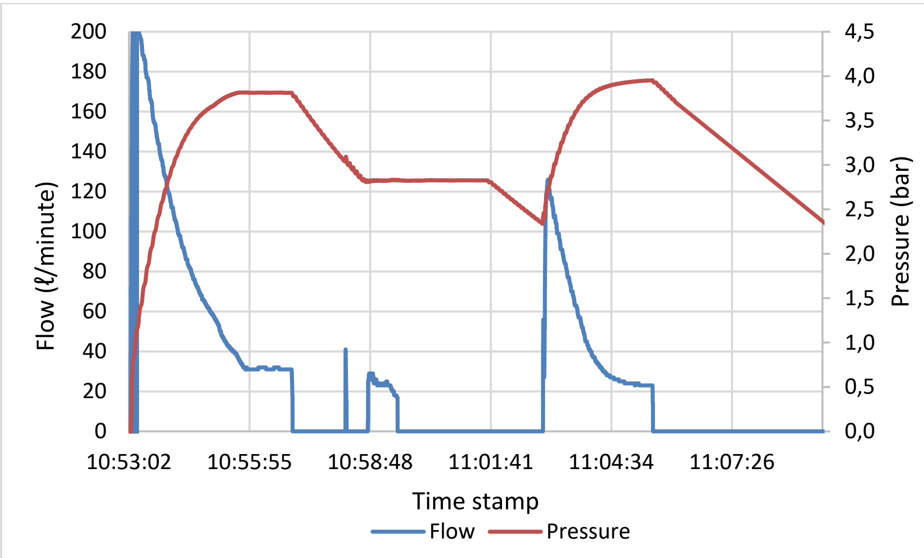

Figure 4.62: Flow and pressure profile of the repeated test

The maximum pressure went up to 3.8 bar and was dropped by 1 bar, and the pressure was allowed to stabilise. It was also noted that the leakage was not very pressure dependant. It was unclear why the results differed as the pipe was isolated by closing valves V1 and V4, as was done in the first attempt. It was also not clear where the leakage flow in the initial test (Figure 4.61) went to, as the pressure upstream and downstream of the GP pipeline was higher than 5 bar, meaning that, should any leak have occurred at the valves, the flow would have been into the GP pipeline and consequently the device would not have been able to pressurise the pipeline.

As a result of the inconsistency between the first two attempts, the test was repeated an hour later. An attempt was made to close the pressure-regulating valve (V3) as well, but due to the low flow and isolation of the pipe, it is not clear whether the pressure-regulating valve closed completely. The results of the third test attempt, illustrated in Figure 4.63, still did not match those of the first test.

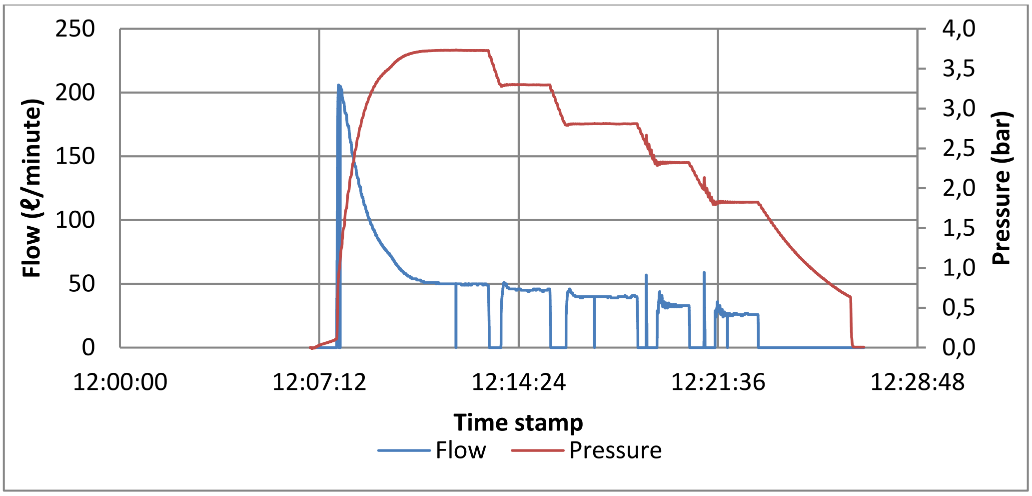

Figure 4.63: Flow and pressure data after the second attempt

It was still unclear why the test results differed because the only change between the two initial tests was the opening and closing of the control valve, and some adjustment to one of the two bypass valves that were already closed.

To investigate this inconsistency further, the hosepipe was disconnected to check whether there was any flow coming out of the test pipe via the connection point. A small inconsistent outflow was observed from the connection point. It appeared as if the flow was alternating between an outflow and inflow through the connection point.

A number of possibilities for the inconsistency are discussed:

Possibility 1:

It was possible that water was drawn off the main pipeline, possibly by an illegal connection, but the operators believed this to be highly unlikely.

Possibility 2:

As the pipe drained after the isolation valve at Garsfontein, and the supply from the reservoir was isolated, air was sucked into the pipe to compensate for the volume of water leaving the pipe through a leak. When the supply to the reservoir was opened again, an air lock could have formed in the pipeline and collected at a high point as illustrated in Figure 4.64.

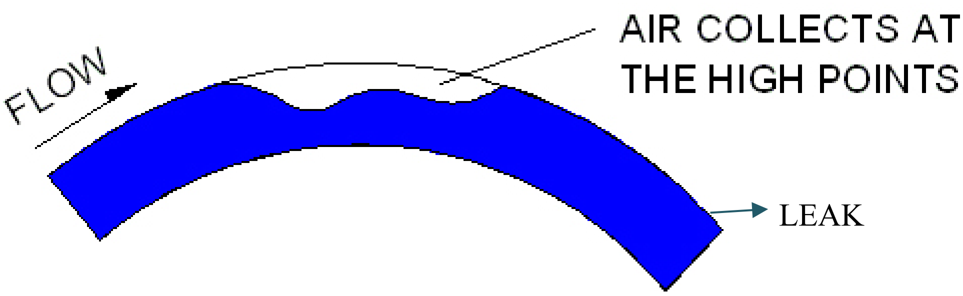

Figure 4.64: Air pocket collecting at a high point in a pipe

Note the associated reduced pipe diameter as a result of the air pocket in Figure 4.64. Water will trickle over the elbow and fill the pipe from the other side. If the leak is on the downstream side of the pipeline, the water level on the other side will continue to drop due to the downstream leak. As the pressure is increased, the level before the elbow rises due to the compression of the air. This possibly results in a higher flow rate over the bend. It would therefore appear as though water is lost through a leak, yet most of the flow is only filling the pipeline and compressing air.

Possibility 3:

The third and final possibility explains why the first attempt experienced a high leakage rate, and then a much lower leakage rate. This could have happened because air was sucked into the pipe through a small leak in order to replace the volume lost through the larger leak downstream. Then, as the pipe was pressurised, the air was forced back out through the same leak at which it entered. The flow rate of the air through the leak was, however, much higher than that of water. Therefore, while the leaking of air contributed to the replacement of water pumped into the pipe, it appeared as if there was a huge leak. Once all the air was out, the rate reduced, as water will not leave the pipe at the same rate as air. Due to the uncertainty about leaking valves, and the large number of valves on the tested pipe, it was decided to repeat the test by isolating the pipe with valve V2, rather than the pressure-regulating valve or valve V4. This effectively ensured that the ineffective isolation of the off-take pipes would not influence the results.

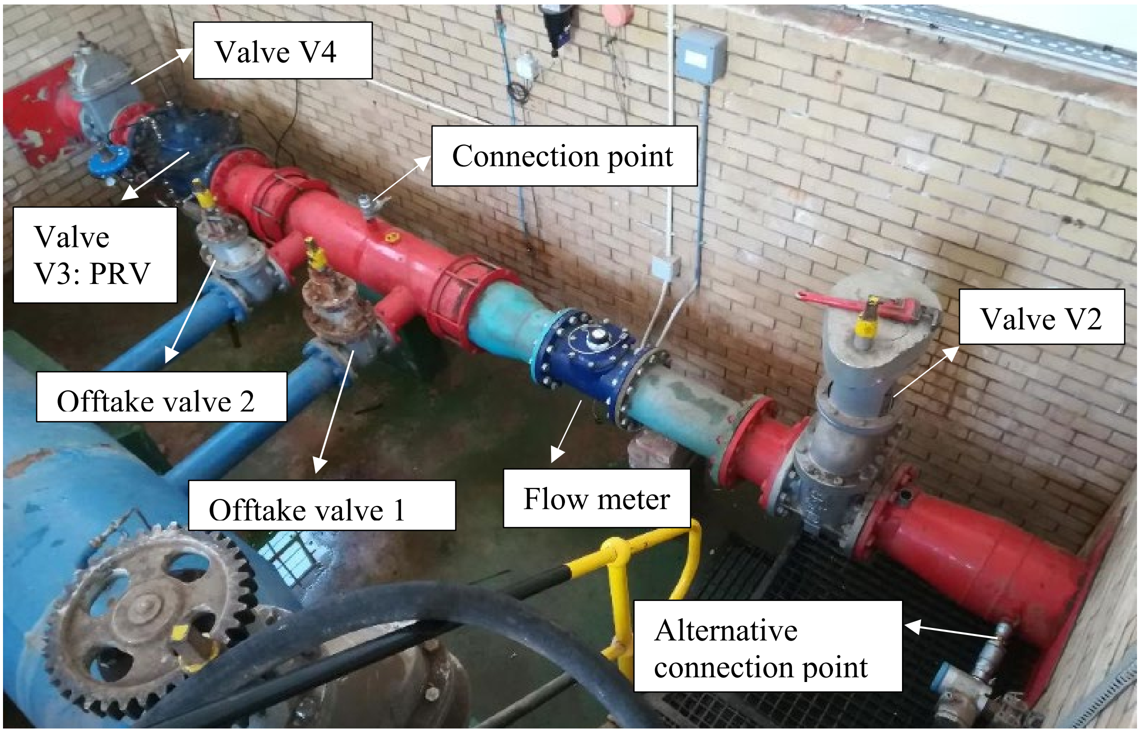

Figure 4.65: Alternative connection point

A close-up image of the alternative connection point is shown in Figure 4.66. The alternative connection point was a 25 mm connection point. The tank was filled from this alternative connection point. Once the tank was full, isolation valve V2 was closed instead of V3, which had been closed previously.

Figure 4.66: Alternative connection point

Unfortunately, even though an effort was made to keep the pipe pressurised, air entered the pipe through the connection point during the disconnection and reconnection of the testing equipment, because the connection point could not be isolated.

To assess whether valves V1 and V2 closed effectively, the level of water in the tank was monitored over a period. The water level in the tank appeared to drop, rather than rise, indicating that water was flowing back into the GP pipeline. If the valves were not sealing, the water level in the tank would be expected to rise, since the pressures just downstream of valve V1 and just upstream of valve V2 were higher than those in the pipe, and would therefore result in flow entering the GP pipeline, and subsequently filling the water tank; hence, the water would rise. In addition, the operators were confident that these valves did not leak.

Unfortunately, after connecting to the pipe, there was air in the pipeline that could not be discarded. Nonetheless, the test was carried out. Figure 4.67 shows the flow and pressure results of the test.

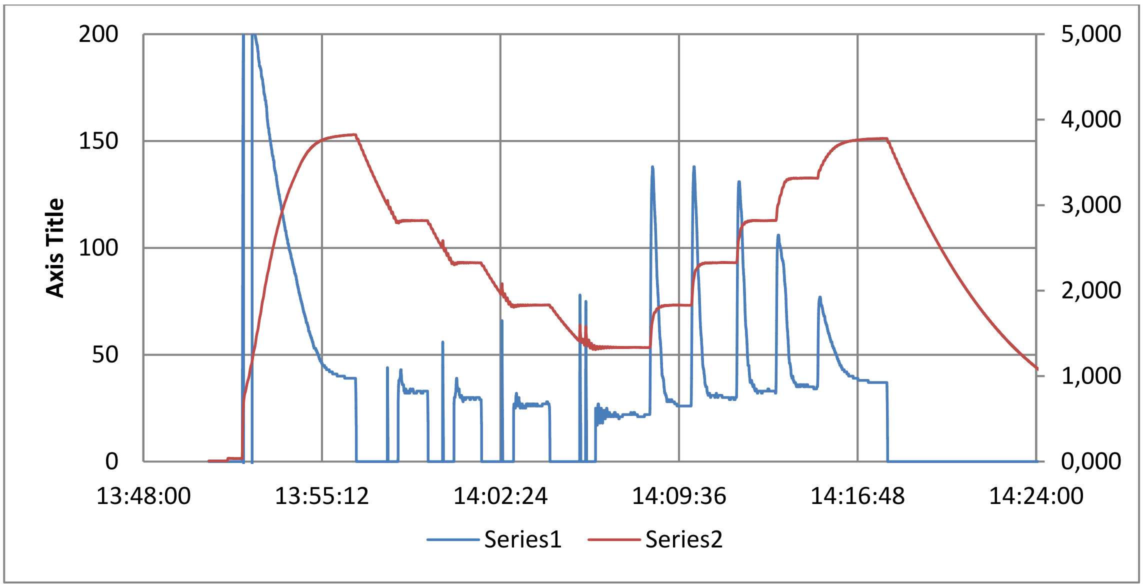

Figure 4.67: Flow and pressure data from the alternative connection point

There was much more confidence in this test, and a general consensus that a leak was identified, although not as large as expected in the first attempt. The higher fluctuation in the flow that can be seen when the pressure is incrementally increased could be due to the air pockets in the pipeline, which potentially dampened the effect of a change in pressure.

4.10.3 Results

4.10.3.1 Data analysis procedure

Figure 4.68 shows the elevation profile section of the GP pipeline. The pipeline starts at valve V1. It then dips by 27 m to “Bottom Valley 1”, and rises by 13.96 m to “Top of valley”. Then it dips again by 29.74 m to “Bottom Valley 2”, and rises again to the final isolation valves, V2, V3 and V4.

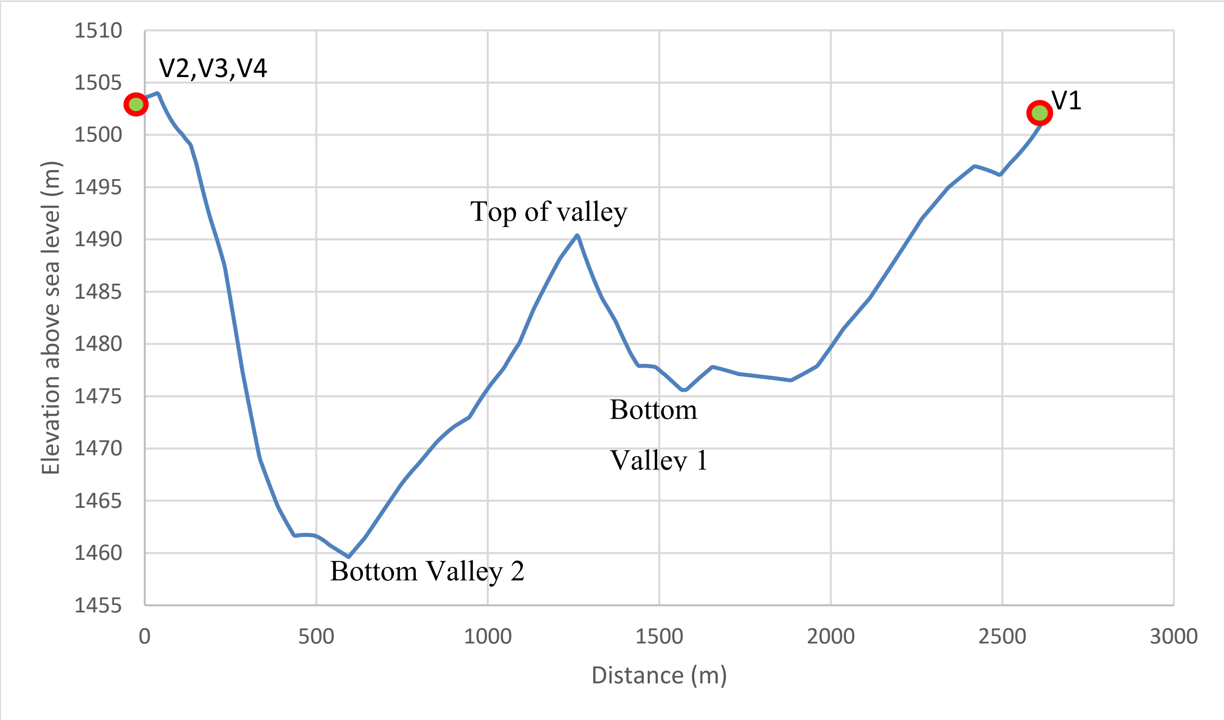

Figure 4.68: Elevation profile of the GP pipeline

Nodes were assigned at critical points on the pipeline as shown in Figure 4.69. The downstream valve, V1, where the pipe starts, was assigned Node 4. The lowest point of the pipe, “Bottom Valley 2”, was assigned Node 3. Node 2 was the isolation valve at the end of the pipe. The connection point on the pipeline was assigned Node 1. Finally, the PCAE pressure sensor was assigned Node 0.

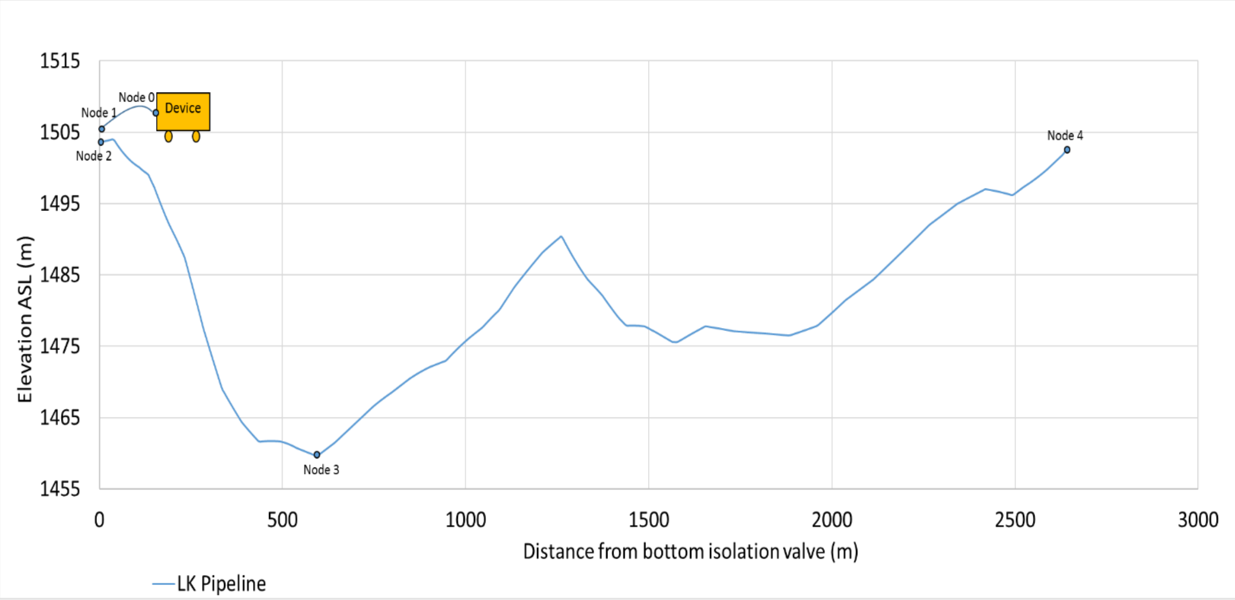

Figure 4.69: Elevation profile with nodes

A summary of the pipe properties between each node is given in Table 4.16. These pipe properties are used to calculate the head losses between each node and therefore adjust the pressure accordingly for each node. Since the pressure head at Node 0 is known (the measured pressure head), the analysis starts from Node 0 and ends at Node 4. The minor loss coefficients, *k*, and absolute roughness, *e*, are obtained from Finnemore and Franzini (2009).

Table 4.16: Pipe properties between each node

Pipe properties	Node 0 to Node 1	Node 1 to Node 2	Node 2 to Node 3	Node 3 to Node 4
Pipe section identity	Delivery hosepipe	Connection	Test pipe	Test pipe
Diameter, d (mm)	50	25	500	500
Absolute roughness, e (mm)	0.3	0.03	0.15	0.15
Minor loss coefficient, k	0.3	0.33	0.5	0
Elevation difference, Δz (m)	1.85	0.8	56.92	-47
Length of pipe, l (m)	10	0.8	600.00	2040.16
e/d	6.00E-03	1.80E-03	3.00E-04	3.00E-04
Pipe area, A (m^2)	1.96E-03	4.91E-04	1.96E-01	1.96E-01

4.10.3.2 Data interpretation

The raw flow and pressure data obtained from the PCAE recorder is plotted against time in Figure 4.70. As can be seen from the figure, the pressure was varied at increments of 0.5 bar, and the flow rate was allowed to stabilise before another pressure increment was set. The flow rate detected suggests that a leak exists in the pipeline.

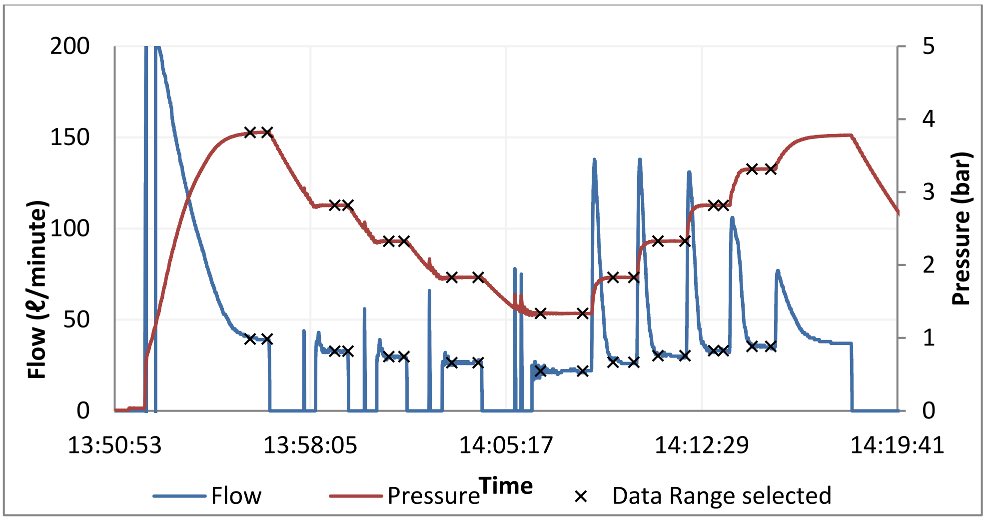

Figure 4.70: Flow and pressure data showing the stabilised data range selected

While the pressure curve showed clear transitions between steps, the flow curve dropped below the stabilised value at the start of each downward step, and above the stabilised value at the start of each upward step. The reason for this behaviour is the contraction and expansion of the pipe diameter (and thus internal volume) as a result of the changes in pressure. The higher flow fluctuation at the start of each upward step can be attributed to the potential air pockets in the pipeline. The air pockets may have had a dampening effect as the pressure changes.

The x-markers on the graphs in Figure 4.70 indicate the periods of stable flow and pressure that were used for further analysis. The measured pressure values were adjusted for each node. This was done by taking the elevation difference, pipe friction and minor losses between the pressure sensor and each node into account.

Table 4.17 gives a summary of the pressure at each node. It is important to note that Node 0 represents the device and thus the measured pressure.

Table 4.17: Flow and adjusted pressure for each node

Q (m^3/s) flow rate	h at Node 0	h at Node 1	h at Node 2	h at Node 3	h at Node 4
6.57E-04	38.93	40.74	41.45	94.6981	47.698
5.45E-04	28.75	30.57	31.31	84.5588	37.559
4.95E-04	23.73	25.56	26.30	79.5522	32.552
4.40E-04	18.66	20.50	21.25	74.5029	27.503
3.64E-04	13.62	15.46	16.23	69.4812	22.481
4.45E-04	18.66	20.50	21.25	74.5017	27.502
5.05E-04	23.74	25.56	26.31	79.5569	32.557
5.50E-04	28.75	30.57	31.30	84.5521	37.552
5.90E-04	33.82	35.64	36.36	89.6141	42.614

It can be seen from Table 4.17 that the highest pressures were found to occur at Node 3, the lowest point of the pipe (see Figure 4.69). The lowest pressures occurred at Node 0, as expected because this was the highest point of the analysis. Due to the conservation of mass principal, the flow rate, *Q*, measured at Node 0, was assumed to be the same for each node.

For the leakage modelling analyses (power equation and MOE), only the nodes located on the test pipe were used for analysis. These included nodes 2, 3 and 4.

4.10.3.3 Power equation leakage parameters

The flow and adjusted pressure values for nodes 2, 3 and 4 in Table 4.17 are plotted in Figure 4.71. The reason why only nodes 2, 3 and 4 are plotted is because these nodes are located on the GP pipeline, and therefore, the leakage parameters obtained at these nodes provide an envelope of possible leakage parameters on the pipe.

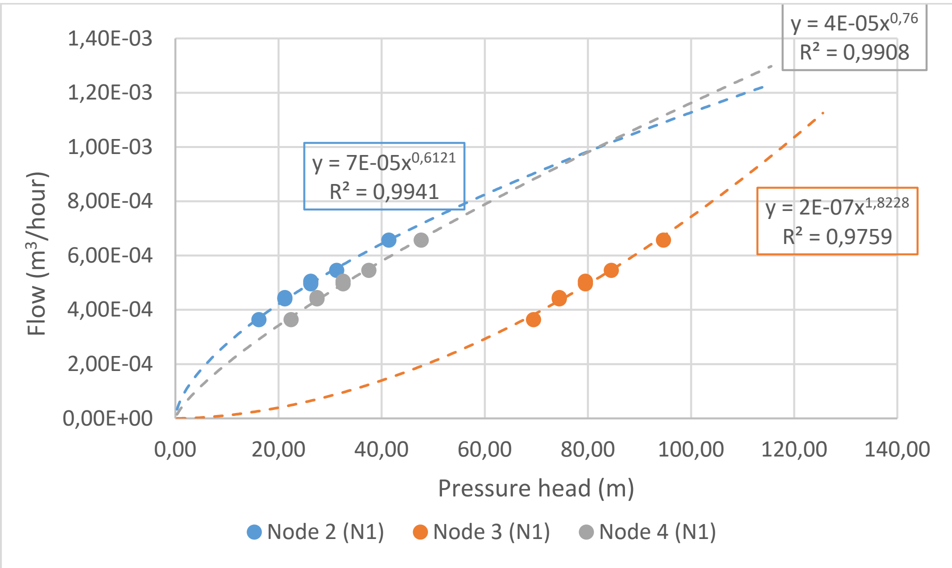

Figure 4.71: Flow against pressure data for nodes 2, 3 and 4

A power equation is fitted on the data points as indicated in Figure 4.71. From the power equation, the leakage coefficient, *C*, and the leakage exponent, *N1*, were obtained for each node, and are given in Table 4.18.

Table 4.18: Power equation leakage parameters for nodes 2, 3 and 4

Node	Leakage coefficient, C	Leakage exponent, N1
2.	7×10^{-5}	0.61
3.	2×10^{-7}	1.82
4.	4×10^{-5}	0.76

It can be seen that the largest leakage exponent, *N1* = 1.82, was obtained at Node 3, which had the highest pressures (see Table 4.18), followed by *N1* = 0.76 at Node 4, and finally *N1* = 0.61, obtained at Node 2. Generally, it can be seen that the nodes with higher pressures also had the largest leakage exponents, but the lowest leakage coefficient.

Since the GP pipeline is a steel pipeline, it can be classified as a rigid pipe. Consequently, the *N1* exponent would be expected to be around 0.5. However, nodes 2, 3 and 4 all had *N1* exponents greater than 0.5. These higher leakage exponents can occur in rigid pipes due to excessive corrosion. Therefore, the leakage exponent results could suggest that the pipeline had potentially undergone some excessive corrosion; particularly for the section of pipe between nodes 3 and 4.

4.10.3.4 Modified orifice equation

The effective leakage areas at each pressure were calculated for nodes 2, 3 and 4. The results are shown in Table 4.19. It can be seen from Table 4.19 that the largest leakage areas were found to occur at Node 2, even though this node had the smallest averaged pressure heads. This is because the flow rate is assumed to be the same at each node. From the data in Table 4.19, it is clear that, for the same flow rate, if the pressure head, h, is reduced, then the leakage area increases.

Table 4.19: Head-area slope and adjusted pressure for each node

	Node 2		Node 3		Node 4	
Q flow rate	**h (m)**	**A'_2 (mm²)**	**h (m)**	**A'_3 (mm²)**	**h (m)**	**A'_4 (mm²)**
6.57E-04	41.45	23.03	94.70	15.23	47.70	21.46
5.45E-04	31.31	21.99	84.56	13.38	37.56	20.07
4.95E-04	26.30	21.81	79.55	12.54	32.55	19.60
4.40E-04	21.25	21.55	74.50	11.51	27.50	18.94
3.64E-04	16.23	20.38	69.48	9.85	22.48	17.31
4.45E-04	21.25	21.80	74.50	11.64	27.50	19.16
5.05E-04	26.31	22.22	79.56	12.78	32.56	19.97

The effective leakage area, A', against the pressure head was plotted for nodes 2, 3 and 4, as shown in Figure 4.72. A linear function was fitted to the data points. The intercept of each linear line with the area axis (y-axis) gave the effective initial leak area, A'_0, and the slope of the line gave the effective head-area slope, m'.

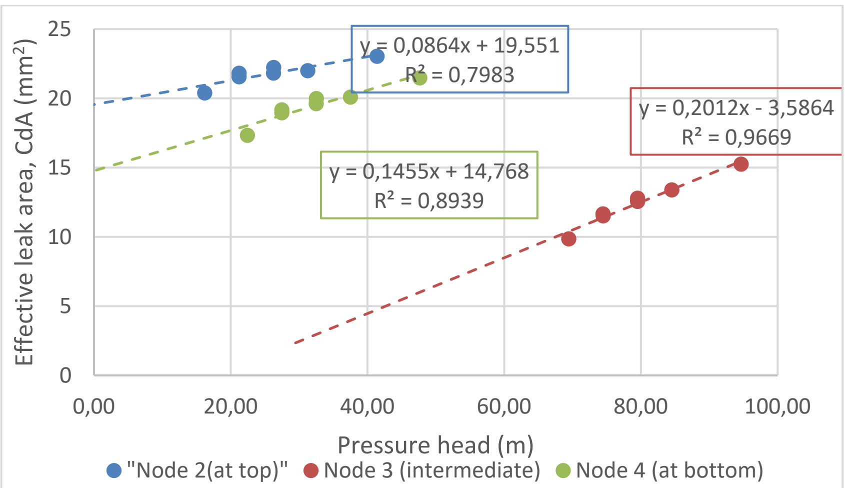

Figure 4.72: Effective leak area against pressure

The results shown in Figure 4.72 show that all nodes had leaks with positive head-area slopes, but with varying magnitudes. Node 3 had the largest head-area slope of 0.19 mm^2/m, followed by Node 4 with 0.15 mm^2/m, and finally Node 2 with a head-area slope of 0.04 mm^2/m. A summary of the results is provided in Table 4.20.

Table 4.20: Modified orifice equation leakage parameters

Node	Effective initial leakage area	Effective head-area slope	Leak characteristic
2.	21.69	0.043	Round hole
3.	-3.54	0.19	Longitudinal crack
4.	13.74	0.15	Longitudinal crack

The results in Table 4.20 show that if all the leakage occurred at Node 2, the leak could be characterised as a round hole. This is because of the small expansion rate of about 0.043 mm^2/m on the pressure head, which is characteristic of a round hole. The initial leakage area of approximately 21.69 mm^2 would then imply that the round hole has a diameter of 5 mm.

The results obtained for Node 3 show that if the leakage occurred at Node 3, the expansion rate would be 0.19 mm^2/m of pressure applied. A negative initial leakage area was obtained. While this is not physically possible, this result suggests that the leak remained closed and only started to open up at a pressure head of about 18.2 m (the x-axis intercept).

The results for Node 4 show that if all the leakage was located at Node 4, the leakage area would be expanding at 0.15 mm^2/m of pressure. This positive expansion rate is consistent with a longitudinal crack with an initial leakage area of approximately 13.74 mm^2.

4.11 BRICKFIELDS TO CONSTANTIA RESERVOIR

4.11.1 Introduction

The Brickfields to Constantia Reservoir steel bulk pipeline (the BC pipeline) was a rising main, fed by gravity. The pipeline was ±5 000 m in length with a nominal diameter of 450 mm.

The layout of the BC pipeline is shown in Figure 4.73. The section of the pipeline that was tested starts from isolation valve V1 (the butterfly valve) and ends at isolation valve V2 (the pressure-regulating valve). The elevation difference between the operating system pressure upstream of valve V1 was approximately 10 bar, and downstream of V2 it was approximately 3 bar.

BRICKFIELDS → CONSTANTIA

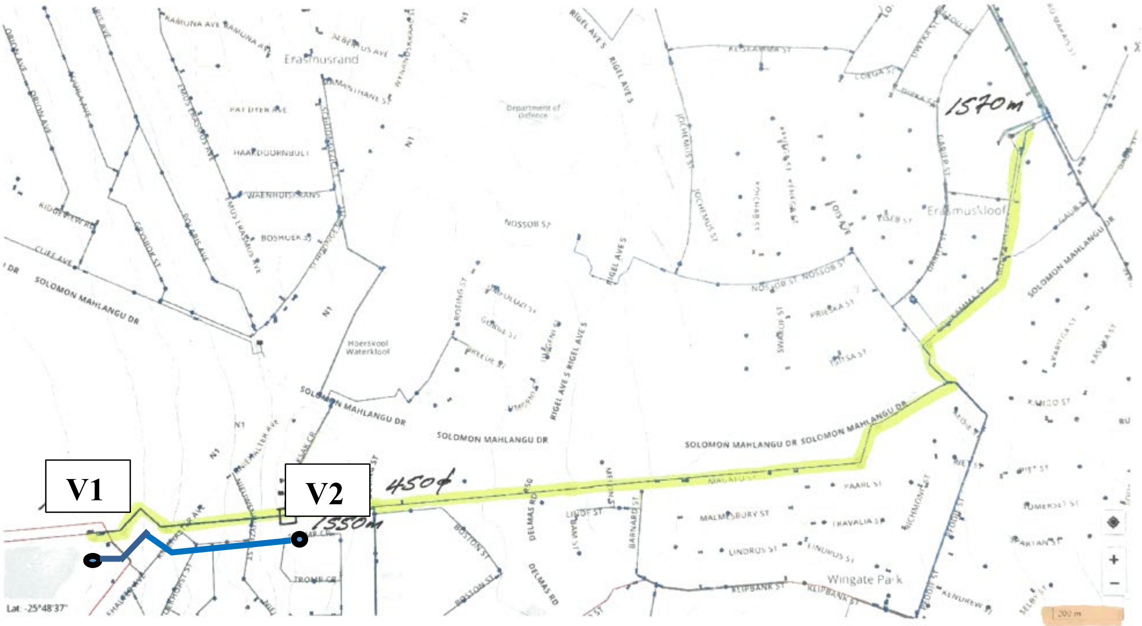

Figure 4.73: Layout of pipeline route starting at V1 and ending at V2

4.11.2 Procedure

The test began at isolation valve V2, where the operational team isolated a pressure-regulating valve housed in an underground chamber. It was observed that the pipes near this chamber were not in a good condition. Some of the pipes were excessively corroded, and it appeared as though a large area near the chamber had recently been excavated to fix a leak.

The operational team then drove to Brickfield to close isolation valve V1 (the butterfly valve). After two hours, the operational team returned to isolation valve V2, and explained that valve V1 did not seal at all. A large flow still passed the valve in its closed position. Based on this and the recommendation by the operational team, it was decided to abandon this test.

4.11.3 Results

No results were obtained for this test because the butterfly valve, at isolation valve V1 from which the pipeline is fed, did not seal. A large flow was heard passing through the butterfly valve in its closed position. Furthermore, this was a complex pipeline that required a number of isolation valves to be closed.

4.12 FORT KLAPPERKOP RESERVOIR TO CARINA STREET PIPELINE

4.12.1 Introduction

The Fort Klapperkop Reservoir to Carina Street steel bulk pipeline (the FC pipeline) is a gravity-fed, rising pipeline. It is directly supplied by the bulk water supplier, Rand Water. The pipeline is 2 700 m in length, with a nominal diameter of 406 mm and an internal thickness of 3.15 mm.

The layout of the FC pipeline is shown in Figure 4.74. The section of pipe tested starts at the isolation valve V1 (the gate valve) at the Fort Klapperkop Reservoir. The pipeline then rises to a maximum height after dropping to the final isolation valve V2 (the gate valve) at Carina Street, where it ends. Isolation valve V1, at the bottom, was pressurised by a Rand Water line to a pressure of at least 5 bar. The isolation valve V2, at the top, was pressurised to approximately 0.3 bar.

Figure 4.74: Pipeline route starting at V1 (5 bar+) and ending at V2 0.3 bar+)

A Google Earth image of the reservoir configuration at Carina Street is shown in Figure 4.75, with the location of the chamber that housed the gate valve used to isolate the pipe at V2.

Figure 4.75: Google Earth image of the reservoir configuration at Carina Street

It was observed that the chamber housing of isolation valve V2 had a number of pressure-regulating valves on branches, as shown in Figure 4.76, all of which had to be closed to isolate the pipeline. It was also noted that a strainer on the tested pipe had a significant leak, resulting in a spray of water in the room. The spray appeared to be pressure dependant, as it reduced significantly immediately after the pipe was isolated. The size of this leak is unknown.

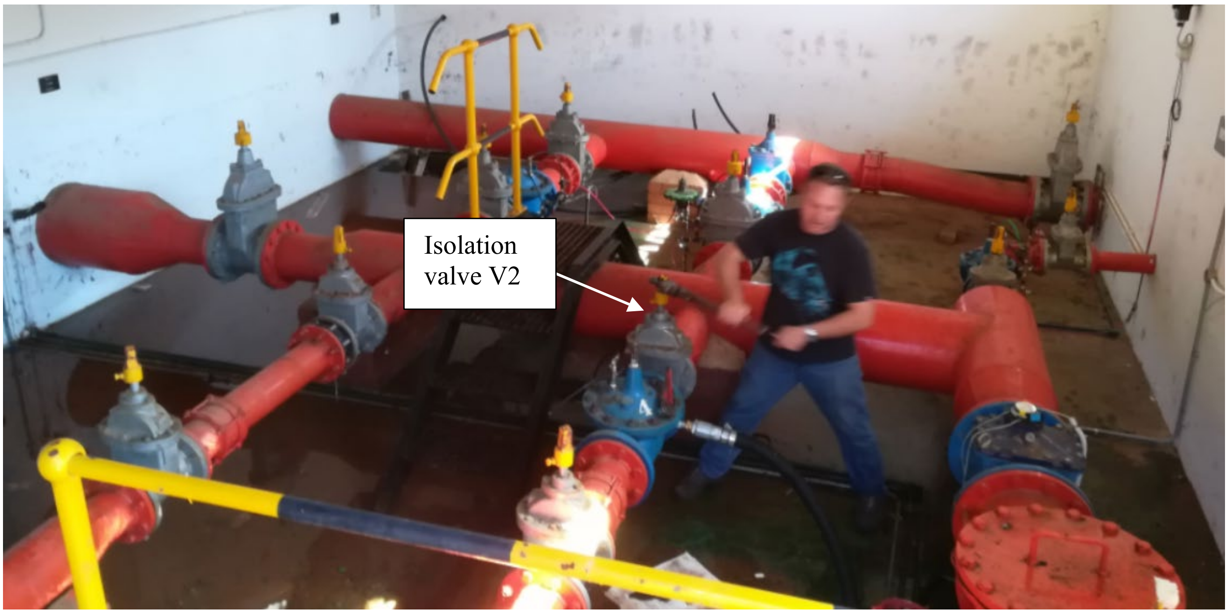

Figure 4.76: Carina Street chamber housing the isolation valve V2

A Google Earth image of the Fort Klapperkop Reservoir setup is shown in Figure 4.77. The FC pipeline is directly supplied by a Rand Water pipe and isolated on the site by a pressure-regulating valve. The pipeline is not related to the reservoirs in this figure.

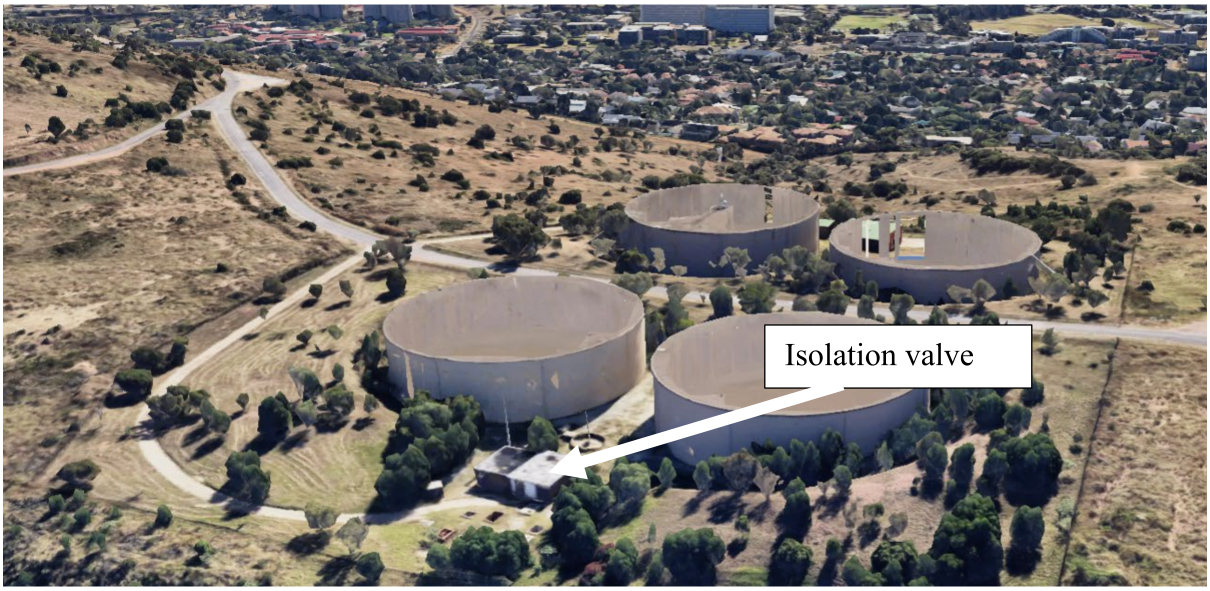

Figure 4.77: Fort Klapperkop Reservoir setup

4.12.2 Procedure

The test began at isolation valve V1 at the Fort Klapperkop Reservoir (Figure 4.77), where the FK pipeline was supplied by a Rand Water pipe. An operator remained at the valve to operate the valve once the tests commenced.

The rest of the team then drove to the Carina Street chamber that housed isolation valve V2, shown in Figure 4.78. This chamber was approximately 2.7 km from isolation valve V1. Four pressure-regulating valves in the chamber had to be closed to isolate the FC pipeline.

In addition, three gate valves also isolated this pipeline, but two of the three were already in a closed and sealed position. The third gate valve was downstream of the pressure-regulating valve to which the testing equipment was connected. This means that seven valves had to be closed in this chamber to isolate the pipe. The operator was confident that all seven valves closed fully. The bottom valve feeding the pipe was definitely closed because the pressure in the pipe dropped to much lower levels than would be expected if the valve was even slightly open.

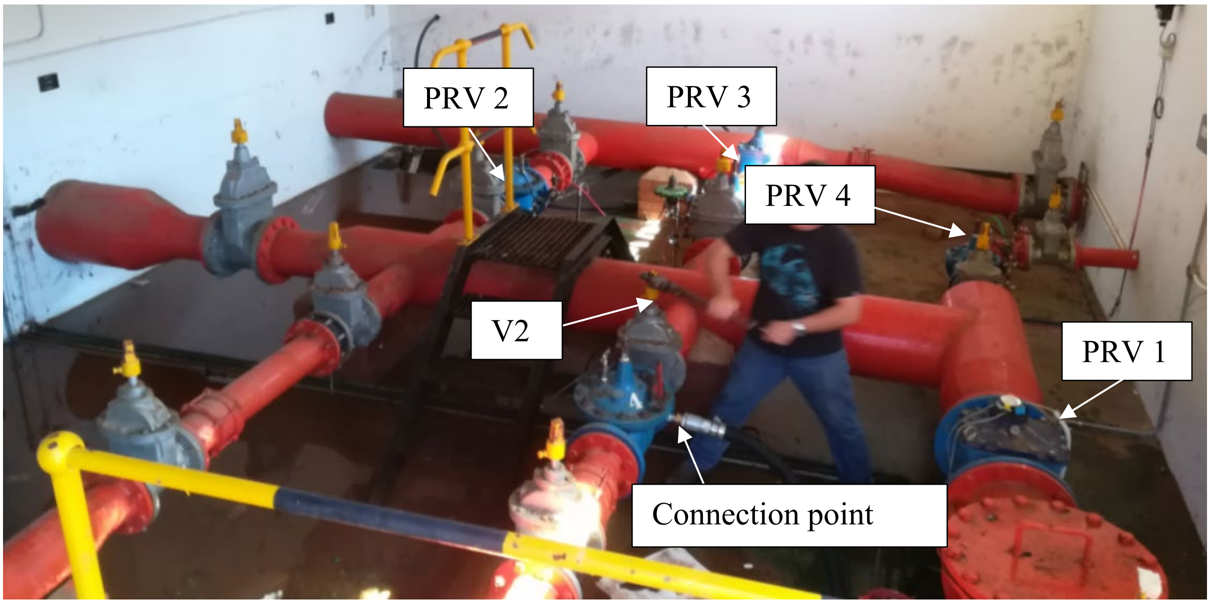

Figure 4.78: Pressure-regulating valves that were closed to isolate the pipe

A closer view of the connection point is shown in Figure 4.79. The connection point was a 20 mm (3/4 inch) connection to a pressure-regulating valve directly on the main pipe and just downstream of isolation valve V2.

Figure 4.79: Connection point on the pressure-regulating valve

The hose of the testing device was then connected. The operator who remained at valve V1 was instructed to open the valve to provide pressure to fill the tank. After filling the tank, the pipeline was isolated on both sides using V1 and V2.

Once the FC pipeline was fully isolated, the PCAE pump was activated at maximum pressure. The pressure could not be raised higher than 1.6 bar, indicating that there was a leak in the pipe. The pressure was then dropped at increments of 0.1 bar up to 0.73 bar, and increased again at increments of 0.1 up to 0.9 bar, as shown in Figure 4.80. For each pressure step, the flow was allowed to stabilise.

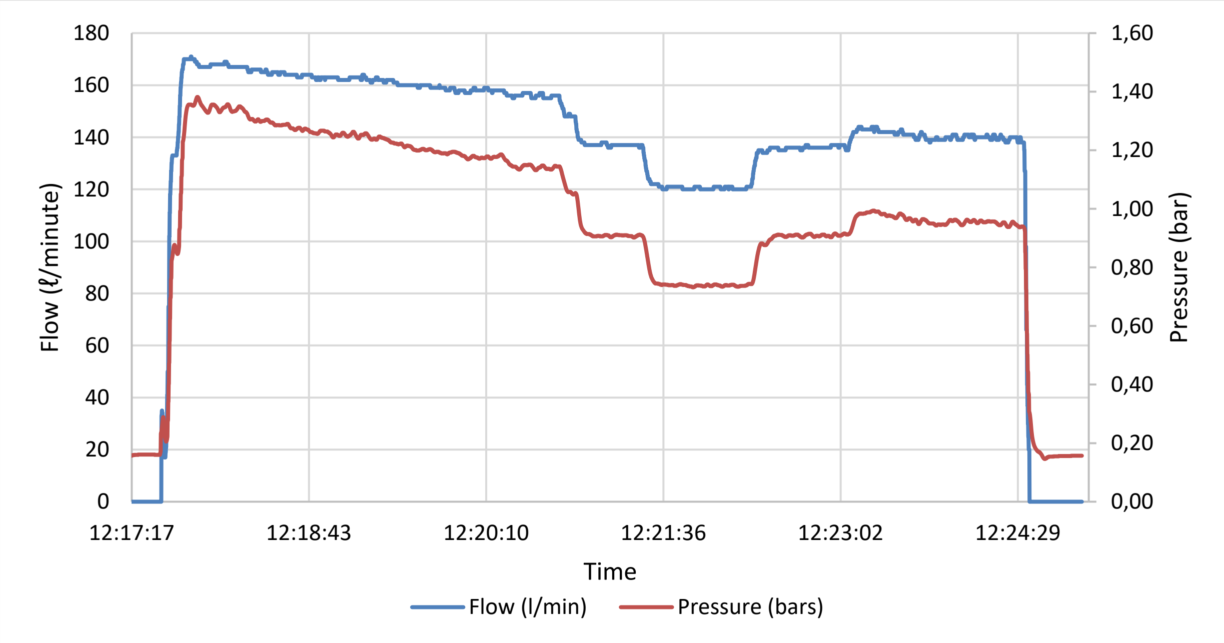

Figure 4.80: Pressure and flow data for the first attempt

A second attempt was made to check if the pressure and flow data would be similar to the first attempt. The PCAE tank was filled again by requesting the operator at valve V1 to open the valve and pressurise the FC pipeline to fill the tank. Once the tank was filled, the pipeline was isolated again by closing valves V1 and V2. The test was repeated. The pressure and flow results for this second attempt are shown in Figure 4.81.

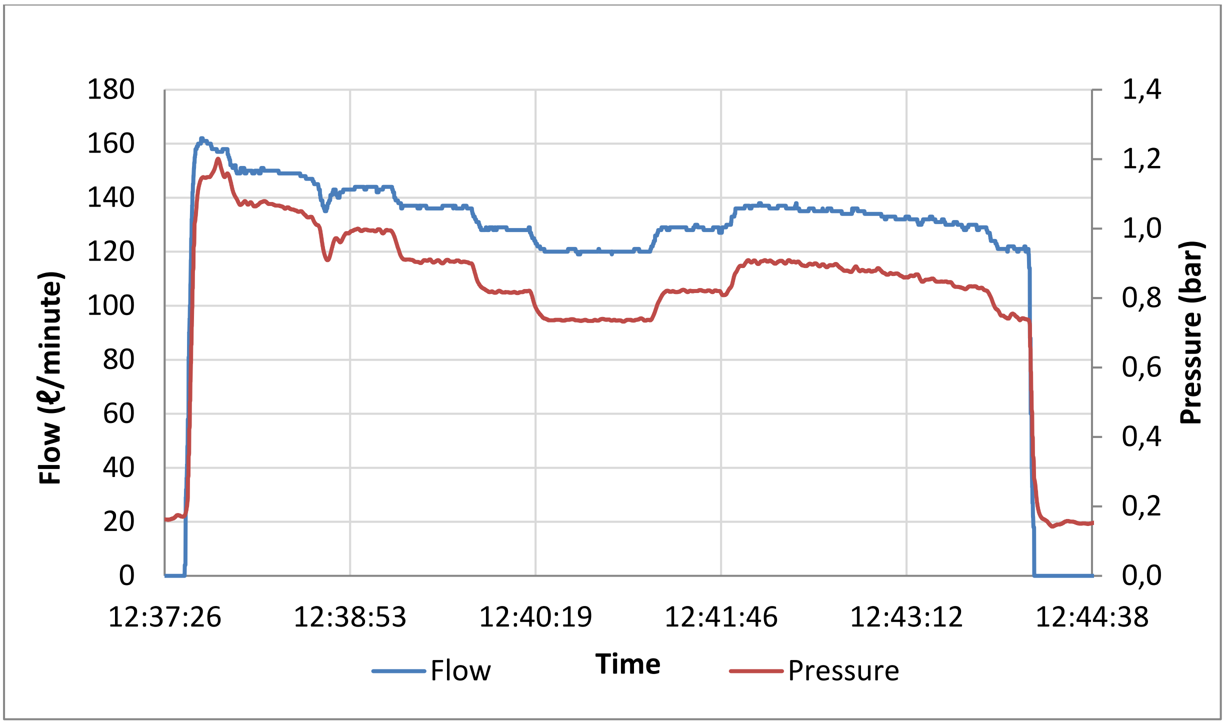

Figure 4.81: Pressure and flow data for the second attempt

The results obtained for the second attempt show similar results to the first attempt. A very clear leak was detected that was also pressure dependent. Furthermore, the leakage flow rate obtained in the second attempt was similar to the leakage flow rate obtained in the first attempt, with the lowest pressures giving a leakage flow rate of 120 ℓ per minute. The data obtained in the second attempt was used for further analysis.

A very clear leak was detected that was strongly pressure dependent. It was investigated whether the leakage was through the valves, but it did not appear that it was, as the pressure dropped to levels lower than would be expected from the downstream reservoir. The upstream valve was definitely closed as the pressure dropped to much lower levels than would be expected if the valve was even slightly open.

4.12.3 Results

The elevation profile of the FK pipeline is shown in Figure 4.82. Nodes were assigned at critical points on the pipeline. The downstream isolation valve V1 was assigned Node 4. The pipeline consistently rises, and an intermediate point between Fort Klapperkop and the Carina Street Reservoir was assigned Node 3. The pressure continues to rise until the Carina Street Reservoir where the connection point was assigned Node 2. The isolation valve V2 was assigned Node 1. The location of the PCAE device was assigned Node 0.

Figure 4.82: Elevation profile of the FK pipeline

A summary of the pipe properties between each node is given in Table 4.21. These pipe properties are used to calculate the head losses between nodes. The pressure head at Node 0 (the device) is known because the pressure is measured by the pressure sensor. The analysis starts from Node 0, and ends at Node 4. The minor loss coefficients, *k*, and absolute roughness, *e*, are obtained from Finnemore and Franzini, 2009.

Table 4.21: Summary of pipe properties between nodes

Pipe properties	**Node 0 to Node 1**	**Node 1 to Node 2**	**Node 2 to Node 3**	**Node 3 to Node 4**
Pipe section identity	**Delivery hosepipe**	**Connection**	**Test pipe**	**Test pipe**
Diameter, *D* (mm)	50	25	400	400
Absolute roughness, *e* (mm)	0.3	0.03	0.15	0.15
Minor loss coefficient, *K*	0.3	0.33	0.5	0
Elevation difference, Δz (m)	1	0.08	27.00	27
Length of pipe, *l* (m)	10	0.08	1 305.89	1 305.89
e/D	6.00×10^{-3}	1.80×10^{-3}	3.75×10^{-04}	3.75×10^{-04}
Pipe area, *A* (m^2)	1.96×10^{-03}	4.91×10^{-04}	1.26×10^{-01}	1.26×10^{-01}

The raw flow and pressure data obtained from the PCAE recorder is plotted against time in Figure 4.83. As can be seen from the figure, a clear leak was detected that was pressure dependent. The pressure was dropped at increments of 0.1 bar, and a flow rate was detected, suggesting that a leak existed in the pipeline. The leakage flow rate was then allowed to stabilise before another pressure increment was set.

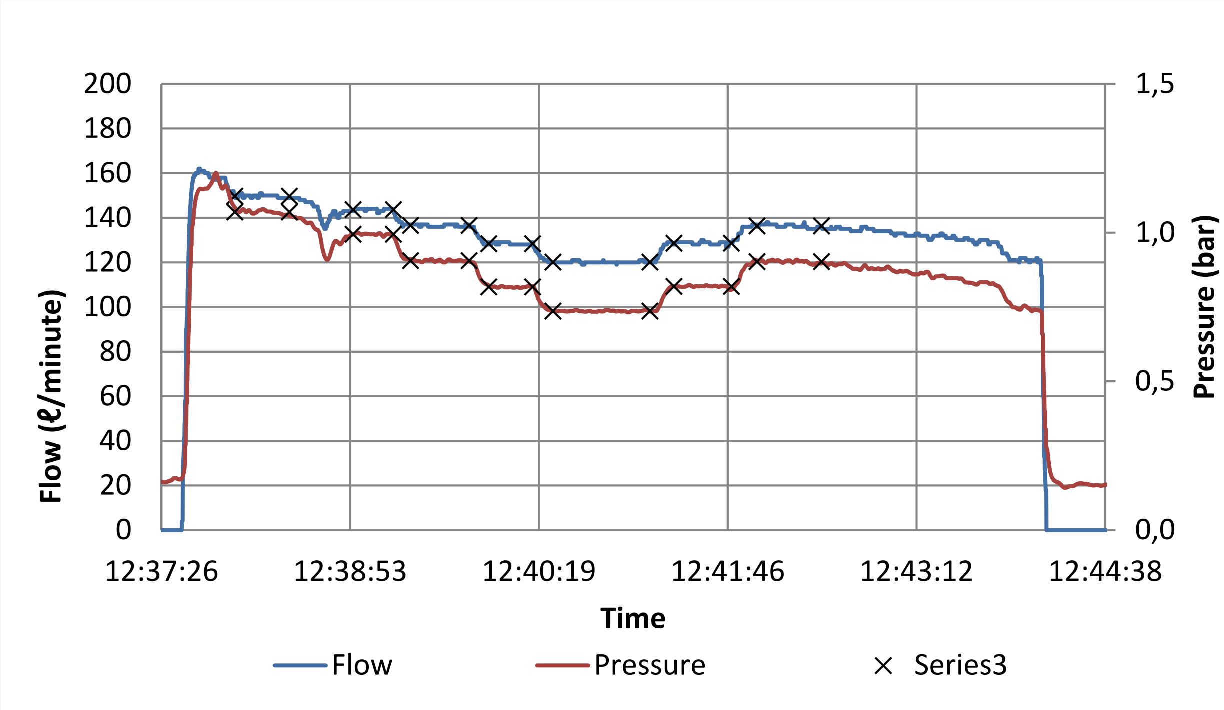

Figure 4.83: Flow and pressure data showing the stabilised data ranges selected

The graph clearly shows a step-down and step-up pattern repeated for both the pressure and flow data profile. The stabilised data range of each pressure and flow step was used for further analysis. The selected stabilised range of the pressure and flow rate is shown by the cross markers in Figure 4.83.

While the measured flow rate represents the water flowing from the tank into the pipeline and out of the pipeline through leakage, the measured pressure represents the pressure at the sensor and is not necessarily the pressure at each node. In order to obtain the pressure at each node, the measured pressure must be adjusted to take the elevation and other parameters that influence the pressure into account. The pressure was adjusted at each node. A summary of the pressure at each node is given in Table 4.22.

Table 4.22: Summary of the flow and adjusted pressures for each node

Q (m^3/s)	Head at 0, h0 (m)	Head at 1, h1 (m)	Head at 2, h2 (m)	Fead at 3, h3 (m)	Head at 4, h4 (m)
2.50E-03	10.908	11.356	10.905	37.903	64.901
2.39E-03	10.145	10.636	10.228	37.226	64.224
2.28E-03	9.239	9.779	9.417	36.416	63.414
2.14E-03	8.337	8.931	8.621	35.619	62.618
2.00E-03	7.511	8.155	7.894	34.893	61.891
2.14E-03	8.355	8.947	8.636	35.634	62.633
2.27E-03	9.205	9.746	9.386	36.385	63.383

From Table 4.22, it can be seen that the highest pressures occurred at Node 4, followed by Node 3. Finally, the nodes at the top (nodes 2, 1 and 0) had the lowest pressures. This was expected because the pipeline was pressurised from the top. Subsequently, due to the elevation difference (see Figure 4.82), the pressure will increase downstream of the pipeline.

For further analysis, only the pressure at nodes 2, 3 and 4 will be used as these nodes are located on the pipeline.

The flow and pressure data for nodes 2, 3 and 4, from Table 4.22, are plotted in Figure 4.84. The reason only nodes 2, 3 and 4 were selected was because these nodes are located on the pipeline. Therefore, the leakage parameters obtained for each of these nodes provides an envelope of possible leakage behaviour at different locations on the pipeline. Of these, the most realistic solution would probably be a good indicator of the leakage behaviour and possibly location.

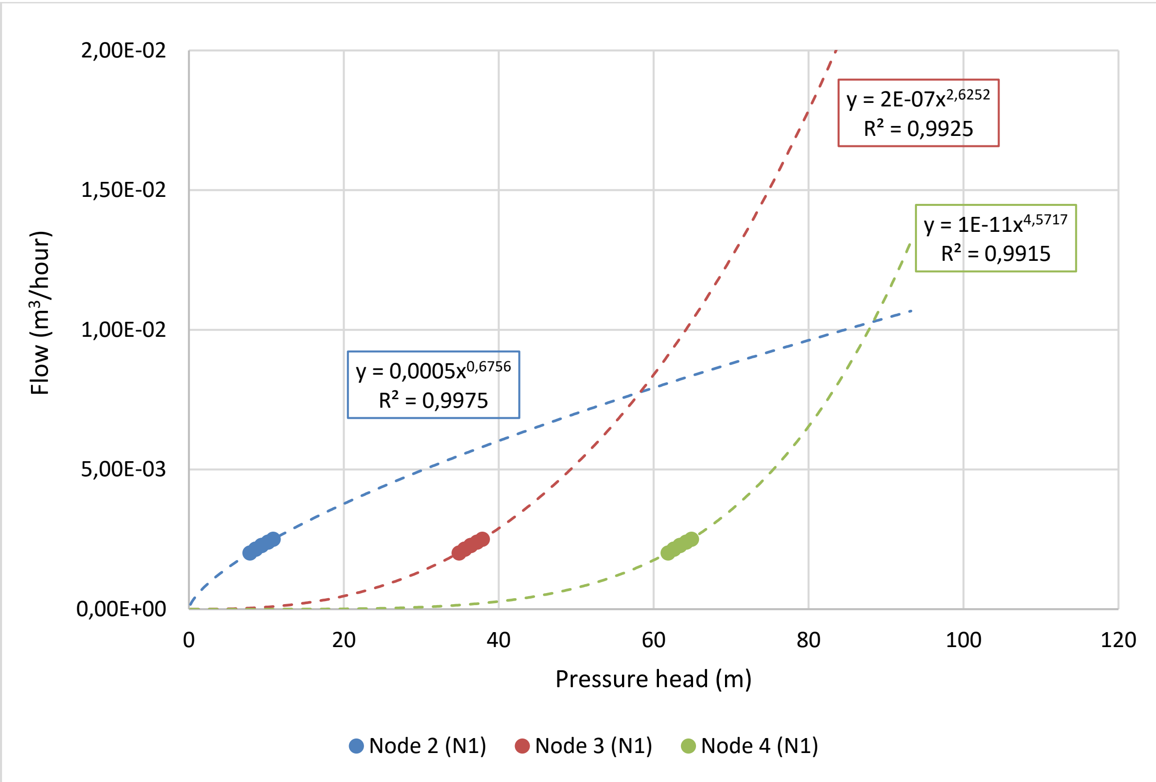

Figure 4.84: Flow against pressure for nodes 2, 3 and 4

From Figure 4.84, it can be seen that Node 2 had a leakage exponent of 0.67, which was the smallest, and perhaps the most realistic, when compared to nodes 3 and 4 that had leakage exponents of 2.62 and 4.57, respectively. Furthermore, it can be seen that, as the leakage exponent increases, the leakage coefficient becomes smaller and smaller, seemingly approaching zero. A summary of the power equation leakage parameters is provided in Table 4.23.

Table 4.23: Summary of the power equation leakage parameters

Node	Leakage coefficient, C	Leakage exponent, N1
2.	5×10^{-4}	0.67
3.	2×10^{-7}	2.62
4.	1×10^{-11}	4.57

From Table 4.23, it can be seen that if all the leakage occurs at Node 2, the leakage exponent would be 0.67 and the leakage coefficient 5 x 10^{-4}. This result is within the exponent range that can be explained by the MOE, 0.5 < N1 < 1.5. This result is synonymous with the leak that was observed on the strainer at Node 2.

If all the leakages occurred at Node 3, the leakage exponent would be 2.62 and the leakage coefficient 2 x 10^{-7}. A leakage exponent greater than 1.5 could occur due to an isolation valve bridge or data error. However, for this test, it is known that the isolation valve sealed properly and the data obtained had no errors. This indicated that a leak was unlikely.

If all the leakages occurred at Node 4, the leakage exponent would be 4.57 and the leakage coefficient 1 x 10^{-11}. This high leakage exponent is also unlikely to be due to an isolation valve bridge or errors in the data. This could also indicate an unlikely result.

4.12.3.1 Modified orifice equation leakage parameters

The effective leakage areas at each pressure was calculated for nodes 2, 3 and 4. The results are shown in Table 4.24. It can be seen from Table 4.24 that the largest leakage areas were found to occur at Node 2, followed by Node 3 and finally Node 4. This was expected because of the format of the effective leakage area equation in which the leakage flow rate is a numerator and the pressure is a denominator. Subsequently, if the leakage flow rate at each node is assumed to be the same, the nodes with large pressures (Node 4) will have a smaller effective leakage area, while nodes with small pressures (Node 2) will have larger leakage areas.

Table 4.24: Summary of effective leak area and pressure for each node

Flow rate, Q (m^3/s)	Head at 2, h_2 (m)	Effective leak area, CdA_2 (mm^2)	Head at 3, h_3 (m)	Effective leak area, CdA_3 (mm^2)	Head at 4, h_4 (m)	Effective leak area, CdA_4 (mm^2)
2.50E-03	10.91	170.57	37.90	91.49	64.90	69.92
2.39E-03	10.23	169.03	37.23	88.60	64.22	67.45
2.28E-03	9.42	167.44	36.42	85.15	63.41	64.52
2.14E-03	8.62	164.50	35.62	80.93	62.62	61.04
2.00E-03	7.89	160.86	34.89	76.51	61.89	57.45
2.14E-03	8.64	164.69	35.63	81.08	62.63	61.15
2.27E-03	9.39	167.43	36.38	85.04	63.38	64.43

The effective leakage area A' against the pressure head was plotted for nodes 2, 3 and 4, and a linear function was fitted to the data points, as shown in Figure 4.85. The intercept of each linear line with the area axis (y-axis) gave the effective initial leak area, A'_0, and the slope of the line gave the effective head-area slope, m'.

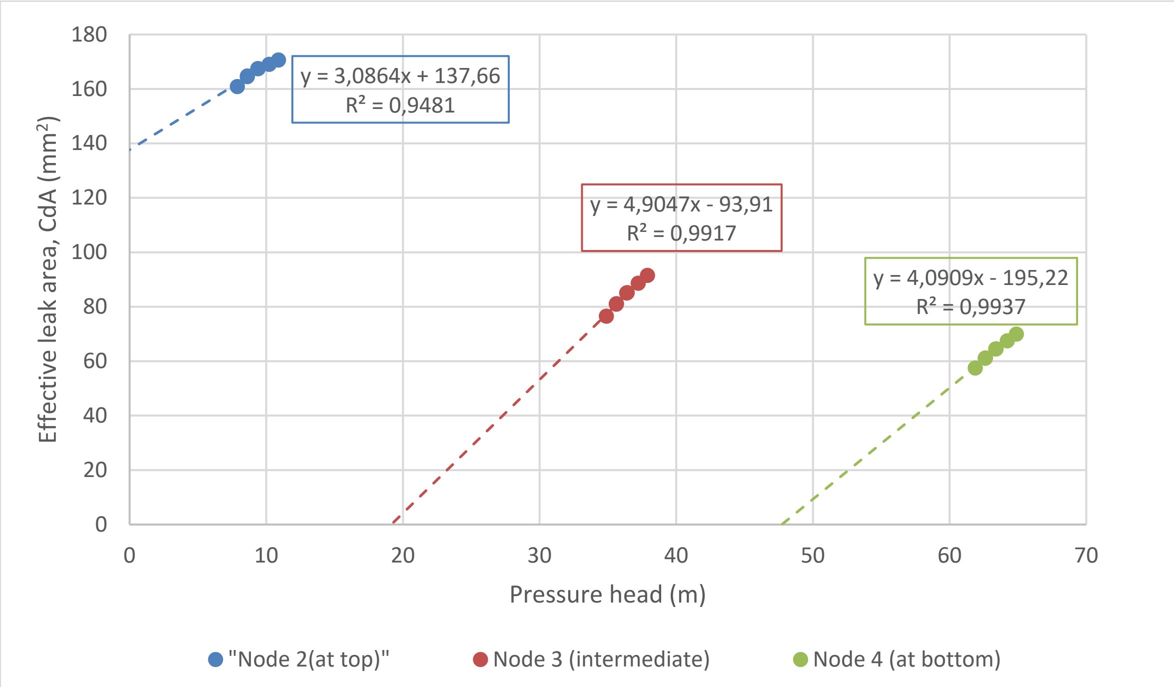

Figure 4.85: Effective leakage area against pressure head for nodes 2, 3 and 4

The results shown in Figure 4.85 show that all nodes had leaks with positive head-area slopes, but with varying magnitudes. Node 3 had the largest head-area slope of 4.9 mm^2/m, followed by Node 4 with 4.09 mm^2/m, and finally Node 2 with the smallest head-area slope of 3.08 mm^2/m. A summary of the results is provided in Table 4.25.

Table 4.25 Summary of the results

Node	Effective initial leakage area	Effective head-area slope	Leak characteristic
2.	137.66	3.0864	Excessive corrosion
3.	-93.91	4.9047	Longitudinal crack
4.	-195.22	4.0909	Longitudinal crack

Table 4.25 shows that the results obtained for Node 2 suggest that if all the leakage occurred at Node 2, the effective head-area slope would be 3.086 mm^2/m, implying that the leakage area would expand by 3.086 mm^2 for every meter of internal pressure to which the pipeline is subjected. Furthermore, at zero internal pressure, the results obtained suggest that the size of the effective leakage area is approximately 137.66 mm^2. This is a significant leak size and can be associated with the leak that was observed on the strainer on the tested pipeline at Node 2.

The results obtained for Node 3 suggest that if all the leakage occurred at Node 3, the effective head-area slope would be 4.90 mm^2/m, implying that the leakage area expands by 4.9 mm^2 for every meter of internal pressure to which the pipeline is subjected. At zero internal pressure, a negative effective initial leakage area was obtained. While a negative effective initial leak area is not physically possible, this result implies that the leak remains closed until a certain pressure is reached. For Node 3, the internal pressure required for the leakage area to open is approximately 19 m.

The results obtained for Node 4 suggest that if all the leakage occurred at Node 4, the effective head-area slope would be 4.09 mm^2/m, implying that the leakage area expands by 4.09 mm^2 for every meter of internal pressure to which the pipeline is subjected. At zero pressure, a negative effective initial leak area was obtained. While a negative effective initial leakage area is not physically possible, this result implies that the leakage area remains closed at Node 4 until a certain pressure is achieved, after which the leakage area starts opening. For Node 4, the internal pressure required for the leakage area to start opening is about 48 m.

The results obtained for the effective initial leakage area at nodes 3 and 4 suggest that the leakage is not corrosion, because corrosion damage deteriorates the material and consequently results in a positive effective initial leak area, such as at Node 2. For this reason, the results for nodes 3 and 4 perhaps indicate that leakage is unlikely to occur at these nodes. The most realistic result is the result obtained for Node 2.

4.13 DISCUSSION

The study was able to conduct 12 field tests, which is many more than originally planned. The tests allowed the equipment and proposed methodology to be thoroughly tested, showing that it provides a feasible, efficient and cost-effective method to evaluate bulk pipelines in the field.

A summary of the tests conducted is given in Table 4.26, providing the leakage characteristics of the pipe, as well as the leakage rate at a pressure head of 50 m. A summary of the main test findings are shown graphically in Figure 4.86.

Table 4.26: Results of real losses calculated from the modified orifice equation

Test	A_0' (mm^2)	m' (mm^2/m)	Leakage at 50 m (ℓ/min)	Leakage at 50 m (m^3/a)	Comment
BS 8 pipeline Test 1	8.50	0.0032	16	8 600	Leaks confirmed in the field and repaired.
BS 8 pipeline Test 2	29.57	0.51	103	54 000	Test done several weeks after Test 1. Large new leak evident.
Wingfield Test 1-1	0	0	0	0	No leak on section between valves V2 and V3.
Wingfield Test 1-2	11.56	3.41	342	180 000	Leak found between valves V2 and V4.
Wingfield Test 2	-	-	-	-	Failure on hydrant – no test possible.
Wingfield Test 3	-	-	-	-	No test possible due to large leak occurring in pipe while not in use.
UCT pipeline	-	-	3.4	1 800	Leak found, but too small for the meter to register. Half of meter starting flow assumed.
Simon Vermooten to Murrayfield Reservoir	-	-	-	-	No test possible due to isolation not sealing properly.

Test	A_0' (mm^2)	m' (mm^2/m)	Leakage at 50 m (ℓ/min)	Leakage at 50 m (m^3/a)	Comment
Lynnwood Road to Koedoesnek Reservoir	22.68	0.13	55	29 000	
Garsfontein to Parkmore High-level Reservoir	17.72	0.10	42	22 000	
Brickfields and Constantia Reservoir	-	-	-	-	No test possible due to isolation not sealing properly.
Fort Klapperkop Reservoir to Carina Street pipeline	137.66	3.09	549	288 000	
Average	**32.5**	**1.0**	**139**	**73 000**	

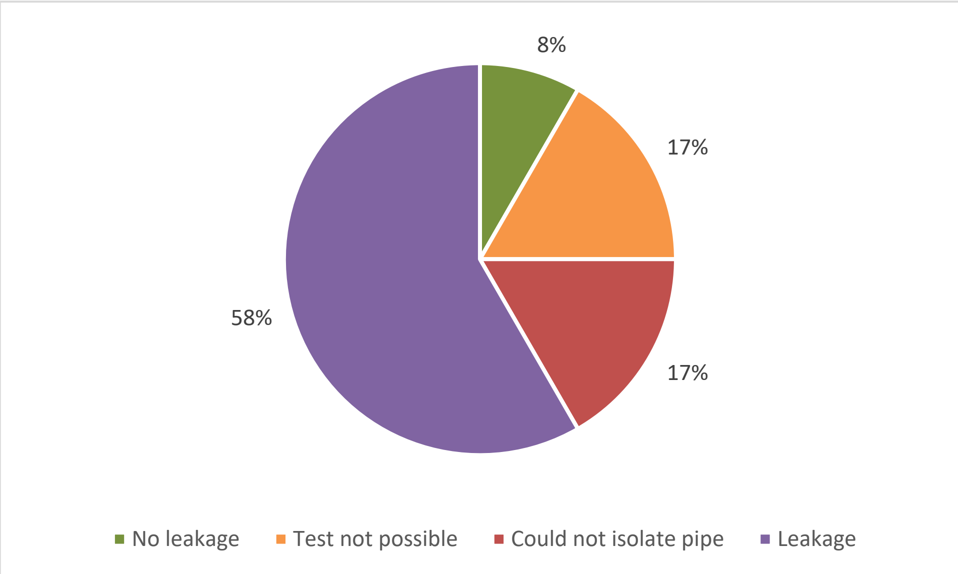

Figure 4.86 Summary of field test results

It was only possible to determine the leakage characteristics in eight (67%) of the 12 tests. Two tests, both on the Wingfield pipeline, were not possible due to very large leakage on the pipe. This line was not in active use, which may have contributed to its rapid deterioration. Two of the other tests could not be completed due to isolation valves not sealing properly, which is important additional information for the municipality to have. Should the pipe have to undergo repairs, non-sealing isolation valves may hamper this process and thus it is recommended that these valves be repaired.

Of the eight successful pipe tests, only one (12.5%) pipe section was found to have no leakage. The other seven tests (87.5%) found leakage varying between 3.4 and 549 ℓ per minute, or between 1 800 and 288 000 m^3/a (see Figure 4.87). Assuming a production cost of R5/m^3, the leaks represent an annual loss of between R90 000 and R1 440 000.

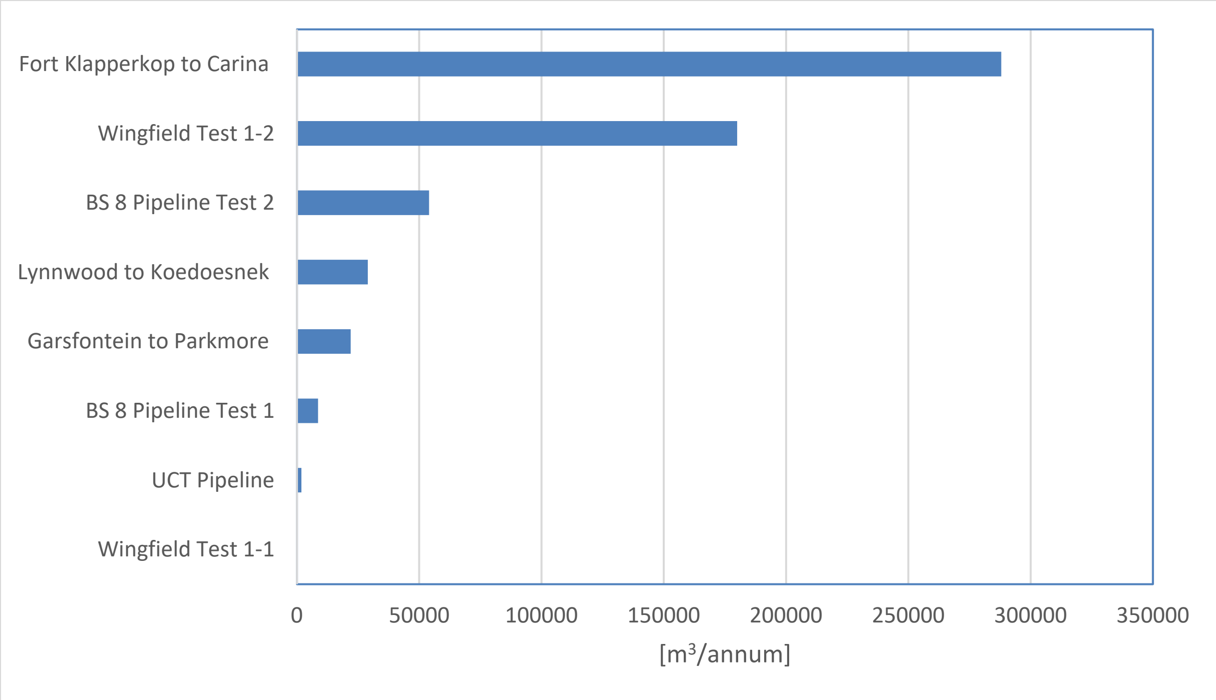

Figure 4.87: Annual leakage for the tested pipelines

CHAPTER 5: CONCLUSION

The aim of this project was to investigate the extent of leakage in bulk pipelines using novel PCAE conceptualised in earlier research. A larger version of the PCAE was constructed to allow bulk pipes to be tested. It consisted of a 1 000 ℓ tank installed on a mobile trailer, variable speed pump, pressure controller, sensors and pipework.

The PCAE used a pressure-testing technique in combination with the latest leakage models and data analysis techniques to characterise leakage on bulk pipelines. A method to test bulk pipes was developed, verified in the laboratory and refined.

Several tests were conducted on a wide range of bulk pipelines of different pipe materials, pipe diameters and lengths. Twelve tests were conducted and documented in detail to show the applicability of the method and problems experienced in the field.

Of the 12 tests, two could not be completed due to very large leaks on a disused pipe that clearly deteriorated rapidly while not in use. Another two tests failed due to the isolation valves not sealing properly. Of the remaining eight tests, leaks were found on seven pipelines. The leakage rates (estimated at a pressure of 50 m) varied between 3.4 ℓ and 549 ℓ per minute, equivalent to between 1 800 and 288 000 m^3/a. Assuming a production cost of R5/m^3, the leaks represent an annual loss of between R90 000 and R1 440 000.

The tests showed that the PCAE provides an efficient, non-intrusive and cost-effective method to assess the condition of bulk pipelines. It seems that the vast majority of pipelines have some measure of leakage and that this leakage can have severe financial implications for water suppliers.

REFERENCES

BENNIS S, FARES R, GUEMOURIA N and DUBOIS M (2011) Theoretical modeling and experimental validation of leakage in drinking water networks. Journal American Water Works Association **103 (12)** 61–72.

BURSTALL T (1997) *Bulk water pipelines,* Thomas Telford Publications, London, UK.

CASSA AM and VAN ZYL JE (2013)

CASSA AM and VAN ZYL JE (2014) Predicting the leakage exponents of elastically deforming cracks in pipes. Procedia Engineering **70** 302–310. http://doi.org/10.1016/j.proeng.2014.02.034.

CASSA AM and VAN ZYL JE (2011) *Linking the power and FAVAD equations for modelling the effect of pressure on leakage*. Centre of Water Systems, College of Engineering Mathematics and Physical Science, University of Exeter, Exeter, UK.

CASSA AM, VAN ZYL JE and LAUBSCHER RF (2010) A numerical investigation into the effect of pressure on holes and cracks in water supply pipes. Urban Water Journal **7 (2)** 109–120. http://doi.org/10.1080/15730620903447613.

CATALDO A, PERSICO R, LEUCCI G, DE BENEDETTO E, CANNAZZA G, MATERA L and DE GIORGI L (2014) Time domain reflectometry, ground penetrating radar and electrical resistivity tomography: A comparative analysis of alternative approaches for leak detection in underground pipes. NDT & E International **62** 14–28. http://doi.org/10.1016/j.ndteint.2013.10.007.

CATALDO A, CANNAZZA G, DE BENEDETTO E and GIAQUINTO N (2012) A new method for detecting leaks in underground water pipelines. IEEE Sensors Journal **12 (6)** 1660–1667.

CATALDO A, DE BENEDETTO E, CANNAZZA G, PIUZZI E and GIAQUINTO N (2015) Embedded TDR wire-like sensing elements for monitoring applications. Measurement: Journal of the International Measurement Confederation **68** 236–245. http://doi.org/10.1016/j.measurement.2015.02.050.

CHARALAMBOUS B (2005) Experiences in DMA redesign at the Water Board of Lemesos, Cyprus. Leakage **2005** 1–11.

CLAYTON CRI and VAN ZYL JE (2007) The effect of pressure on leakage in water distribution systems. Water Management **160** 109–114. http://doi.org/10.1680/wama.2007.160.2.109.

COLOMBO AF, LEE P and KARNEY BW (2009) A selective literature review of transient-based leak detection methods. Journal of Hydro-Environment Research **2 (4)** 212–227. http://doi.org/10.1016/j.jher.2009.02.003.

COSTELLO SB, CHAPMAN DN, ROGERS CDF and METJE N (2007) Underground asset location and condition assessment technologies. Tunnelling and Underground Space Technology **22 (5–6)** 524–542. http://doi.org/10.1016/j.tust.2007.06.001.

COUNCIL FOR SCIENTIFIC AND INDUSTRIAL RESEARCH (CSIR) (2005) Water supply. In: *Guidelines for human settlement planning and design*, CSIR, Pretoria, South Africa. http://doi.org/10.1007/SpringerReference_85090.

DE MIRANDA S, MOLARI L, SCALET G and UBERTINI F (2014) A physically-based analytical relationship for practical prediction of leakage in longitudinally cracked pressurized pipes. Engineering Structures **79** 142–148. http://doi.org/10.1016/j.engstruct.2014.08.011.

DE WIT M and STANKIEWICZ J (2006) Changes in surface water supply across Africa with predicted climate change. Science **311 (5769)** 1917–1921. http://doi.org/10.1126/science.1119929.

DEYI M, VAN ZYL J and SHEPHERD M (2014) Applying the FAVAD concept and leakage number to real networks: A case study in Kwadabeka, South Africa. Procedia Engineering **89** 1537–1544. http://doi.org/10.1016/j.proeng.2014.11.450.

ENVIRONMENTAL PROTECTION AUTHORITY (EPA) (2007) *Leakage management technologies*, American Water Works Association, Denver, CO, USA.

FARLEY M (2003) Non-revenue water. In: *12th Annual CWWA Water, Wastewater and Soil Waste Conference,* Paradise Island, Bahamas, 28 September to 3 October 2003.

FERRANTE M (2011) Experimental investigation of the effects of pipe material on the leak law: Leak in a steel pipe. Journal of Hydraulic Engineering (under revision) 736–743. http://doi.org/10.1061/(ASCE)HY.1943-7900.0000578.

FERRANTE M, BRUNONE B, MENICONI S, CAPPONI C and MASSARI C (2014) The leak law: From local to global scale. Procedia Engineering **70** 651–659. http://doi.org/10.1016/j.proeng.2014.02.071.

FERRANTE M, MASSARI C, BRUNONE B and MENICONI S (2011) Experimental evidence of hysteresis in the head-discharge relationship for a leak in a polyethylene pipe. Journal of Hydraulic Engineering **137 (7)** 775–780. http://doi.org/10.1061/(ASCE)HY.1943-7900.0000360.

FINNEMORE EJ and FRANZINI BJ (2009) *Fluid mechanics with engineering applications,* McGraw Hill, New York, NY, USA.

FRAUENDORFER R and LIEMBERGER R (2010) *The issues and challenges of reducing non-revenue water,* Asian Development Bank, Metro Manila, Philippines.

GAO Y, BRENNAN MJ, JOSEPH PF, MUGGLETON JM and HUNAIDI O (2005) On the selection of acoustic/vibration sensors for leak detection in plastic water pipes. Journal of Sound and Vibration **283** 927–941. http://doi.org/10.1016/j.jsv.2004.05.004.

GREYVENSTEIN B (2004)

GREYVENSTEIN B (2005)

GREYVENSTEIN B and VAN ZYL JE (2007) An experimental investigation into the pressure – leakage relationship of some failed water pipes. Journal of Water Supply: Research and Technology – AQUA **56 (2)** 117–124. http://doi.org/10.2166/aqua.2007.065.

HANNAFORD MA and MELIA WJ (2010) An advanced method of condition assessment for large-diameter mortar-lined steel pipelines. In: *Hetch Hetchy Water and Power Project,* Public Utilities Commission, San Francisco, CA, USA.

HAO T, ROGERS CDF, METJE N, CHAPMAN DN, MUGGLETON JM, FOO KY, WANG P, PENNOCK SR, ATKINS PR, SWINGLER SG, PARKER J, COSTELLO SB, BURROW MPN, ANSPACH JH, ARMITAGE RJ, COHN AG, GODDARD K, LEWIN PL, ORLANDO G, REDFERN MA, ROYAL ACD and SAUL AJ (2012) Condition assessment of the buried utility service infrastructure. Tunnelling and Underground Space Technology Incorporating Trenchless Technology Research **28** 331–344.

HENAN WEIN INDUSTRY CO., LTD (2012, 1 November) Henan Wein Industry Co., Ltd. http://www.hawein.com/a/product/Ductile_Iron_Product/2012/0830/5.html.

HERBST P and RALETJENA M (2015) No drop in the context of water security. In: *5th Regional African Water Leakage Summit,* Stellenbosch, South Africa, 23–24 June 2015.

HIKI S (1981) Relationship between leakage quantity and pressure. Journal of Japan Waterworks Association **51 (5)** 50–54.

HUNAIDI O and GIAMOU P (1998) Ground-penetrating radar for detection of leaks in buried plastic water distribution pipes. In: *7th International Conference on Ground Penetrating Radar,* Lawrence, KS, USA.

HUNAIDI O, WANG A and BRACKEN M (2004) Acoustic methods for locating leaks in municipal water pipe networks. In: *International Conference on Water Demand Management*, Dead Sea, Jordan, 30 May to 3 June 2004.

INNOSPECTION (n.d.) Remote field eddy current technique. http://www.innospection.com/pdfs/Remote Field Eddy Current.pdf. (Accessed 1 April 2016).

KARNEY B, KHANI D and HALFAWY MR (2009) A simulation study on using inverse transient analysis for leak detection in water distribution networks. *Journal of Water Management Modeling* **17** 399–416. http://doi.org/10.14796/JWMM.R235-23.

KINGDOM B, LIEMBERGER R and MARIN P (2006) *The challenge of reducing non-revenue water (NRW) in developing countries. How the private sector can help: A look at performance-based service contracting*. Water Supply and Sanitation Sector Board Discussion (No. 8), The World Bank, Washington, DC, USA.

KROON DH, LINDEMUTH D, SAMPSON S and VINCENZO T (2011). Corrosion protection of ductile iron pipe, 1–15. http://www.corrpro.com/mm/files/Corrosion Protection of Ductile Iron Pipe.pdf

LAI WWL, CHANG RKW, SHAM JFC and PANG K (2016). Perturbation mapping of water leak in buried water pipes via laboratory validation experiments with high-frequency ground penetrating radar (GPR). Tunnelling and Underground Space Technology **52** 157–167.

LAMBERT A (2000) What do we know about pressure leakage relationships in distribution systems? In: *IWA Conference: System approach to leakage control and water sistribution system management*, Brno, Czech Republic, May 2000.

LAMBERT (2001)

LAMBERT A and HIRNER W (2000) Losses from water supply systems: Standard terminology and recommended performance measeures. IWA: The Blue Pages **3**.

LAVEN K (2012)

LAVEN K and LAMBERT AO (2012) What do we know about real losses on transmission mains? Component analysis concepts applied to unreported leak data.

LEINOV E, CAWLEY P and LOWE MJ (2015) Guided wave attenuation in pipes buried in sand. AIP Conference Proceedings **1650 1** 227–236. http://doi.org/10.1063/1.4914614

LIU Z and KLEINER Y (2013) State of the art review of inspection technologies for condition assessment of water pipes. Measurement: Journal of the International Measurement Confederation **46 (1)** 1–15.

LIU Z, KLEINER Y, RAJANI B, CONDIT W and WANG L (2012) *Condition assessment technologies for water transmission and distribution systems*. Environmental Protection Agency (EPA), Washington, DC, USA.

LIU H (2003) Pipeline engineering. https://books.google.com/books?id=v_THSIAdx60C&pgis=1.

MAY JH (1994) Leakage, pressure and control. In: *BICS International Conference Leakage Control Investing in Underground Assets*.

MALDE R (2015) An analysis of leakage parameters of individual leaks on a pressure pipeline through the development and application of a standard procedure. Masters dissertation, University of Cape Town, Cape Town, South Africa.

MCKENZIE R, SIQALABA Z and WEGELIN W (2012) *The state of non-revenue water in South Africa (2012)*. Water Research Commission, Pretoria, South Africa.

MPESHA W, GASSMAN S and CHAUDHRY H (2001) Leak detection in pipes by frequency response method. Journal of Hydraulic Engineering **127** 134–147.

NSANZUBUHORO RM and VAN ZYL JE (2016) Leakage characterization of bulk water pipelines. Pipe condition assessment device design report.

NSANZUBUHORO RM, VAN ZYL JE and ZINGONI A (2016). Predicting the head-area slopes of circular holes in water pipes. In: *18th Conference on Water Distribution System Analysis,* Cartagena, Columbia, 24–28 July 2016.

OGURA (1979)

OLIVEIRA F, ROSS T and TROVATO A (2011) Smartball: A new pipeline leak detection system, and its survey of two petrobras/transpetro pipelines field tests. In: *8th Rio Pipeline Confernce,* Rio de Janeiro, Brazil, 20–22 September 2011.

ORAZEM ME (2014) *Underground pipeline corrosion – detection, analysis and prevention*, Woodhead Publishing, Sawston, UK.

ORAZEM ME and TRIBOLLET B (2008) List of symbols. Electrochemical Impedance Spectroscopy **7 (1)** 481–493. http://doi.org/10.1093/jicru/ndm007.

OSTAPKOWICZ P (2016) Leak detection in liquid transmission pipelines using simplified pressure analysis techniques employing a minimum of standard and non-standard measuring devices. Engineering Structures **113** 194–205. http://doi.org/10.1016/j.engstruct.2016.01.040.

PIPELINE INSPECTION AND CONDITION ANALYSIS CORPORATION (PICA CORP.) (n.d.) RFT technology described. http://www.picacorp.com/technology/entryid/144/rft-technology-described.aspx. (1 April 2016).

PHILLIPS RV (1972) Pipeline problems – brittle fracture, joint stresses, and welding. Journal od the American Water Works Association **64 (7)** 421–429.

PRINSLOO K, WRIGGLESWORTH M and WEBB M (2011) Advancement of condition assessment techniques for large diameter pipelines. *SAICE Civil Engineering Magazine* 20–26. http://reference.sabinet.co.za/sa_epublication_article/civeng_v19_n9_a7.

RAJANI B and KLEINER Y (2003) Protection of ductile iron water mains against external corrosion: Review of methods and case histories. Journal American Water Works Association **95 (11)** 110–125.

ROGERS D (2014) Leaking water networks: An economic and environmental disaster. Procedia Engineering **70** 1421–1429. http://doi.org/10.1016/j.proeng.2014.02.157.

SCHWALLER J and VAN ZYL JE (2014) Implications of the known pressure-response of individual leaks for whole distribution systems. Procedia Engineering **70** 1513–1517. http://doi.org/10.1016/j.proeng.2014.02.166.

SCHWALLER J, VAN ZYL JE and KABAASHA AM (2015) Characterising the pressure-leakage response of pipe networks using the FAVAD equation. Water Science and Technology: Water Supply **15 (6)** 1373–1382. http://doi.org/10.2166/ws.2015.101.

SSOZI EN, MALEKPOUR A, KARNEY BW and NAULT J (2015) Physical understanding of sudden pressurization of pipe systems with entrapped air: Energy auditing approach. ASCE Journal of Hydraulic Engineering **138** 642–652. http://doi.org/10.1061/(ASCE)HY.1943-7900.

STAMPOLIDIS A, SOUPIOS P, VALLIANATOS F and TSOKAS GN (2003) Detection of leaks in buried plastic water distribution pipes in urban places – a case study. In: *2nd International Workshop on Advanced Ground Penetrating Radar*, Delft, The Netherlands, 14–16 May 2003.

THORNTON J and LAMBERT A (2005) Progress in practical prediction of pressure: Leakage, pressure: Burst frequency and pressure: Consumption relationships. http://www.miya-water.com/fotos/artigos/10_progress_in_practical_prediction_of_pressure_leakage_pressure_burst_frequency_and_pressure_consumption_relationships_16541036425a328d4c63c6c.pdf.

TPLI METAL CASTING INDUSTRIES (2010)

TSE PW and WANG X (2009) Semi-quantitative analysis of defect in pipelines through the use of technique of ultrasonic guided waves. Key Engineering Materials **413–414** 109–116. http://doi.org/10.4028/www.scientific.net/KEM.413-414.109.

TURKOWSKI M and BRATEK A (2007) Methods and systems of leak detection in long range pipelines. Journal of Automation, Mobile Robotics and Intelligent Systems **1** 39–46.

UNITED NATIONS (2012) *The United Nations World Water Development Report 4: Managing water under uncertainty and risk*. United Nations Educational, Scientific and Cultural Organization (UNESCO), Paris, France.

UNITED NATIONS (2015). *The United Nations World Water Development Report 2015: Water for a sustainable world*. United Nations Educational, Scientific and Cultural Organization (UNESCO), Paris, France.

VAN DEN BERG C (2015) Drivers of non-revenue water: A cross-national analysis. Utilities Policy **36** 71–78. http://doi.org/10.1016/j.jup.2015.07.005.

VAN VUUREN SJ (2014). Theoretical overview of surge analysis. University of Pretoria, Pretoria, South Africa.

VAN ZYL JE (2014) Theoretical modeling of pressure and leakage in water distribution systems.

Procedia Engineering **89** 273–277. http://doi.org/10.1016/j.proeng.2014.11.187.

VAN ZYL JE, LAMBERT A and COLLINS R (2017) Realistic modeling of leakage and intrusion flows through leak openings in pipes. Journal of Hydraulic Engineering **143 (9)** 1–7.

WALSKI T, BEZTS W, POSLUZNY E, WEIR M and WHITMAN B (2006) Modelling leakage reduction through pressure control. Journal of the American Water Work Association **98 (4)** 147–152.

WALSKI T, WHITMAN B, BARON M and GERLOFF F (2009) Pressure vs flow relationship for pipe leaks. World Environmental and Water Resources Congress **(1)** 93–102. http://doi.org/10.1061/41036(342)10.

World Bank (2016) *High and dry: Climate change, water and the economy*. World Bank Group, Washington, DC, USA.

WU (2011)